Corona Pulses And Radio Interference Levels Of High Voltage Direct Current Transmission Lines.

CORONA PULSES AND RADIO INTERFERENCE LEVELS OF HIGH VOLTAGE DIRECT CURRENT TRANSMISSION LINES

BY

Beegamudré Rakosh-Das

A Dissertation

Presented to the Graduate Faculty

of Lehigh University

in candidacy for the Degree of

Doctor of Philosophy

in

the Department of Electrical Engineering

Lehigh University

1968

Approved and recommended for acceptance as a dissertation in partial fulfillment of the requirements for the degree of Doctor of Philosophy.

March 5, 1968
(date)

Professor in Charge

Accepted March 14, 1968
(date)

Special committee directing the doctoral work of Mr. B. Rakosh-Das

(Chairman)

ACKNOWLEDGEMENTS

The author is most grateful to Dean L.V. Bewley and Dean J.J. Karakash for giving him the opportunity to come to North America in 1957 by providing him with an instructor's position at the Lehigh University at his request. He is also indebted to these two gentlemen for their continued interest and encouragement throughout his doctoral work. He is thankful to the latter for providing him an instructor's position at Lehigh for the academic year 1967-68 during the finishing stages of this dissertation.

Portions of the experimental work carried out by the candidate while he was regularly employed by the National Research Council of Canada, Ottawa, have been used in this dissertation with permission from the Director, Radio and Electrical Engineering Division. They have been taken from published work by the author as unclassified research reports and technical papers. The author is highly thankful to the Director for this permission.

He is also thankful to Professor J.B. Jordan of the Universté Laval, Quebec, for consenting to review the work and to Professors E.H. Cutler and D. Leenov of Lehigh University for their consent to act as members of the candidate's doctoral committee.

TABLE OF CONTENTS

A B S T R A C T

Design of a d-c transmission line requires a knowledge of the proper size of conductor and its configuration in order that its radio noise level may be kept below tolerable limits. This dissertation is concerned with the interrelation between the basic characteristics of corona pulses occuring under the high applied d-c voltage and the level of resulting radio interference.

Hitherto, investigation of radio interference from conductors at high d-c voltages has been mostly concerned with measurement of radio noise levels by a noise meter under all possible experimental conditions. There has been little or no effort made to correlate basic characteristics of corona pulses with the observed radio noise levels, which will permit prediction of noise levels to be made so that the proper size and configuration of conductors might be selected for planned transmission lines of higher voltages that will be used in future.

In such a problem, the following basic pulse characteristics are considered important:

1. Shape and duration of a single corona current pulse;
2. Charge content and current amplitude of single pulse;
3. Repetition rate of corona pulses in a train;
4. Characteristics of radio influence voltage (RIV) caused by the pulses from short lengths of conductor in the laboratory in a co-axial cylindrical electrode system;
5. RIV from large conductors tested outdoors.

All the above five properties have been measured. A theoretical analysis has been made of the shape and repetition rate of positive pulses and pertinent values for the parameters involved in the analysis have been obtained from experimental results.

The next aspect of the overall problem is a discussion of a fundamental nature of radio noise meter characteristics and the noise levels of transmission lines indicated by them. There is at present no general agreement between engineers responsible for radio noise investigation on (a) whether it is the r-f power at the measuring frequency in corona pulse activity that is indicative of the radio noise level of a line, or, (b) whether it is the response characteristics of the noise-measuring circuit that is considered as the radio noise level. The authorby his analysis of the problem has shown that in so far as corona-type pulses are concerned, the response of the quasi-peak weighting circuit used in conventional noise meter bears a definite relation to the r-f power of the corona pulses. At first this isdone for periodically-occuring pulses of constant amplitude and shape. Then by the application of autocorrelation function and spectral density techniques, it is extended to include randomly-occuring corona pulses.

The final part of the dissertation deals with the predetermination of noise levels of transmission lines caused by corona pulses. Mathematical models are evolved which describe the behavior of radio noise of conductors of any given size

and configuration under different weather conditions. Before actually carrying out the design of long transmission lines for given operating d-c voltage, the distribution of r-f electric field intensity at ground level in the vicinity of a line of finite length which is open-circuited at both ends has been made. Conversion of data obtained from such short lines to the design values of a long line has been put on a theoretical foundation by establishing proofs for the methods used. Calculation of the near-field requires numerical methods which necessitates the use of digital computer.

Finally, prediction of radio-noise levels of long d-c lines has been carried out on the basis of the mathematical model developed. Validity of these models have been proved by comparison with experimental results available to the author. A fundamental difference between the energies involved in the different modes of propagation of a bipolar d-c line and those from a-c transmission lines has been found, and forms the basis of the mathematical models in addition to the description of RI levels from the power content of the corona pulses.

I N T R O D U C T I O N

Radio interference from direct-current transmission line conductors occurs when pulses are generated during a self-sustained corona discharge on them under high voltage stresses beyond a critical value known as the corona-inception gradient. The level of radio interference (RI) of a line is governed chiefly by the characteristics of these pulses originating in the corona discharge, since if there are no pulses there is no radio interference.

This dissertation is concerned with the interrelation between basic characteristics of pulses and the RI level of a d-c transmission line on which they originate and propagate. A quantitative evaluation of RI levels when pulses do occur depends upon several factors which are listed below:

1. Amplitude, shape, and repetition rate of pulses;
2. Response characteristics of noise-measuring circuit;
3. Size of conductor and line configuration;
4. Excitation voltage;
5. Propagation characteristics of pulses on the conductors;
6. Variation of Radio Influence Voltage (RIV) of pulses with excitation voltage;
7. Surface condition of conductors;
8. Weather conditions and wind; and
9. Lateral attenuation of the high-frequency electric or magnetic field intensity in the vicinity of the transmission line.

A complete evaluation of radio noise levels incorporating all of the above factors is an aim worth achieving in order that a transmission line might be designed with absolute certainty as to its behavior. In practice, however, it is not possible to achieve complete certainty on account of the random nature of some of the above factors. It is only possible to approach an accuracy that is tolerable as a complaint-free design.

Investigation of radio interference from high-voltage d-c power transmission lines has so far been mostly concerned with observing noise-meter readings under all possible experimental conditions, (1 - 8)*. These conditions involve

(a) variation of conductor size and number;

(b) variation of spacing between conductors on a tower, (proximity of conductors);

(c) variation of radio noise with voltage; and

(d) variation of radio noise with weather conditions.

Very little or no effort has been directed towards a systematic correlation between the basic characteristics of the source of interference, namely the pulses generated by corona, and the noise levels of transmission lines. The present work is primarily directed towards filling this gap. In so doing, the plan of attack involves four steps leading from the pulse characteristics to the final calculation of noise levels of a transmission line with given configuration of conductors on which these pulses originate and propagate. These steps are:

---

* Numbers in parentheses refer to Bibliography on page 164.

1. determination of basic characteristics of corona pulses;
2. analysis of response characteristics of noise-measuring instrument to the basic pulse characteristics;
3. determination of performance of short experimental lines when subjected to corona pulse excitation; and
4. analysis of performance and prediction of RI levels of long transmission lines for chosen voltages.

These four steps have been selected by the author as being the logical processes leading from the source of RI to the final phase of design of transmission lines. They form the subject of Chapters I to IV of this dissertation. Development and design engineers have followed some of these steps in practice depending upon the final results they were seeking and the expenditure they were prepared to incur, as well as the most important factor, the time at their disposal.

There is a general lack of agreement between engineers responsible for design of transmission lines from the RI-point of view, on whether it is the pulse characteristics and the r-f energy content in the pulse train that defines the radio interference level or whether it is the characteristics of the noise meter that constitutes what is termed radio interference. Engineers are divided broadly into two camps. The first group holds the idea that the high-frequency energy content of corona pulses forms the basic interference level, while the second group of engineers assumes that the peak value of the pulse (or a quantity proportional to the

peak value of the pulse called the quasi peak) forms the basic interference level, (9,10). The first group have based their idea on the assumption that a radio receiver experiences a high level of interference when the long-term average energy content of the noise source is high, regardless of the actual time variation of current or voltage of the noise source. This has necessitated their description of noise levels in terms of spectral density and auto-correlation function of the noise source. The second group have based their idea on the assumption that the level of interference to an apparatus used for radio reception is as much a property of the source as it is of the characteristics of the apparatus itself, namely its response to the source. This implies that two different noise sources with identical root mean square values but widely different time variation of noise voltage cause different levels of inconvenience to a listener. Conversely, two different noise-measuring circuits may yield entirely different responses to the same noise input.

Out of these two points of view has grown the enormous amount of good work that has been accomplished by engineers in the field of Radio Interference. The chief advantage of the r.m.s. view-point lies in the fact that the energy of the noise source is amenable to mathematical calculation and hence some sort of an analytical prediction of noise level could be made for preliminary design purposes, (11 - 14). At least the noise levels of two different sizes and configurations

of conductors can be compared, and if the noise level of one of them is determined from experiments then the noise level of the second or alternative arrangement can be ascertained from calculation. The second method requires that before a line could be designed, several alternative designs should be actually tested, even on a small scale, and compared for their noise level, (15). In order to obviate the basic difficulty involved in this method, designers have accepted the empirical rule that the voltage gradient on the surface of a conductor in any given configuration constitutes a primary design factor upon which an acceptable design could be evolved, (16). This takes away the direct importance attached to the actual r-f energy of the source of interference.

It is the object of this dissertation to advance the view that the noise level ofa a given transmission line shold be based on a combination of (a) an accurate knowledge of characteristics of corona pulses, (b) variation of these characteristics with voltage, and (c) response of noise meter to these pulses. The interference level should correspond more closely to the noise source characteristics as a primary quantity and the noise meter characteristics should be the secondary quantity. With this object in view, response characteristics of a noise meter and the statistical variations of the properties of the noise source, namely the corona pulses, are analyzed in detail, and finally the design of a d-c transmission line is related to the noise power of these pulses.

C H A P T E R - I

CHARACTERISTICS OF CORONA PULSES GENERATED UNDER HIGH D-C STRESSES

I.1 INTRODUCTION

This chapter describes characteristics of pulses generated by conductors when subjected to the influence of voltage stresses beyond the corona-inception value. The characteristic feature of a high pressure (760 mm of mercury) gas discharge is that partial discharges occur only in non-uniform field geometries. Uniform field geometry gives rise to a complete discharge between the electrodes, when once some type of discharge is initiated in the cathode region and the applied voltage is such as to cause ionization of the medium between the electrodes. Partial discharges are classified as corona discharges regardless of their type and method of initiation, (1). A complete discharge between electrodes is a breakdown phenomenon and has been investigated more extensively than partial discharges, chiefly on account of its importance in gas-discharge apparatus and for design of high-voltage insulations.

Of the many types of partial discharges, or corona, only those conditions that yield pulse-like self-sustained discharges obtained under high direct-voltage stresses will be discussed. It may sometimes prove interesting, however, to compare corona pulse phenomena occuring under d-c stresses with those obtained under a-c stresses. This will be done in

this chapter to some extent although this dissertation does not concern itself with a-c corona nor with the design of a-c transmission lines.

Pulses generated during a corona discharge contain energy at frequencies upto about 25 MHz, (megacycles per second). In this range, however, the energy content falls off rapidly at frequencies above 2 MHz. Since broadcast band ranges from 0.5 to 1.8 MHz, the energy content of corona pulses interferes with radio reception, if receivers are located close enough to a transmission line. It is the aim of an engineer topredict the interference of his line in order that radio equipment used in military or civilian communications sites and residential areas can be properly located to have a high signal-to-noise (S/N) ratio in the broadcast band. Corona pulses yield a negligibly small interference in the television range of frequencies and therefore do not affect video reception.

Since pulses form the source of radio interference (RI), it is first of all necessary to understand their characteristics before proper design of a transmission line can be carried out. These characteristics are:

1. shape of a corona current pulse;
2. current amplitude and charge content of a single pulse;
3. repetition rate of the pulses;
4. magnitude or level of Radio Influence Voltage (RIV) generated by these pulses from a given electrode

geometry as a function of excitation voltage; and

5. frequency spectra of this RIV.

All of the above characteristics were investigated and will be described in this chapter.

I.2 EXPERIMENTAL SETUP

Experimental determination of the shape of corona current pulse was carried out from a co-axial cylindrical geometry. Figure 1 shows the circuit layout. One of the main difficulties involved in an accurate measurement of the shape of a single pulse is the distortion caused by the electrode geometry to the measuring circuit. This is because of the capacitance between the discharge electrodes themselves. The shapes of a single corona pulse obtained by different investigators have shown differences in duration of these pulses because of the large time constants of the measuring circuits, (2 - 6). This author was fortunate enough to procure extremely high speed oscillographs with very low rise-times for the amplifiers. Also by suitably designing the electrode system, the shape and duration of a single pulse was measured as accurately as has been possible with the available technology. The work was carried out at the National Research Council of Canada.

A second limitation in the accurate measurement of pulse shapes is the necessity for properly connecting the electrodes to ground in order that reflections of pulses having very high rates of rise are eliminated from the ends

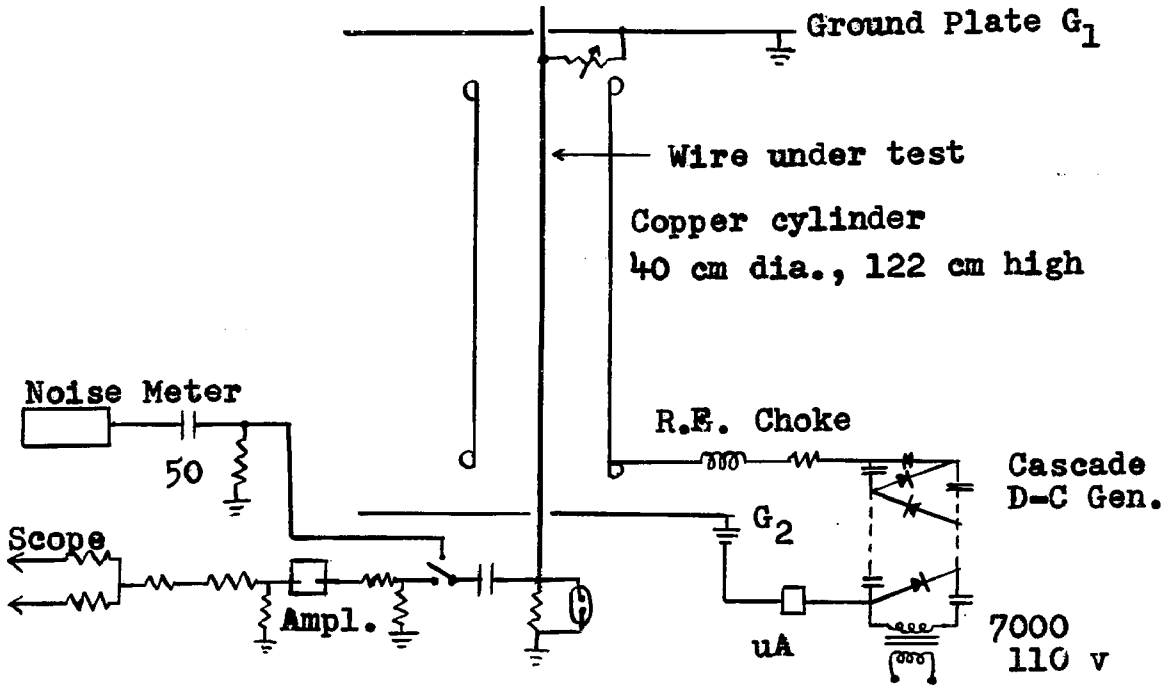

Figure 1. Circuit Diagram

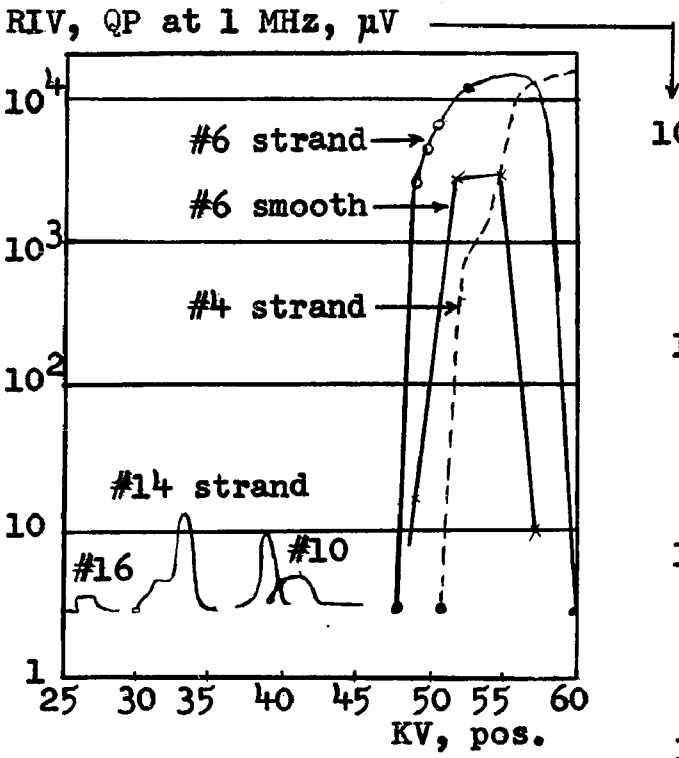

Fig.2 Occurence of Pulses
Laboratory tests

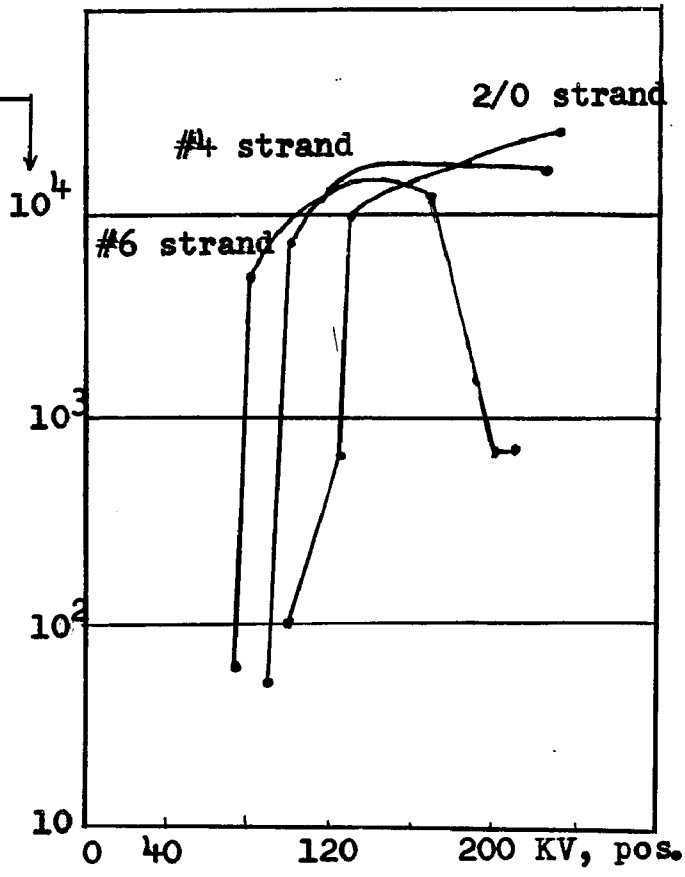

Fig.3 RIV of conductors
Outdoor tests

of the wire. Corona pulses last for less than 500 nano-seconds (ns) and therefore matching of components in the measuring circuit is of paramount importance.

These two limitations to the accurate measurement of the fast-rise short-duration corona pulses were recognized by the author and were minimized to the extreme by the following procedure:

1. The conductor on which corona discharge occured was placed near ground potential and the outer cylinder was connected to the high-voltage supply;
2. Intermediate amplifiers were kept to a minimum when photographing single pulses and the oscillograph used had a very high sensitivity;
3. An extremely fast-rise pre-amplifier with less than 1.5 ns rise time was used in the oscillograph;
4. A delay cable from the pulse source to the oscillograph with as low a capacitance as possible was used;
5. Impedance matching networks at every junction between components as well as at the trigger and input terminals of the oscillograph were used; and
6. The inner conductor was connected to ground by a resistance nearly equal to the calculated value of surge impedance of the co-axial cylindrical arrangement.

Using the conductor at ground potential makes the matching extremely convenient. It also eliminates the high-voltage capacitor required to provide a high impedance

between conductor and ground in order that measuring instruments may be used at ground potential. When the conductor is at nearly ground potential, a resistance will suffice to provide the necessary voltage to drive the vertical deflection plates of the oscilloscope. This makes the termination independent of frequency and a true shape of the pulse can be obtained. The terminations were tested with great care experimentally before final values of matching resistances were decided upon to achieve a completely reflection-free termination. This was carried out with a pulse generator giving pulses of 50 ns duration and the oscilloscope. The entire measuring circuit had a rise time of less than 5 ns.

The high-voltage supply consisted of a 60-kv rectifier chain of the Cockroft-Walton type and was connected to the outer cylinder 16 inches in diameter and 4 feet in height. The wire under test was clamped concentric to the cylinder and connected to ground plates at its two ends through proper terminating resistances. Characteristics of the corona current pulse were determined from measurements made at one end of the wire. The current pulse thus measured is one half of the total current induced in the conductor by the change in the bound charge occuring during a discharge.

Reflections were prevented from occuring at the ends of the wire, and thereby distort the pulse shape, by terminating each end in a resistance equal to the characteristic impedance of the cylinder-to-wire arrangement. Values of

matching resistances used for different wire sizes are shown in Column 4 of Table I, on page 16. These values were obtained experimentally and are nearly equal to the surge impedance of the cylinder-to-wire arrangement, Column 3.

Radio Influence Voltage (RIV) developed by the corona pulse was measured on a Stoddart NM20-A type of noise meter connected to the lower end of the wire through the 50-ohm matching impedance of the meter, as shown in Figure 1.

I.3 OCCURENCE OF PULSES

Before describing the shape of the pulse, it will be worthwhile mentioning here that pulses do not occur on conductors at all voltages. This is true of laboratory studies, but may not be entirely true on large conductors used on transmission lines which have a rough surface and are subject to contamination. A good review of this topic has been made by Loeb, (7), who has described conditions for formation of pulseless glow discharges called the Hermstein glow. Uhlig, (8), has discovered that a glow discharge occrs on extremely thin wires at high negative gradients which he has called the Ultra Corona. These glow discharges have been attributed to possible secondary mechanisms as well as the transformation of the non-uniform field distribution in the vicinity of the wire into a more uniform distribution due to the presence of space charges. Boulet and Jakubczyk, (9,10), have obtained experimental results of pulse activity when very thin wires are wrapped around a large conductor

TABLE I. WIRE SIZES AND TERMINATING RESISTANCES

Wire Size	Outside diameter, inches	Calculated surge impedance $Z = 60\ \mathrm{Ln}(R/r_o)$	Actual value of terminating resistance used, ohms
Smooth No. 16	0.051	345	375
Smooth No. 14	0.064	330	360
Stranded No. 14	0.073	323	
Smooth No. 10	0.102	303	320
Stranded No. 10	0.116	295	
Smooth No. 6	0.162	275	295
Stranded No. 6	0.184	268	
Stranded No. 4	0.231	250	250

TABLE II. AMPLITUDE AND CHARGE CONTENT OF PULSES

Wire Size	Pol.	KV	Peak Ampl., mA	Charge Content, μμC	
				Pulse Front	Complete Pulse
Stranded No. 4	Pos.	55.0	133	5100	19,200
Stranded No. 6	Pos.	48.7	66	2625	10,500
		51.4	116	3625	18,300
		54.0	122	3825	17,800
	Neg.	48.6	30	420	1,900
		51.5	50	750	3,450
		54.4	45	565	2,650
		57.0	54	900	3,800
Stranded No.10	Neg.	41.0	37	500	2,250
		48.0	38.4	500	2,450

in order to obtain a diminished pulse activity, under a-c excitation.

Commencing with No.16 smooth wire, when the wire is negative with respect to the cylinder, pulses and RIV are generated at all voltages above 26 kv, which is the corona onset voltage. But when the wire is positive, pulses occured only in a narrow region of about 1 kv near the onset voltage. However, even though the pulses vanished altogether at higher positive voltages the average direct current representing the power input during corona increased steadily with increasing voltage. This region is the Hermstein glow region as we know it now.

The same type of behavior is observed from larger conductors. The voltage range in which pulses occur increases with conductor size and with stranding. A smooth No.6 size of wire gave pulses within a voltage range of 50 to 55 kv while a stranded conductor with the same gauge number yielded pulses within the range of 48 to 60 kv, positive. Pulse activity is indicated by a measurement of the RIV at 1 MHz, as shown in Figure 2, page 12. Within the range of available voltages it was not possible to subject all sizes of wire through the entire range of occurence of pulses; but as may be observed from Figure 2, RIV began to fall for No.4 stranded wire after reaching a maximum value, indicating a diminished pulse activity.

Figure 3, page 12, shows results of RIV measurements

from an outdoor setup using 20-foot lengths of conductor 15 feet above ground. Once again diminishing of pulse activity is indicated on some of the wires as voltage is increased.

I.4 PULSE SHAPE

Oscillograms of corona current pulses show distinctly different shapes for pulses generated by the two polarities of excitation. These pulse shapes do not vary appreciably either with change of voltage or wire size. In a recent paper, Perel'man and Chernobrodov, (4), have obtained pulse shapes on larger conductors and it is interesting to note that the pulse shape is nearly the same as from smaller wire sizes obtained by the author.

i. Positive Pulse

The positive pulse, Figure 4, shows that its shape can be approximated to a double-exponential type of variation with time. It rises to its peak value in 50 ns. The full line shows a typical observed pulse and the broken line a calculated 50/150-ns double-exponential curve having the same peak value. It can be described by the equation

$$i(t) = A \left(e^{-\alpha_p t} - e^{-\beta_p t} \right) , \qquad (1)$$

where A, α_p, and β_p are constants. They depend upon t_1, the time to reach peak value, t_2 the time to reach one-half the peak value on the tail, and I_p, the peak value of the pulse, as shown in Figure 4.

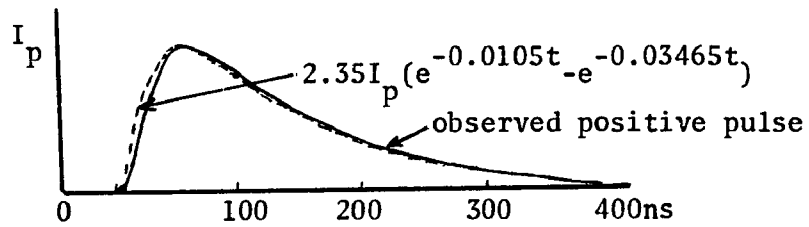
I_p
$2.35I_p(e^{-0.0105t}-e^{-0.03465t})$
observed positive pulse
0
100
200
300
400ns

Fig. 4

2.9 β_p/α_p
2.5
2.0
1.5
1.1
$\alpha_p t_1$
I_p/A
β_p/α_p
$\alpha_p t_1$
I_p/A
β_p/α_p
$\alpha_p t_1$
I_p/A
0.9 0.4
0.8 0.3
0.7 0.2
0.6 0.1
0.5 0.0
2.7
2.75
2.8
2.85
2.9
t_2/t_1

Fig. 5

A theoretical explanation for the shape of positive pulse has been derived in Section I.8. Numerical values for the constants A, α_p, and β_p in equation (1) can be obtained from the following three conditions:

i) at $t=t_1$, $i=I_p$. $\therefore$ $I_p = A\,(e^{-\alpha_p t_1} - e^{-\beta_p t_1})$.

ii) at $t=t_2$, $i=\frac{1}{2}I_p$. $\therefore$ $\frac{1}{2}I_p = A\,(e^{-\alpha_p t_2} - e^{-\beta_p t_2})$.

iii) at $t=t_1$, $di/dt=0$. $\therefore$ $0 = A\,(\beta_p e^{-\beta_p t_1} - \alpha_p e^{-\alpha_p t_1})$.

From (iii), $$\beta_p e^{-\beta_p t_1} = \alpha_p e^{-\alpha_p t_1} . \qquad (2)$$

From (i) and (ii), $$e^{-\alpha_p t_2} - e^{-\beta_p t_2} = \tfrac{1}{2}\,(e^{-\alpha_p t_1} - e^{-\beta_p t_1}) \qquad \ldots\ldots (3)$$

Instead of using A, α_p, and β_p as variables, it is convenient to use $\alpha_p t_1$, β_p/α_p, and t_2/t_1 as new parameters. In terms of these three parameters, equations (2) and (3) can be written as follows:

$$\alpha_p t_1 = \mathrm{Ln}\,(\beta_p/\alpha_p)\,/\,(\beta_p/\alpha_p - 1), \qquad (4)$$

and $$2 = (e^{-\alpha_p t_1} - e^{-\beta_p t_1})\,/\,(e^{-(\alpha_p t_1)(t_2/t_1)} - e^{-(\alpha_p t_1)(\beta_p/\alpha_p)(t_2/t_1)}) \qquad \ldots\ldots (5)$$

where Ln stands for the natural logarithm. Evaluation of $\alpha_p t_1$ and β_p/α_p from known values of t_2/t_1 is not straight forward. Instead, the value of t_2/t_1 for corresponding values of $\alpha_p t_1$ and β_p/α_p is found by the following method:

From equation (4), β_p/α_p is calculated for assumed values of $\alpha_p t_1$, and using these values the ratio t_2/t_1 is found from equation (5). A set of curves are drawn giving $\alpha_p t_1$ as a function of t_2/t_1, and β_p/α_p also as a function of t_2/t_1, as shown in Figure 5, page 19. For lightning-type discharges, Bewley has calculated these values in his Fig.6 of Chapter 2, reference (11).

The double-exponential type of equation, equation (1), does not apply for all values of t_2/t_1. In order for this equation to be valid, the time t_2 to half value on the tail must have a minimum value of 2.678 t_1 and is given as the solution to the equation

$$t_2/t_1 - \text{Ln}\,(t_2/t_1) = 1 + \text{Ln}\,2 \quad . \qquad (6)$$

This condition is derived as follows:

When $\alpha_p = \beta_p$, the expressions on the right side of equations (4) and (5) both become equal to the indeterminate quantity 0/0. Therefore the limits of these expressions have to be evaluated by applying L'Hospital's rule, namely by differentiating both the numerator and denominator with respect to β_p/α_p and setting the result equal to the value when β_p/α_p equals unity. This gives

$$\alpha_p t_1 = 1 \ , \qquad (7)$$

and $$(\alpha_p t_1)\,(t_2/t_1 - 1) = \text{Ln}\,2(t_2/t_1) \ , \qquad (8)$$

or $$t_2/t_1 - \text{Ln}\,(t_2/t_1) = 1 + \text{Ln}\,2 \ . \qquad (6)$$

A trial and error solution to equation (6) is $t_2/t_1 = 2.678$.

Having determined $\alpha_p t_1$ and β_p/α_p for a given value of t_2/t_1, the amplitude factor, A, is given by

$$A = I_p \left[e^{-\alpha_p t_1} - e^{-(\alpha_p t_1)(\beta_p/\alpha_p)} \right]^{-1} . \quad (9)$$

For a 50/150- ns positive pulse, theratio $t_2/t_1 = 3.0$. From Figure 5, $\alpha_p t_1 = 0.5$ and $\beta_p/\alpha_p = 3.5$. If time is measured in nanoseconds, α_p and β_p become 0.01 and 0.035, respectively, and $A = 2.3\ I_p$. Thus the equation to the 50/150-ns positive pulse is

$$i = 2.3\ I_p\ (e^{-0.01\ t} - e^{-0.035\ t}) . \quad (10)$$

ii. Negative Pulse

The negative pulse is shorter and steeper than the positive pulse and its amplitude is nearly 30% of that of the positive pulse. It rises to its peak value I_n in 20 ns and decays to half value on the tail in 50 ns. Its shape does not correspond to equation (3), that is, the negative pulse is not a double-exponential. Since the negative pulse is of great importance in the study of breakdown of gaps, its shape has been theoretically derived by several investigators, chiefly by Fletcher (12), Heintz (13), and Raether (14). An equation derived by Heintz for the negative pulse, based on the analysis of Fletcher in the calculation of formative time-lag of gaps, is

$$i_n(t) = B\, t^{-3/2}\, e^{-(\alpha_n/t + \beta_n t)} \qquad (11)$$

It is plotted in Figure 6 and shows good agreement with the measured shape except on the final portion ofthe tail. A true double-exponential equation of the type of equation (1) cannot be fitted to a pulse having a ratio of $t_2/t_1 = 50/20 = 2.5$. But by taking $t_2/t_1 = 2.7$ and $t_1 = 20$ ns, a double-exponential curve has been fitted to show that the negative pulse deviates appreciably from equation (1). A simple formula derived by the author for the declining portion of the negative pulse is given in Section I.8 to be

$$i(t) = I_n\,(1 + \gamma_n\, t)^{-2}\,. \qquad (12)$$

It is also plotted in Figure 6 and describes the tail of the pulse very closely.

The constants B, α_n, and β_n in equation (11) are functions of I_n, t_1, and t_2, and are calculated as follows: The three known conditions are

i) at $t = t_1$, $i = I_n$. $\therefore$ $I_n = B\, t_1^{-3/2}\, e^{-(\beta_n t_1 + \alpha_n t_1^{-1})}$.(13)

ii) at $t = t_2$, $i = \frac{1}{2} I_n$. $\therefore$ $\frac{1}{2} I_n = B\, t_2^{-3/2}\, e^{-(\beta_n t_2 + \alpha_n/t_2)}$.(14)

iii) at $t = t_1$, $di/dt = 0$. $\therefore$ $0 = B\, t_1^{-5/2}\, e^{-(\beta_n t_1 + \alpha_n/t_1)} \times (\alpha_n/t_1 - \beta_n t_1 - 3/2)$. (15)

From (15), $\alpha_n/t_1 = 3/2 + \beta_n t_1$. (16)

From (13) and (14), $2 = (t_2/t_1)^{3/2}\, e^{\beta_n(t_2 - t_1) + \alpha_n(1/t_2 - 1/t_1)}$ ..... (17)

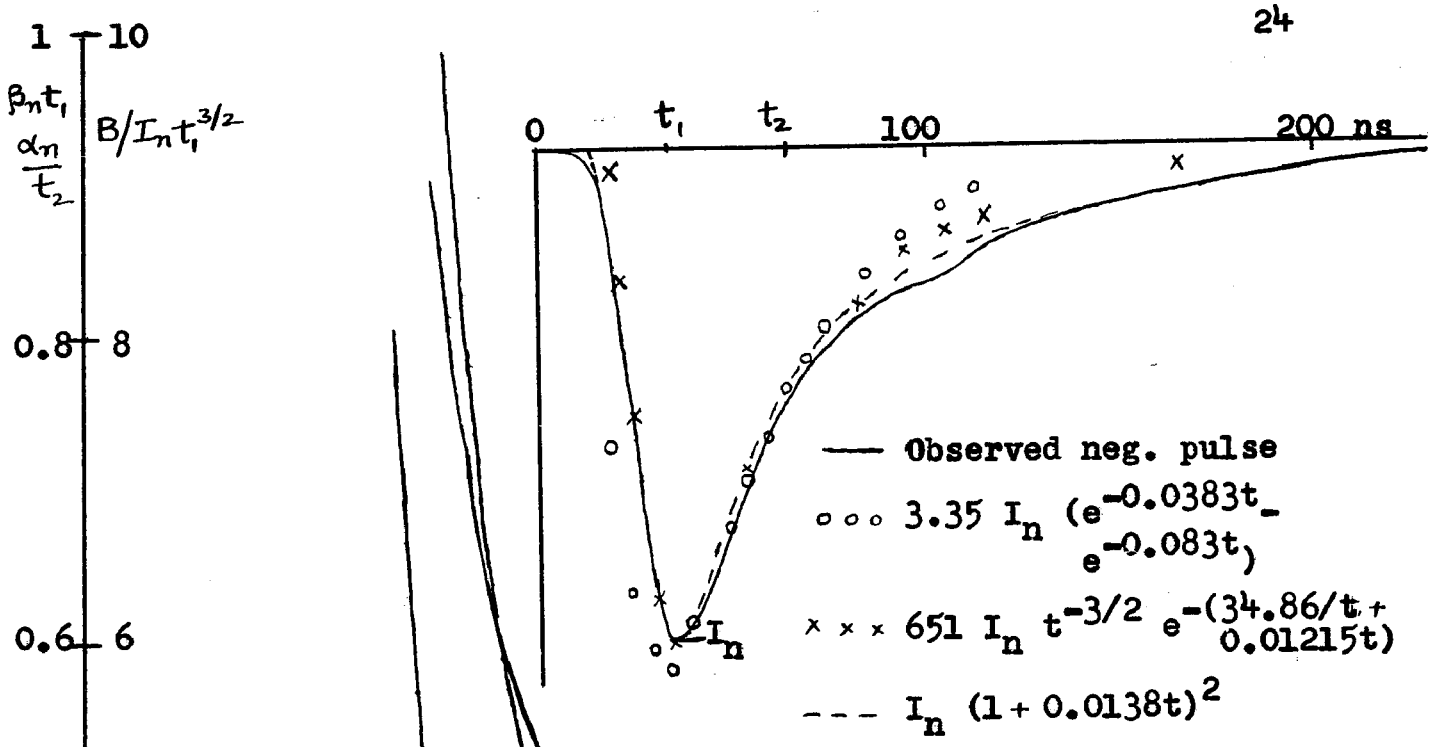

Figure 6. Negative Corona Pulse

Figure 7. Calculation of α_n, β_n, and B of equation (11)

Using equation (16) in (17), $\beta_n t_1$ is obtained as a function of t_2/t_1 thus:

$$\beta_n t_1 = \frac{\text{Ln } 2 - (3/2)\text{ Ln } (t_2/t_1)}{(1 - t_1/t_2)(t_2/t_1 - 1)} + \frac{3}{2}\,\frac{1}{(t_2/t_1) - 1} \qquad (18)$$

Therefore from equations (13) and (16),

$$B\, I_n^{-1}\, t_1^{-3/2} = e^{(\alpha_n/t_1 + \beta_n t_1)} = e^{2\,\beta_n t_1 + 3/2}\,. \qquad (19)$$

Figure 7 shows values of $\beta_n t_1$, α_n/t_2, and $B\, I_n^{-1}\, t_1^{-3/2}$ as functions of t_2/t_1, calculated from equations (16), (18), and (19). When t_1 and t_2 are known for any given pulse, the values of BI_n^{-1}, α_n, and β_n are obtained from this figure. For the 20/50- ns pulse, for which $t_2/t_1 = 2.5$, Figure 7 gives

$$\alpha_n t_1 = 0.243,\ \alpha_n/t_2 = 0.697,\ \text{and}\ B\, I_n^{-1}\, t_1^{-3/2} = 7.287.$$

When time is measured in nanoseconds, there are

$$\beta_n = 0.01215,\quad \alpha_n = 34.85,\quad \text{and}\quad B = 651\, I_n. \qquad (20)$$

The equation to the messured negative pulse is therefore

$$i_n(t) = 651\, I_n\, t^{-3/2}\, e^{-(34.85/t\, +\, 0.01215\, t)}\,. \qquad (21)$$

This is plotted in Figure 6.

An extremely important analysis has been carried out by Würstlin, (15,16), of the shape of the positive and negative pulses from basic consideration of the random motion of ions and electrons near the highly stressed electrode. His analysis has utilized the autocorrelation function and

spectral density of the statistical fluctuations of velocity and energy acquired by the charge carriers. The frequency spectrum of these positive and negative pulses obtained from their shape are discussed in Section I.9.

I.5 AMPLITUDE AND CHARGE CONTENT OF SINGLE PULSE

The response of a conventional noise meter to sharp corona-type pulses depends upon the amplitude and charge content of the pulse as will be shown in Chapter II. On any given conductor, the amplitude of a pulse is low at the commencement of the corona discharge. A slight increase in voltage nearly doubles the amplitude, but thereafter there is no appreciable increase in amplitude despite higher voltages. The peak value and charge content of single pulses obtained from three different sizes of wire are given in Table II, page 16. Amplitudes and charge contents show no definite relationship with voltage gradients and there is considerable overlapping of their values.

The final amplitude of the positive pulse is nearly 120 mA (milli-amperes) which is about 2.5 times that of the negative pulse.

The charge content of the positive pulse is nearly 18,000 micro-micro coulombs and is about 5 times that of the negative pulse. The charge in the rising portion of the pulse, that is the pulse front, is nearly 25% of that of the entire pulse at both polarities.

I.6 REPETITION RATE

Repetition rate of pulses in a train governs the level of radio influence voltage in conjunction with the amplitude and charge content of a single pulse. In a band-width-limited filter used in a noise meter, the relation between repetition rate in pulses per second and the numerical value of the band-width in cycles per second is a more important quantity than the actual value of the repetition rate, as will be shown in Chapter II.

Unlike a single point in corona from which pulses originate with strict regularity, the separation between pulses from a long conductor in corona is random because there are a large number of points from which corona pulses originate and these points are all uncorrelated. The repetition rate reported here is an average value obtained by measuring the time duration of about 50 pulses. This was obtained on an oscilloscope with a slow sweep rate, as shown in Figure 8.

Oscillograms of positive pulses show that there is no overlapping of pulses. The average repetition rate is in the order of 1000 to 2000 pulses per second, as shown in Figure 9. On laboratory samples of conductor, progressive increase in voltage brings about the Hermstein glow and therefore the pulse repetition rate at first shows an increase with voltage and then decreases, finally reaching zero at the incidence of the Hermstein glow. Since American noise meters have a bandwidth of nearly 5000 Hz, the repetition rate of

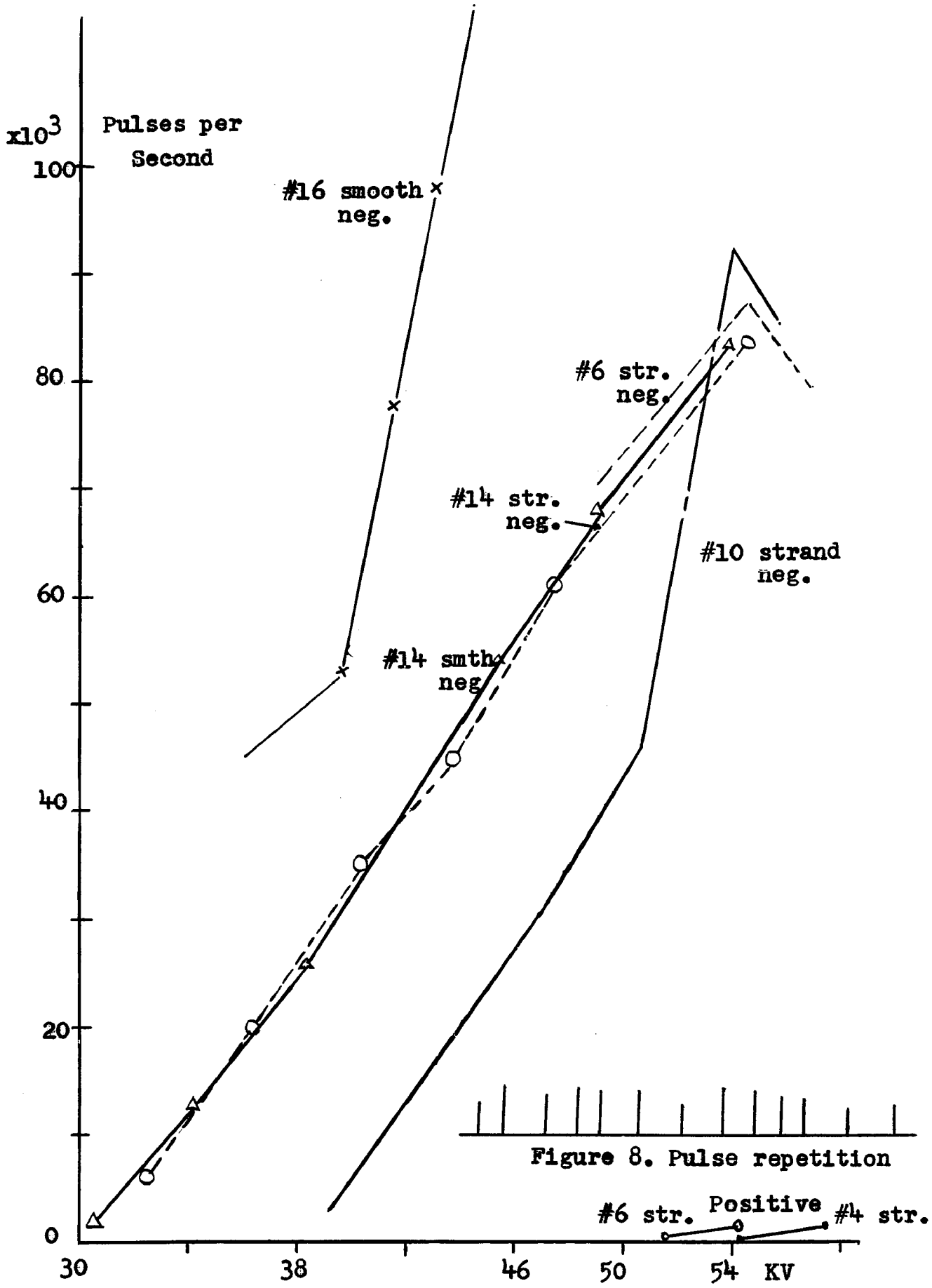

Figure 8. Pulse repetition

Figure 9. Repetition rate of Pos. and Neg. Pulses

positive pulses is numerically below the bandwidth of the meter and the noise reading is nearly independent of the repetition rate of the pulses when they are assumed to occur periodically. As shown in Chapter II, when a random repetition rate is assumed and the noise meter reading is correlated with the spectral density of the corona pulses, the average repetition must be known. Also, since the individual pulses do not overlap, the noise is defined as impulsive.

A theoretical analysis of the repetition rate of positive pulses is carried out in Section I.7.

Negative pulses have a very high repetition rate as compared to positive pulses, as shown in Figure 9. The number of pulses per second now have a numerical value which is higher than the bandwidth of the meter in cycles per second. Except at the higher voltages negative pulses also do not overlap one another. Thus the noise is still impulsive. When pulses overlap, the resulting noise is defined as Random Noise. These distinctions are important because when noise-meter readings are corrected for a bandwidth of 1 KHz, that is if the energy per kilocycle of bandwidth is being evaluated from the measured noise reading, the following corrections have to be applied:

$$\frac{\text{Reading for 1 KHz bandwidth}}{\text{Reading for actual bandwidth}} = \begin{cases} (BW)^{-1}, & \text{for impulsive,} \\ (BW)^{-1/2}, & \text{for random noise.} \end{cases}$$

When comparing noise readings obtained from two different meters, this correction is important.

I.7 ANALYTICAL CALCULATION OF POSITIVE PULSE REPETITION RATE

The physical mechanism involved for the corona discharge to be self-sustained lies in the scavenging of positive charge cloud formed near the positive conductor by the applied electric field. When the conductro is positive, free electrons near the conductor acquire enough energy to start an electron avalanche which is then drawn towards the positive conductor. In its wake the electron avalanche leaves behind a cloud of positive ions which start drifting towards the cathode. During this process the electric field in the space between the positive conductor and the positively charged ions is lower than when there is no positive charge cloud near the positive conductor. A fresh avalanche does not start until the positive charge cloud has moved sufficiently far away from the conductor such that the field gradient near the conductor regains the critical corona-inception value.

It is therefore necessary to determine first the distance to which the positive cloud should move in order that the field strength at the conductor may regain the corona-inception gradient, and second, to calculate the time taken for the positive charge cloud to move this distance under the applied field.

Considering Figure 10 which shows co-axial cylinders of radii r_o and R with charges of $+Q$ and $-Q$ per unit length, the field strength at any radius ρ ($r_o < \rho < R$) at an applied voltage V is

$$E = V/(\rho \, Ln(R/r_o)) = V C/ 2\pi\epsilon\rho \, . \qquad (22)$$

Also, $$E_{r_o} \, r_o = E_\rho \cdot \rho = E_R \, R \, . \qquad (23)$$

The capacitance per unit length of the cylinders is

$$C = 2\pi\epsilon / \, Ln \, (R/r_o) \, . \qquad (24)$$

If now a third cylinder with a positive charge q per unit length is introduced at r_i, as shown in Figure 11, it induces negative charges on the conductor and the outer cylinder. The resulting charge distribution on the three cylinders of radii r_o, r_i, and R will be respectively

$$Q - q \frac{Ln \, (R/r_i)}{Ln \, (R/r_o)} \quad , \quad + q \quad , \quad - \left(Q + q \frac{Ln \, (r_i/r_o)}{Ln \, (R/r_o)} \right) \qquad (25)$$

This is derived as follows:

Let the charge induced on the conductor be (-kq) and on the outer cylinder (k - 1) q, where k is less than unity. Then

$$\frac{k \, q}{\text{capacitance of cylinders } r_o \text{ and } r_i} = \frac{(1 - k) \, q}{\text{cap. of R and } r_i}$$

or, $$k \, q \, Ln \, (r_i/r_o) = (1 - k) \, q \, Ln \, (R/r_i) \, . \qquad (26)$$

Solving for k, there is

$$k = Ln \, (R/r_i) \, / \, Ln \, (R/r_o) \quad , < 1 \qquad (27)$$

and $$1 - k = Ln \, (r_i/r_o) / \, Ln \, (R/r_o) \, . \qquad (28)$$

Hence equation (25). In the presence of these charges, at a voltage ΔV in excess of the corona-inception voltage V_o, the voltage gradient on the surface ofthe conductor becomes

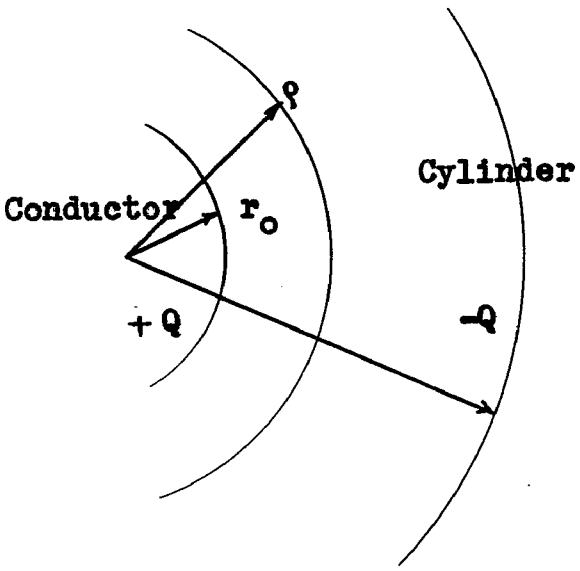

Figure 10

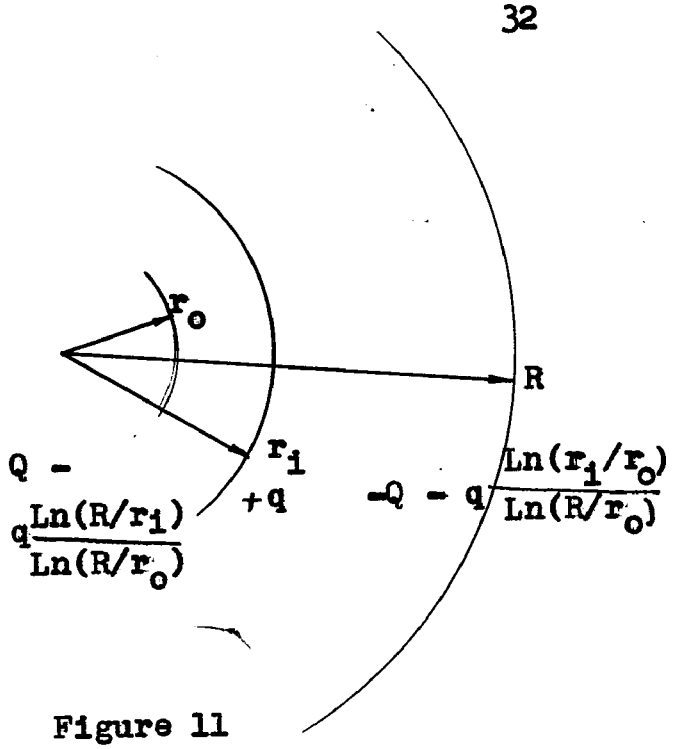

Figure 11

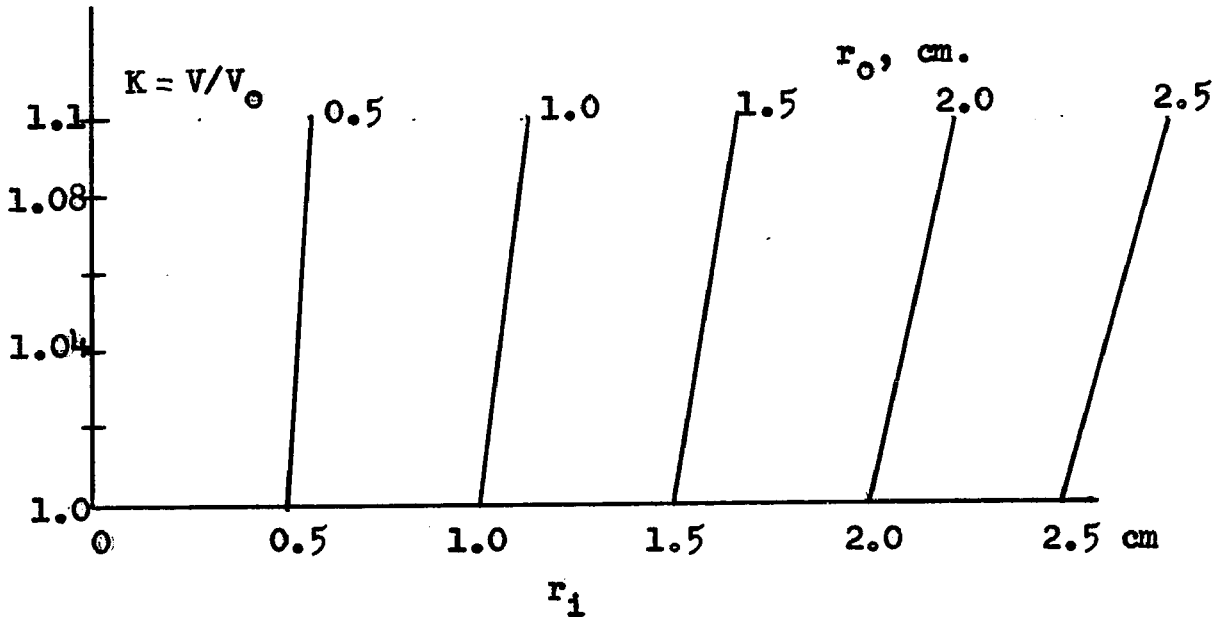

Figure 12. Radius at avalanche formation

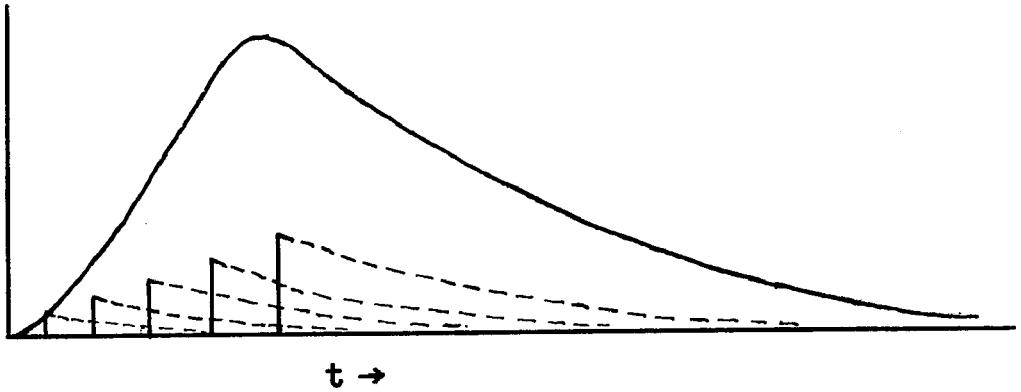

Figure 13. Formation of Positive Corona Pulse

$$\frac{1}{r_o}\ \frac{Q - kq}{2\pi\epsilon} = \frac{1}{r_o}\ \frac{V}{Ln(R/r_o)} - \frac{q}{2\pi\epsilon}\ \frac{1}{r_o}\ \frac{Ln(R/r_i)}{Ln(R/r_o)}$$

$$= E_o + \frac{1}{r_o}\ \frac{\Delta V}{Ln(R/r_o)} - \frac{q}{2\pi\epsilon}\ \frac{1}{r_o}\ \frac{Ln(R/r_i)}{Ln(R/r_o)}\ , \qquad (29)$$

where V = applied voltage $= V_o + \Delta V$,

and E_o = the voltage gradient at corona inception

$= V_o/r_o\ Ln\ (R/r_o)$. (30)

In order that the gradient on the conductor surface may reach the critical corona-inception gradient E_o, the second and third terms on the right side of equation (29) must add to zero, and therefore

$$\Delta V = (\ 2\pi\epsilon\ )^{-1}\ q\ Ln\ (R/r_i)\ . \qquad (31)$$

But $$q = 2\pi\ r_i\ n\delta\ , \qquad (32)$$

where n = number of positive ions per unit area on the surface of cylinder r_i,

and δ = electronic charge.

Therefore, $$\Delta V = n\delta\epsilon^{-1}\ r_i\ Ln\ (R/r_i)\ . \qquad (33)$$

This means that for a given excess voltage above the corona-inception level for the conductor, the sets of values of r_i and n can be obtained when the radius of the outer cylinder R is known. This gives the distance r_i to which the positive-ion cloud should move before a second electron avalanche can be initiated.

In order to find the time taken for the positive charge cloud to move the distance $d = r_i - r_o$, the following

procedure is used:

The velocity of the charge carriers is

$$v = u E = u V / (r \, \mathrm{Ln}(R/r_o)), \qquad (34)$$

where u = mobility ofthe ions.

Then the distance dr moved in a time dt at radius r is

$$dr = v \, dt$$

or $$dt = dr/v = dr. \, r \, \mathrm{Ln}(R/r_o) \, (u V)^{-1} . \qquad (35)$$

Therefore, the time taken for the positive-ion cloud to move from r_o to r_i is

$$T' = \int_{r_o}^{r_i} (uV)^{-1} \, r \, \mathrm{Ln} \, (R/r_o) \, dr$$

$$= \tfrac{1}{2} (uV)^{-1} \, (\mathrm{Ln} \, (R/r_o)). \, (r_i^2 - r_o^2) . \qquad (36)$$

This then gives the time taken for the electric field to regain corona-inception value for creating a fresh electron avalanche and the next positive pulse. The frequency, or repetition rate in pulses per second, is

$$f_r = 1/T' = 2 u V / (\mathrm{Ln}(R/r_o)).(r_i^2 - r_o^2) . \qquad (37)$$

The value of r_i is given from equation (33) as

$$2\pi r_i \, n \, \mathrm{Ln} \, (R/r_i) = 2\pi \epsilon \delta^{-1} \, V . \qquad (38)$$

Numerical example:

As an example of the application of these equations, considering a thin wire of 2-mm radius in a cylinder of 20-cm radius, experimental result gives a repetition rate of 2000 pulses per second at 57 kv, when the corona-inception voltage is 48 kv, as shown in Figure 9, page 28. Therefore,

$V_o = 48{,}000$; $\Delta V = 9{,}000$; $f_r = 2{,}000$; $R = 0.2$; $r_o = 0.002$; $\epsilon = 8.854 \times 10^{-12}$; $\delta = 1.6 \times 10^{-19}$; and $u = 1.5 \times 10^{-4}$. The value for mobility is an average assumed value. Then, from equation (33), solving for r_i and n, there are

$$r_i = 4.3 \times 10^{-2} \text{ meter} = 4.3 \text{ cm.},$$

and $n = 10^{12}$ charge carriers/ sq. meter at the radius r_i.

The total number of charge carriers is $N = 2\pi r_i n = 27.5 \times 10^{10}$ per meter length of wire. Thus the positive-charge cloud will have to move to a radius of 4.3 cm before a second pulse can be formed. The time taken is 1/2000 second, or 0.5 ms.

From equation (37) it may be observed that the repetition rate, f_r, of positive pulses depends on the applied voltage, V, in a complicated manner on account of the presence of r_i^2 in the denominator. The radius r_i to which the positive-ion cloud will have to move, before a second pulse starts, depends upon the excess voltage $\Delta V = V - V_o$ above the corona-inception voltage. Experimental results have shown that the repetition rate varies nearly linearly with voltage within the range of voltage used, Figure 9.

I.8 THEORETICAL ANALYSIS OF SHAPE OF POSITIVE PULSE

The mechanism by which a positive pulse is initiated is different from the mechanism by which a negative pulse is initiated. For a negative pulse to form, the work function of the material of the highly stressed cathode is the basic

governing factor. When the applied voltage on the conductor gives a gradient exceeding the work function, free electrons are ejected out of the metal which acquire sufficiently high kinetic energy to start an electron avalanche. The electron avalanche then travels to the positive cylinder while the positive ions left behind by the avalanche travel to the negative cylinder. The negative charge carriers on the whole have high mobility and the positive ion cloud moves into progressively more intense field near the negative conductor. The negative pulse is therefore of shorter duration than a positive pulse, for which a positive-ion cloud is the main contributing factor for its formation.

When the conductor is positive, on the other hand, electrons are not ejected out of the metal of the conductor. Free electrons in the space between conductor and cylinder acquire high energy by acceleration in the applied electric field and move towards the positive conductor where the field strength is intense. These electrons traveling in the intense field near the conductor possess sufficient energy to create an electron avalanche which is then attracted towards the positive conductor. The positive-ion cloud left behind by the electron avalanche then moves towards the negative cylinder and gives rise to a current flow in the external circuit. The shape and duration of the pulse are governed by the movement of this positive-ion cloud towards the cathode cylinder and of the electron avalanche towards the positive

conductor. The rising portion of the positive pulse is due to the combined contribution of both these activities whereas the decaying portion of the pulse is due entirely to the motion of positive ions towards the negative cylinder.

In order to analyze the positive pulse shape, it is first of all necessary to determine the radius r_i at which the electrons have acquired sufficient energy under the influence of the applied electric field to start the ionization process, i.e. the radius at which the electron avalanche commences. Having obtained this radius it will then be necessary to determine the motion of positive ions towards the negative cylinder and the motion of the electron avalanche towards the positive conductor.

Consider the conductor of radius r_o in a cylinder of radius R between which a voltage V is applied. The voltage gradient at any radius ρ, $(r_o < \rho < R)$ is given by equation (22). From Peek's formula, the voltage gradient for corona inception on a cylinder of radius r_i, at an air density factor of 1, is, (17,18),

$$E_i = 30\, m \left(1 + 0.308\, r_i^{-\frac{1}{2}} \right) \quad \text{kv/cm}, \qquad (39)$$

where $m =$ surface roughness factor, ≤ 1.

At a given applied voltage V, therefore, there exists a radius $r_i > r_o$ at which the field gradient equals the ionization gradient E_i. This is given by the equation

$$V = E_i\, r_i \operatorname{Ln}(R/r_o) = 30\, m\, (1 + 0.308\, r_i^{-\frac{1}{2}})\, r_i \operatorname{Ln}(R/r_o) \,. \qquad (40)$$

Calculations of r_i are simplified if the applied voltage V is written as a multiple of the corona-inception voltage, V_o, on the conductor which is

$$V_o = E_o\, r_o\, \mathrm{Ln}\,(R/r_o) = 30\, m\, (1 + 0.308\, r_o^{-\frac{1}{2}})\, r_o\, \mathrm{Ln}(R/r_o) \quad \ldots\ (41)$$

If $$V = V_o + \Delta V = K\, V_o, \quad K \geq 1, \quad (42)$$

and $$Y = (1 + 0.308\, r_o^{-\frac{1}{2}})\, r_o\,, \quad (43)$$

solving for r_i from equation (40), there is

$$r_i = K\, Y + \tfrac{1}{2}\, 0.308^2 - 0.308\, (K\, Y + \tfrac{1}{4}\, 0.308^2)^{\frac{1}{2}}\,. \quad (44)$$

Figure 12, page 32, shows r_i as a function of r_o and K. From these figures, for K upto 1.1, the ionization radius r_i is very nearly equal to K times the conductor radius r_o.

The surface roughness factor 'm' is taken to correspond to the condition of the conductor surface even though the ionization phenomenon commences very close to the surface of conductor and not on the conductor itself. This assumption is valid because irregularities of field in the immediate vicinity of the conductor are governed by the roughness of the conductor surface to a great extent.

The electron avalanche, commencing at this radius r_i builds up at a more rapid rate on account of the intense field between r_i and r_o than in the case when the avalanche mechanism takes place on a negative conductor from where it moves out into decreasing field-intensity regions. For the avalanche, Townsend's equation gives

$$dn/dr = \alpha n \,, \qquad (46)$$

where the Townsend first ionization coefficient α is a function of the field strength. Its value is given by Loeb, (1), as well as by ver Planck, (19), to have the following variation with field strength:

$$\left.\begin{aligned} &15 < E < 26: \alpha = K_1 e^{aE}, && \text{with } K_1 = 1.67 \times 10^{-5} \text{ and } a = 0.47; \\ &26 < E < 78: \alpha = K_2 (E-b)^2, && K_2 = 0.166 \text{ and } b = 21.5; \\ &78 < E < 200: \alpha = K_3 (E-c), && K_3 = 19.0 \text{ and } c = 50. \end{aligned}\right\} \qquad (47)$$

In the above expressions, E is in kv/cm and α is in ion pairs created in a path of 1 cm in the field direction.

Integration of equation (46) by using equations (22) and (47) yields expressions for 'n' in terms of the number n_o of electrons initiating the electron avalanche at r_i. For the three types of variation of α, there are:

i) $15 < E < 26$:

$$\text{Ln}\,(n/n_o) = r_i\, e^{ap/r_i} - r\, e^{ap/r} + ap\left[\text{Ei}\left(\frac{ap}{r}\right) - \text{Ei}(ap/r_i)\right] \qquad (48)$$

where $p = V/\text{Ln}(R/r_o)$ (49)

and Ei = the exponential integral, $\int \frac{e^x}{x}\, dx$.

Equation (48) is valid for low field strengths and is not of use in practical situations encountered in laboratory setups and outdoor transmission lines for which field strengths are above 26 kv/cm, d-c.

ii) $26 < E < 78$:

$$\text{Ln}\,(n/n_o) = K_2\left[p^2\left(\frac{1}{r_i} - \frac{1}{r}\right) + 2pb\,\text{Ln}\frac{r_i}{r} - b^2(r_i - r)\right]. \qquad (50)$$

This expression covers the range of field strengths normally encountered in practice.

iii) $78 < E < 200$:

$$\text{Ln}\,(n/n_o) = K_3 \left[c\,(r_i - r) - p\,\text{Ln}\,(r_i/r) \right] \quad (51)$$

This expression applies to very thin wires.

Having determined the number of positive ions generated by the electron avalanche at a radius r, $(r_o < r < r_i)$, it is necessary to analyze the characteristics of the motion of these positive ions as well as the electron avalanche as a function of time and evaluate the current induced in the external circuit by the motion of these charges in opposite directions. The total current induced in the external circuit consists of the addition of very sharp pulses generated when the electron avalanche builds up in stages as the electrons move through their mean paths. At $t = 0$ the electron avalanche starts at $r = r_i$. As the n_o initial electrons move through their mean free paths L_1 in time $\Delta_1 t$, they acquire the necessary energy to ionize neutral atoms located at $r_1 = r_i - L_1$. The positive ions liberated at r_1 then move towards the negative outer cylinder. The number of electrons liberated at r_1 is given by equations (48) to (51), depending upon the range of field strength E present at r_1. This action takes place step by step until the electron avalanche reaches the conductor. The mean free paths $L_1, L_2, \ldots$ and the time intervals $\Delta_1 t, \Delta_2 t, \ldots$ are calculated. The resulting positive pulse of current measured in the external circuit will

consist of a large number of small pulses displaced in time by $\Delta_1 t$, $\Delta_2 t$, ... and of increasing magnitude as shown in Figure 13, page 32, qualitatively.

The total number of such small pulses can be calculated by determining the time taken for the avalanche to move from r_i to r_o, and the number of collisions taking place within the distance between r_i and r_o. The energy acquired by an electron moving over a distance dr at a radius r is $\delta E\, dr$, where E is the field strength at radius r according to equation (22). If an electron moves from radius r_1 to r_2 equal to its mean free path for ionization, then the collision taking place with an atom will ionize the atom. The energy required for this to happen is its ionization energy $\delta V_i'$, where V_i' is the ionization potential of the atom.

Hence
$$\int_{r_1}^{r_2} E\, dr = \frac{V}{\mathrm{Ln}(R/r_o)} \int_{r_1}^{r_2} \frac{1}{r}\, dr = V_i' \qquad (52)$$

or,
$$\mathrm{Ln}\,(r_2/r_1)/\,\mathrm{Ln}\,(R/r_o) = V_i'/V\,. \qquad (53)$$

This gives the ratio of r_2/r_1 as

$$r_2/r_1 = (R/r_o)^{V_i'/V}\,. \qquad (54)$$

The mean free path at radius r_1 is

$$L_1 = r_2 - r_1 = r_1\left[(R/r_o)^{V_i'/V} - 1\right] \qquad (55)$$

and in general, the mean free path at radius r is

$$L_{(r)} = r\left[(R/r_o)^{V_i'/V} - 1\right]\,. \qquad (56)$$

The velocity of electrons is

$$v = u E = u V /(r \, \mathrm{Ln}(R/r_o)) . \qquad (57)$$

Therefore, the time between collisions is

$$\Delta t = L/v = \frac{\mathrm{Ln}(R/r_o)}{u V} \left[\left(\frac{R}{r_o}\right)^{V_i'/V} - 1 \right] r^2 . \qquad (58)$$

If the electron starts from zero velocity after experiencing a collision, the time taken is twice that given by equation (58). The radius reached after the k-th collision is

$$r_k = \left[2 - (R/r_o)^{V_i'/V} \right]^k r_i , \qquad (59)$$

and the time interval between the (k-1)-th and k-th collision

$$\Delta_k t = \frac{2 \, \mathrm{Ln}(R/r_o)}{uV} \left[(R/r_o)^{V_i'/V} - 1 \right] r_{k-1}^2 . \qquad (60)$$

This sequence is continued until r_o is reached. The total number of collisions, η, taking place from r_i to r_o is obtained when

$$r_o = r_i \left[2 - (R/r_o)^{V_i'/V} \right]^{\eta}$$

or

$$\eta = \mathrm{Ln}(r_o/r_i) \Big/ \mathrm{Ln} \left[2 - (R/r_o)^{V_i'/V} \right] . \qquad (61)$$

Next, the current induced in the external circuit by the movement of one type of electric charges in the space between the conductor and cylinder is determined by the following analysis:

We consider a region of space in which charges are moving under the influence of an applied electric field between the two concentric cylinder electrodes. In cylindrical coordinates having cylindrical symmetry, the following

equations can be written down for the potential ϕ, velocity v, and charge density ρ at any point r and time t :

Poisson's equation: $$\frac{1}{r}\frac{\partial}{\partial r}\left(r\frac{\partial \phi}{\partial r}\right) = -\frac{\rho}{\epsilon} \qquad (62)$$

Contimuity equation: $$\frac{\partial \rho}{\partial t} + \frac{1}{r}\frac{\partial}{\partial r}(r \rho v) = 0 . \qquad (63)$$

Velocity: $$v = -u\frac{\partial \phi}{\partial r} \qquad (64)$$

The time-dependence of the current induced in the electrodes can be obtained by solving for v and ρ from these three equations. From (62) and (64), upon elimination of $\partial \phi/\partial r$, there is

$$\frac{\partial}{\partial r}(r v) = \frac{u}{\epsilon} r \rho . \qquad (65)$$

This gives

$$r v = \frac{u}{\epsilon}\int r \rho \, dr + \text{an integration constant with respect to } r \text{ and therefore a possible function of } t,$$

$$= \frac{u}{\epsilon}\int r \rho \, dr + u A(t) . \qquad (66)$$

From equations (63) and (66) the equation for charge density ρ, is

$$\frac{\partial \rho}{\partial t} + \frac{u}{\epsilon}\frac{1}{r}\frac{\partial}{\partial r}\left[\rho\int r \rho \, dr + \epsilon \rho A(t)\right] = 0. \qquad (67)$$

A solution assumed for ρ is of the type

$$\rho(r,t) = R(r) \cdot T(t) , \qquad (68)$$

where R(r) is a function of r only and T(t) is a function of t only. From (68) and (67) there is

$$\frac{1}{T^2}\frac{dT}{dt} + \frac{u}{\epsilon}\frac{1}{r R}\frac{d}{dr}\left(R\int rR \, dr\right) + \frac{u}{rR}\frac{A(t)}{T}\frac{dR}{dr} = 0. \qquad (69)$$

Equation (69) can be separated into radial and temporal terms if $A(t)$ is assumed to be of the type

$$A(t) = A\,T\,, \tag{70}$$

where A is a constant. Of all the possible solutions, we shall restrict to such a type of solution. Then

$$\frac{1}{T^2}\,\frac{dT}{dt} = -\,\frac{u}{\epsilon}\,\frac{1}{rR}\,\frac{d}{dr}\left(R\int r\,R\,dr\right) - \frac{uA}{rR}\,\frac{dR}{dr}\,. \tag{71}$$

Since the left side of equation (71) is a function of t only and the right side a function of r only, they can be made equal to a constant, $-k$, independent of both r and t. The two separate equations for T and R now become

$$T^{-2}\quad dT/dt = -\,k, \tag{72}$$

and

$$\frac{d}{dr}\left(R\int r\,R\,dr\right) + \epsilon A\,\frac{dR}{dr} = \frac{k\epsilon}{u}\,r\,R\,. \tag{73}$$

Solution of (72) yields

$$T = (k_1 + k\,t)^{-1}\,, \tag{74}$$

in which k_1 is a constant, independent of r and t. The solution for R in terms of r from equation (73) cannot be obtained explicitly, but an implicit equation will be

$$\mathrm{Ln}\,\frac{R}{R - k\epsilon/u} - \frac{k\epsilon/u}{R - k\epsilon/u} = \frac{k^2\epsilon^2}{u\epsilon^2 A k - B u^2}\,\frac{r^2}{2} + k_2\,, \tag{75}$$

in which B and k_2 are constants, independent of r and t. Having obtained the solutions for R and T, the charge density is found out from equation (68). The velocity, v, can then be obtained from equations (68) and (70) to be

$$v = \frac{u}{\epsilon}\,(B - k\epsilon^2 A/u)\,\frac{1}{r(R - k\epsilon/u)}\,\frac{1}{k_1 + kt} \tag{76}$$

Induced current

The current induced in the electrodes due to the movement of the charges in the applied electric field can be obtained from the expression, (20,21),

$$i = \frac{2\pi h_c}{Ln(r_c/r_o)} \int_{r_o}^{r_c} \rho \, v \, dr \, , \qquad (77)$$

where h_c, r_c = height and radius of cylinder,

and r_o = radius of conductor.

Using the expressions for ρ and v from equations (68), (74) and (76), there is

$$i = \frac{2\pi h_c}{Ln(r_c/r_o)} \frac{u}{\epsilon} (B - k\epsilon^2 A/u) \frac{1}{(k_1 + kt)^2} \int_{r_o}^{r_c} \frac{R \, dr}{r(R - k\epsilon/u)} \quad .... (78)$$

Since the integral with respect to r is a definite integral, the time variation of i will turn out to be

$$i(t) = \Gamma (1 + \gamma t)^{-2} \, , \qquad (79)$$

where Γ and γ include all the constants.

This equation is plotted in Figure 6 to show that it describes the decaying portion of a negative pulse very closely. The positive pulse consists of very sharp pulses following equation (79) which are separated from each other by the times given in equation (58). The number of such sharp pulses which together make up the positive pulse is given by equation (61).

I.9 RADIO INFLUENCE VOLTAGE

RIV measurements are normally carried out on the QP

(quasi peak) weighting circuit of the noise meter. In the laboratory test setup, however, readings on the FI (field intensity) and Peak circuits were also taken to determine the nature of the interference caused by the corona pulses. Oscillograms of pulses taken at a slow speed of sweep showed that except at very high voltages, pulses did not overlap so that the noise is considered impulsive. This allows all PEAK readings to be corrected for a bandwidth of 1 KHz, using the bandwidth data supplied by the meter manufacturer.

i. Negative Polarity

Figure 14 shows RIV readings for several wire sizes as a function of applied voltage and frequency of measurement. Under negative polarity of excitation, the ratio of QP reading to FI reading is nearly 3, while the ratio of PEAK to QP readings is 2. The corrected PEAK values are plotted as full lines in Figure 15(b) for one wire size at different voltages. Denholm, (22), working with a-c corona occuring during the negative half-cycle, proposed that the variation of corrected PEAK values with frequency can be expressed by the equation

$$RIV\,(f) = RIV_o \left[2\, f_o/(\, f + f_o) \right]^{\frac{1}{2}} , \qquad (80)$$

where RIV_o is the corrected PEAK value at a reference frequency f_o, which is taken to be 0.15 MHz. The broken lines in Figure 15(b), according to equation (80), show good agreement with the average trend of variation of corrected PEAK values obtained under negative d-c excitation also.

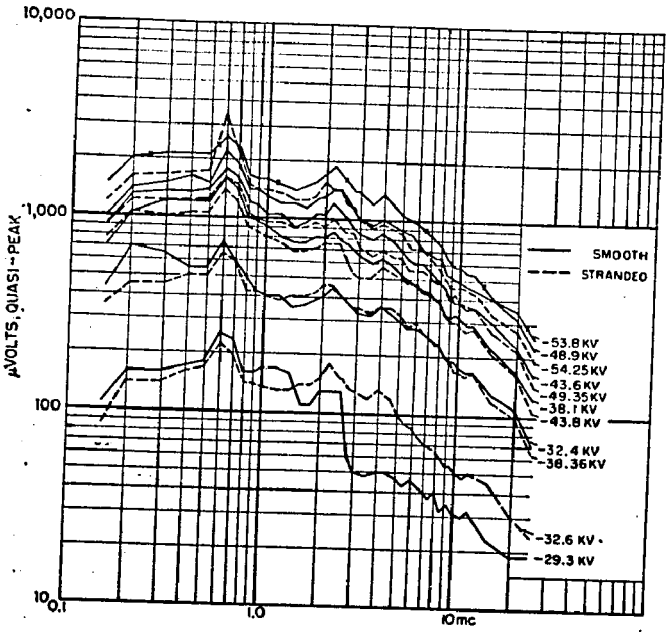

14 Wire Negative

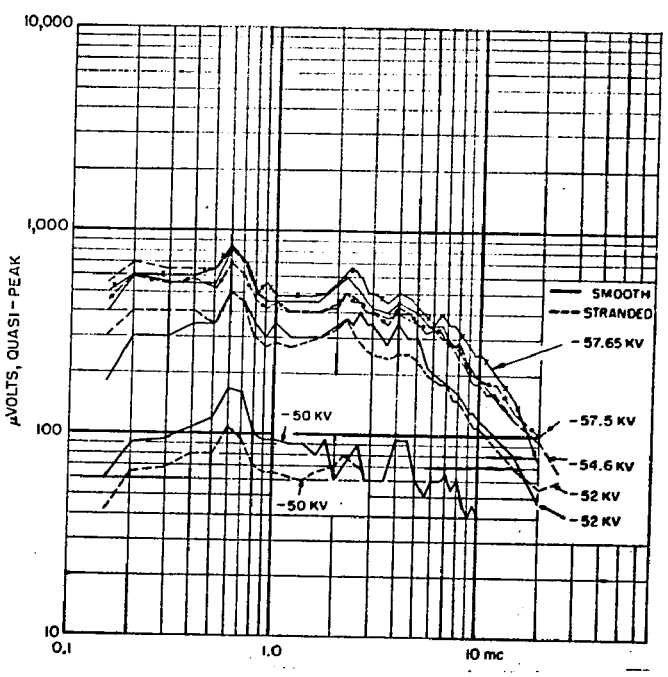

#6 Wire Negative

#6 Smooth. Pos. and Neg.

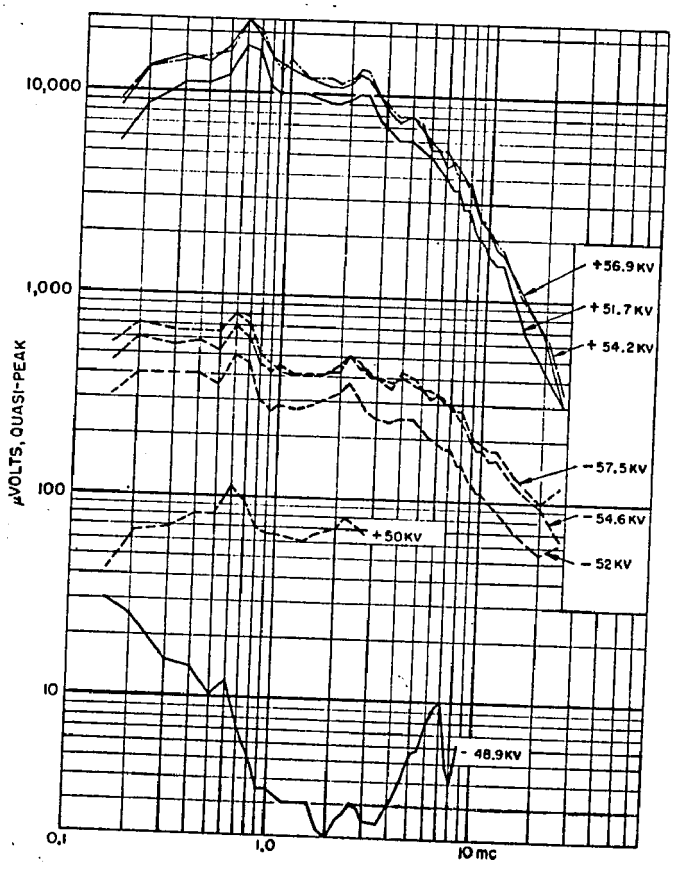

#6 Strand. Pos. and Neg.

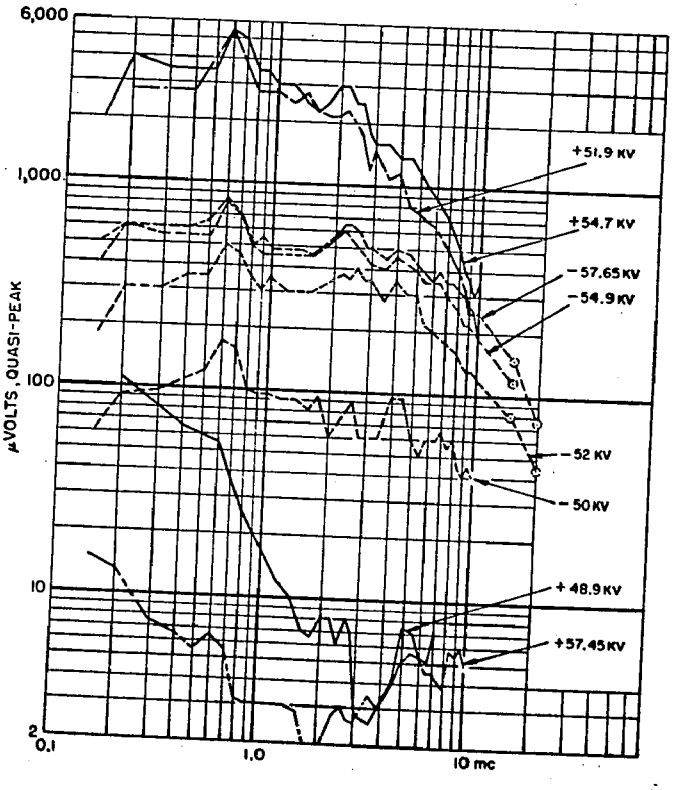

Figure 14

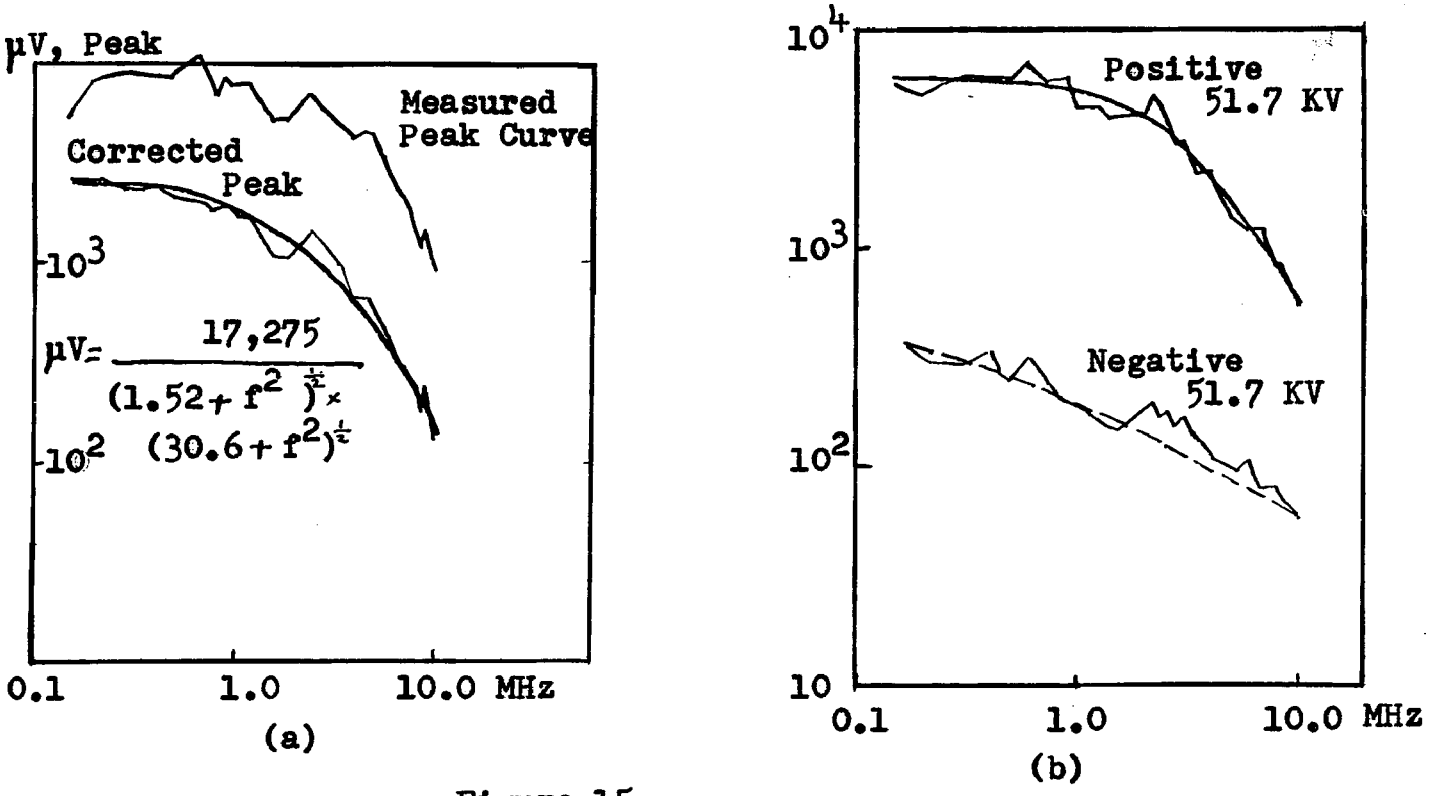

Figure 15

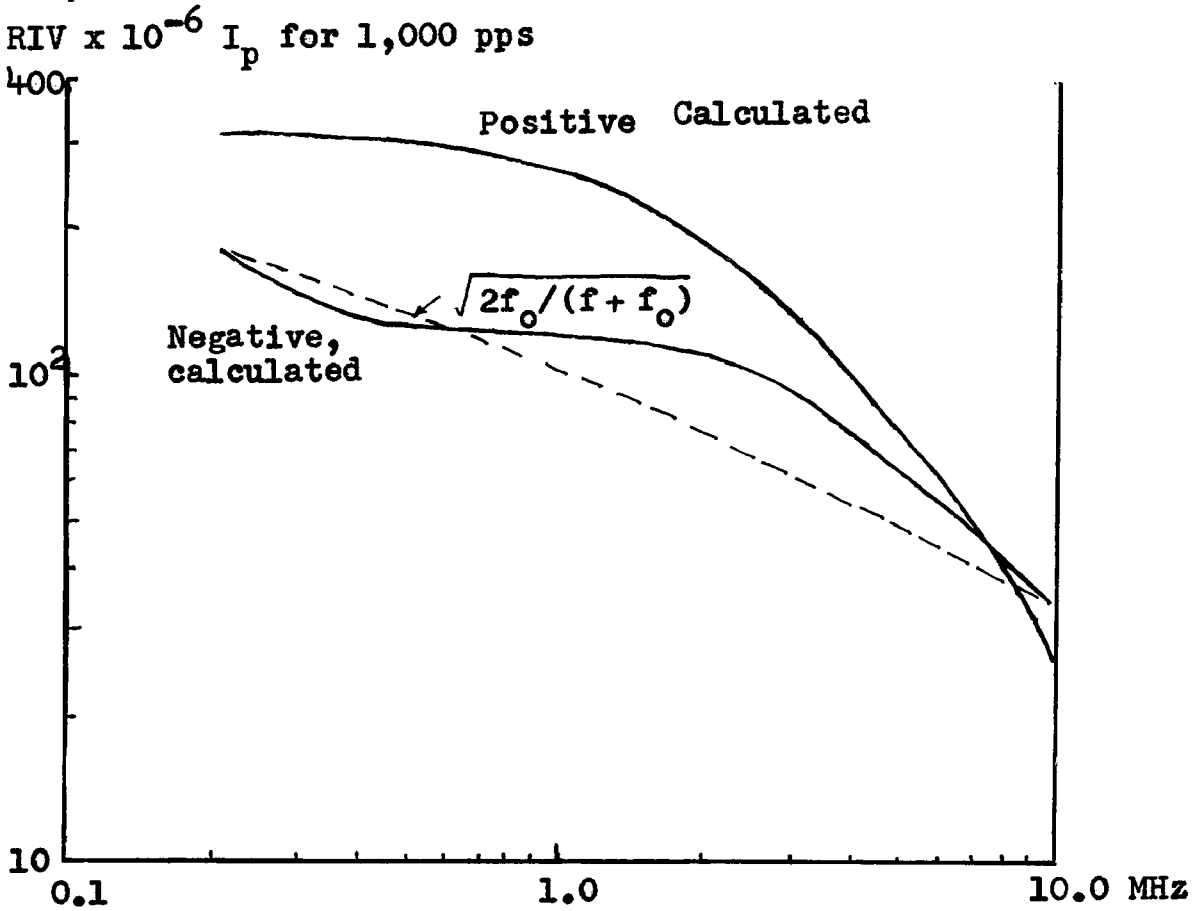

Figure 16. Fourier Frequency Spectrum of Corona Pulses, Calculated.

The measured frequency spectrum of corrected PEAK value shows that it has the same shape as the Fourier frequency transform of a single pulse, as shown in Figure 16. In this figure, RIV is now interpreted as the amplitude of the frequency component in the actual pulse train.

From statistical considerations, Würstlin, (15,16), has found that the amplitude-frequency spectrum of the negative corona discharge current in a co-axial cylinder field follows the equation

$$i_{-}(\omega)/i_{-}(0) = \left[1 + (T_p\,\omega)^2\right]^{-\frac{1}{2}} , \qquad (81)$$

where T_p = a time constant for the positive ions and depends on the ionization coefficient α, the mean free path L, and average drift velocity $\bar{v}_p$ of the positive ions.

This equation shows that at high frequencies for which $T_p\,\omega > 3$, the amplitude varies inversely as the first power of frequency and differs with the observation made by this author that the amplitude varies inversely as the square root of the frequency as shown in equation (80). Furthermore, the author has not found any increase in RIV beyond 2 MHz as reported by Heindl, (6), in his experiments with d-c corona in a co-axial cylindrical field. As pointed out in Section I.2, capacitance between the electrode arrangement and the layout of the experimental setup as a whole can give rise to differences in observation of pulse shapes and hence the measured frequency spectra of RIV.

Figure 17 shows measured QP values of RIV at 1 MHz plotted as a function of surface voltage gradient calculated according to equation (22). The noise level is seen to vary nearly linearly with surface voltage gradient. For smooth conductors, this variation is

$$RIV = 472.4\ r\ (E - E_o)\ , \qquad (82)$$

where E_o is the corona-inception gradient as given by Peek's formula, equation (39) with $m = 1$. The slope of these lines is proportional to the radius of the conductor to which it refers, and is similar to the a-c case obtained by Denholm, (22). For stranded conductors, Figure 17(b) shows that the variation of RIV at 1 MHz is also nearly linear. The slope of these lines is expressible in the form

$$K = 790\ r^{2.4} + 30\ . \qquad (83)$$

The gradient at which any of these lines gives no RIV is slightly less than the values calculated according to equation (39). It was also observed that for any conductor, some RIV was present at all negative voltages above the corona-inception voltage.

ii. Positive Polarity

As shown in Figures 2 and 3, page 12, RIV is only present to a measurable extent on wire sizes No.6 and larger during a definite range of voltage. When RIV occurs the ratio of QP to FI readings is nearly 12 for stranded wires and as high as 500 for smooth wires, as compared to a value

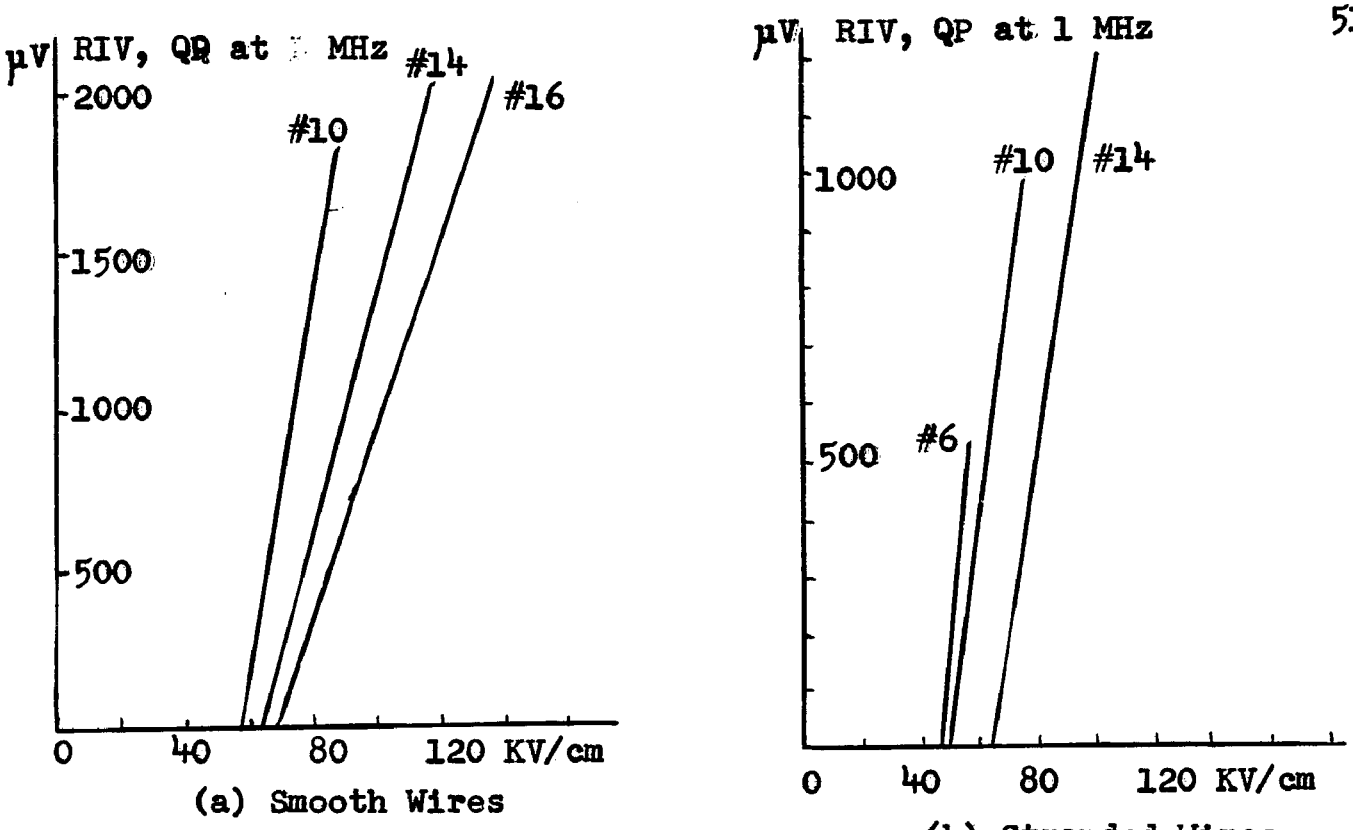

Figure 17
RIV at Negative Excitation

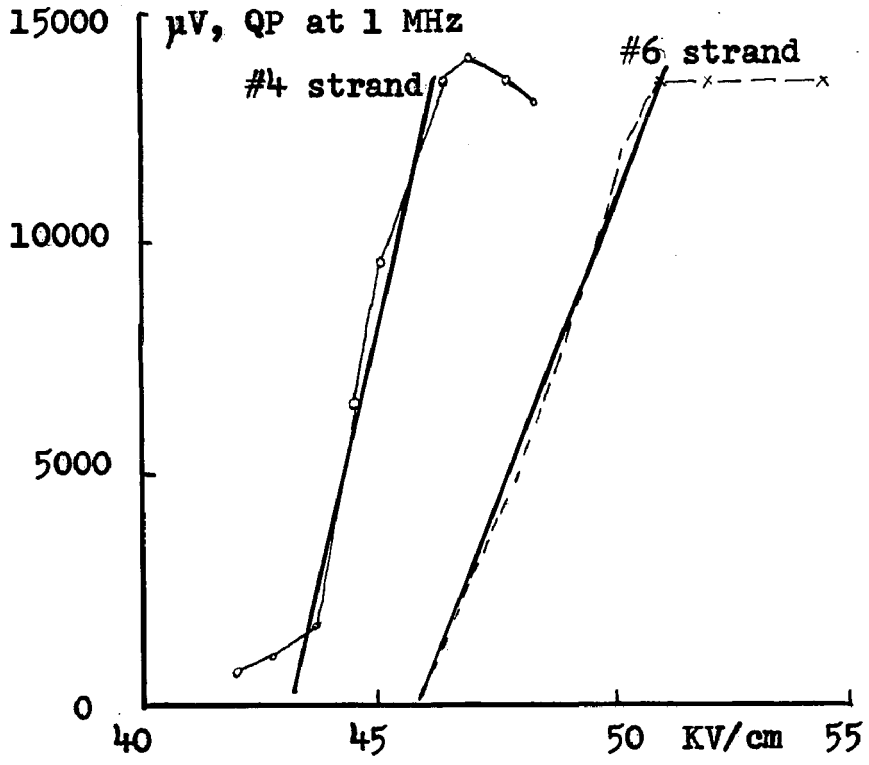

Figure 18. RIV at Positive Excitation

of 3 at negative polarity. This is indicative of the burst of noise occuring on smooth conductors. However, the ratio of PEAK reading to QP reading stays between 2 and 3 for both smooth and stranded wires just as in the case of negative polarity. The general level of RIV is nearly 10 times that at negative polarity.

Figures 14 (d) and (e) show RIV obtained from smooth and stranded No.6 wire at positive voltages. Corresponding PEAK readings are shown in Figures 15 (a) and (b), with both the measured as well as corrected values for a bandwidth of 1 KHz.

The variation of corrected PEAK values with frequency is found to follow a relation of the type

$$\text{RIV} = F_{cp} \left[(p^2 + f^2)\ (q^2 + f^2) \right]^{-\frac{1}{2}} , \qquad (84)$$

where F_{cp}, p, and q are constants and f is the frequency in MHz. This equation is also the Fourier frequency transform of the positive pulse which is a double exponential as shown in Figure 4 and equation (1), page 18. The QP values from long d-c lines in practice also show a similar type of variation of RIV with frequency, as can be seen from Figure 9 of reference (23), which was obtained for a Drake A.C.S.R. conductor, 1.108 inches in diameter at voltages between 300 kv and 500 kv.

Würstlin has obtained the amplitude-frequency spectrum of positive corona discharge as

$$i_+(\omega)/i_+(0) = \left[1 + (T_n\omega)^2\right]^{-\frac{1}{2}} , \qquad (85)$$

which is similar to the negative case, equation (81), but with the positive-ion time constant replaced by the corresponding time constant of negative ions, (15,16). At low frequencies both equations (81) and (85) yield constant value of RIV. But at higher frequencies according to the author's observations the RIV varies inversely as the square of the frequency, while according to equation (85) of Würstlin the amplitude varies inversely as the first power of frequency. Experiments have also confirmed that the Fourier frequency transform of the positive and negative pulses are different while equations (81) and (85) show that they are similar.

Variation of RIV with surface voltage gradient under positive polarity of excitation is shown in Figure 18. For the major portion of the curves they are linear and vary as

$$RIV = K\,(E - E_o) , \qquad (86)$$

where the slope K can be expressed as a function of conductor radius by a relation of the type

$$K = 7.325 \times 10^4\, r^{2.26} . \qquad (87)$$

Comparing equations (83) and (87), one can observe that for stranded conductors, RIV varies linearly with surface voltage gradient and the slope of this linear variation is related to the radius of the conductor, varying as the square of the radius.

Measured RIV from sizes No.6 and larger conductors in an outdoor setup are shown in Figure 3, page 12. The RIV

curves for the three stranded conductors tested show crossover points which indicates that it is not necessarily true that a smaller conductor should have a larger RIV at all positive voltages, that is, it is not necessarily true that higher RIV should be obtained at higher voltage gradients. One could expect RIV to increase as voltage gradients are increased but the conductor radius plays an important role in relating RIV to surface voltage gradient on conductors, under positive d-c excitation.

C H A P T E R II

POWER SPECTRAL DENSITY OF CORONA PULSES AND OUTPUT OF QUASI- PEAK CIRCUIT OF NOISE METER

II.1 INTRODUCTION

A radio noise meter is primarily an apparatus used for assessing the level of interference likely to be caused by a high-voltage line on which corona pulses originate and propagate. In the 1930's a joint committee consisting of members from N.E.M.A., E.E.I., and R.M.A. was formed in the U.S.A., and by the C.I.S.P.R. in Europe, to evolve a design for a radio noise meter and specify methods of measurement of radio noise, (1,2). They recommended that an instrument for assessing interference levels should respond in a manner similar to a radio receiver. The interference level as such was determined from the response of a weighted circuit connected to the output of the last stage of the electronic circuitry of a sensitive superheterodyne type of receiver. The final design of the weighted circuit was accomplished after a large number of tests performed with listeners, whose response to interfering noise of different types was compared with the noise level indicated by the meter. The Quasi-Peak weighted circuit, as incorporated in the original meter is shown in Figure 1. This was later modified, the only change being a decrease in charging time constant of the capacitor from 10 ms to 1 ms.

With the development of mathematical theory of

random variables and its application to communication theory, new tools for prediction of noise levels came into the hands of the engineer, (3,4). These methods were first applied by Dr. G.E. Adams, (5-8), for prediction of corona noise levels of a-c power transmission lines. Attempts were also made to design a new meter to measure the noise power at a definite given frequency, (9,10). But the meter has not yet acquired recognition as a standard for measuring radio noise levels to date, because its performance has not been compared with listeners' response to noise energies. Also, there has been no systematic effort made to correlate the response of the new meter with the response characteristics of the conventional noise meter that was evolved by the recommendations of the NEMA-EEI-RMA joint committee.

In this chapter relationships are derived correlating the response at a given frequency of the quasi-peak weighting circuit of a conventional noise meter to the power content of the corona sources themselves at that frequency. Since corona pulses from a long conductor are not periodic but exhibit a random distribution of intervals, the technique for evaluating their autocorrelation function and power spectral density has to be used. The response of the weighting circuit is then evaluated for the randomly occuring pulses and compared with the spectral density of the input pulses. In doing so it is assumed that all pulses have the same amplitude and shape but that the interval between pulses is

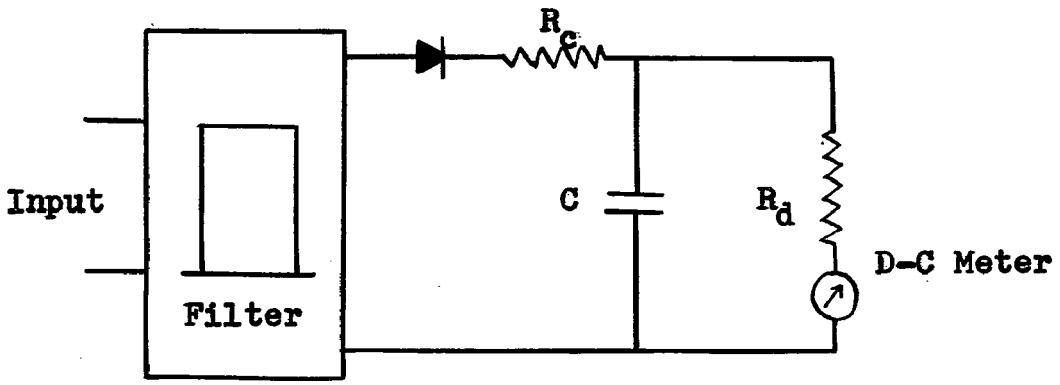

Figure 1. Noise Meter Circuit

Original Time Constants: $R_c C = 10$ ms

$R_d C = 600$ ms

Modified Time Constants: $R_c C = 1$ ms

$R_d C = 600$ ms

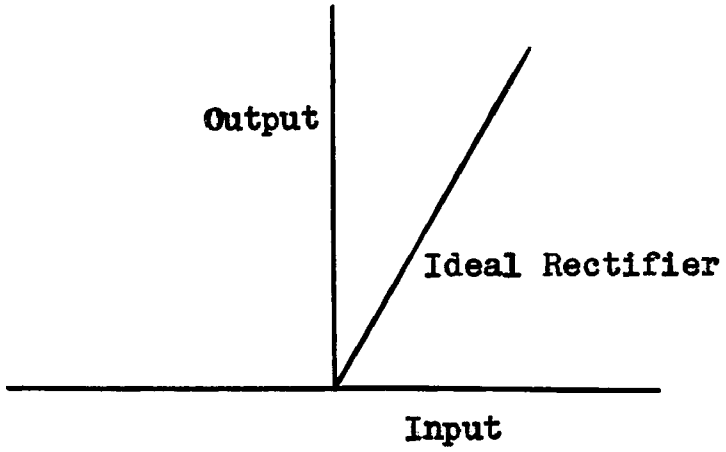

Figure 2

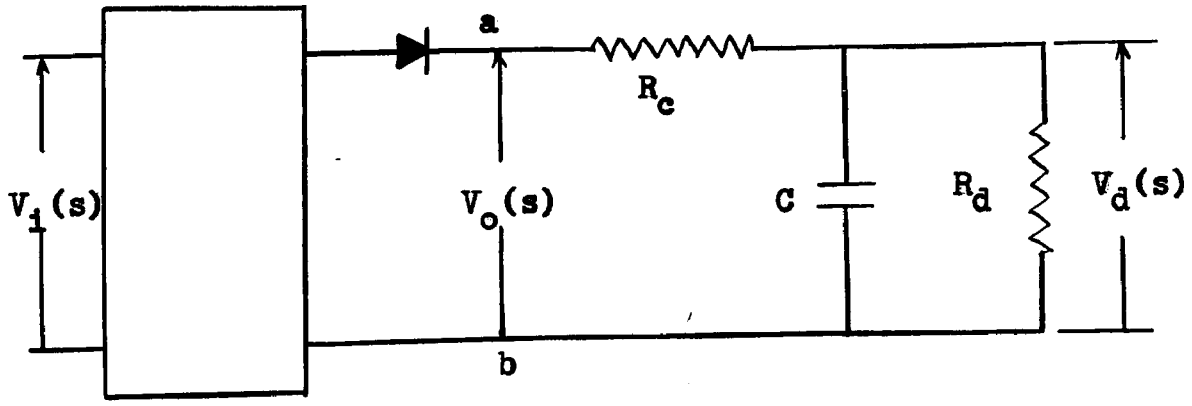

Figure 3

randomly distributed.

During the course of analysis with randomly-occuring positive corona pulses, a discussion of the response of the noise meter to periodically occuring pulse inputs will be made, which will then directly lead to the analysis of random pulse inputs to the noise meter. Experiments were carried out with a Stoddart NM 25T type of noise meter to determine the nature of the detecting circuit, i.e. whether it was linear or followed a square law.

It is the objective of the author to establish the fact that when the shape of corona pulses is a double-exponential as given by equation (1) of Chapter I, radio noise levels of a transmission line can equally well be determined in terms of the power spectral density, repetition rate and the amplitude of the corona pulses themselves just as RI levels have been determined as the output of a quasi-peak weighted circuit.

II.2 RESPONSE OF QUASI- PEAK CIRCUIT TO PERIODICALLY-OCCURING SQUARE- WAVE INPUT

For purposes of analysis, the following assumptions are made:

1. The quasi-peak circuit shown in Figure 1 will be used;
2. The bandwidth-limited filter is ideal with uniform gain and sharp cut-off at frequencies $f_o - \Delta f/2$ and $f_o + \Delta f/2$, where f_o is the frequency to which the meter is tuned, and Δf is the bandwidth. Normally, frequen-

cies of interest are between 0.2 and 10 MHz for f_o, and the bandwidth is nearly 5 KHz in American noise meters.

3. The rectifier used in the circuit is ideal and has a linear input-output characteristic, as shown in Figure 2.
4. Interference level is taken to be the measure of the voltage across discharge resistor R_d, which is related to the meter indication by the simple relation $i = V_d/R_d$, (Figure 1).

Considering the circuit beyond terminals a-b, Fig. 3, the Laplace Transform $V_d(s)$ of voltage across R_d, for an input $V_o(s)$ at terminals a-b, is

$$V_d(s) = \frac{1}{\tau_c} \frac{V_o(s)}{s + \phi_{cd}} , \qquad (1)$$

where τ_c = time constant of charge $= R_c C$, (2)

τ_d = time constant of discharge $= R_d C$, (3)

and $\phi_{cd} = 1/\tau_c + 1/\tau_d$. (4)

For the quasi-peak (QP) circuit, $\tau_c = 1$ ms and $\tau_d = 600$ ms. For the field intensity (FI) circuit, $\tau_c = \tau_d = 600$ ms.

This gives values of nearly 1000 and 3.33 for ϕ_{cd} for the two circuits, respectively. We now proceed to find $V_o(s)$ when the input $v_i(t)$ to the filter is an unrectified square wave with amplitude A and period T' or radian frequency $\omega_r = 2\pi f_r = 2\pi/T'$, Figure 4. The Fourier series for the periodic square wave is

$$\mathcal{F}(\omega_r) = \frac{4}{\pi} A \sum_{\substack{n=1 \\ n \text{ odd}}}^{\infty} \frac{1}{n} \sin n \omega_r t . \qquad (5)$$

Considering the n-th harmonic term of frequency $f = n f_r$, which is very close to the tuned frequency $f_o = \omega_o/2\pi$, its Laplace Transform when rectified by the rectifier will be, (12),

$$V_o(s) = \frac{4A}{\pi} \frac{1}{n} \frac{n \omega_r}{s^2 + n^2 \omega_r^2} \left[1 + e^{-sT/2} + e^{-sT} + \ldots\right] \quad (6)$$

where $T = 1/(n f_r) = T'/n$, the period of the n-th harmonic. (7)

Therefore the operational voltage across R_d is

$$V_d(s) = \frac{4A}{n\pi} \frac{1}{\tau_c} \frac{n\omega_r}{s^2 + n^2 \omega_r^2} \frac{1}{s + \phi_{cd}} \left[1 + e^{-sT/2} + \ldots\right] \quad (8)$$

Its time variation (inverse Laplace Transform) is

$$v_d(t) = \frac{4A}{n\pi} \frac{1}{\tau_c} \frac{n\omega_r}{n^2\omega_r^2 + \phi_{cd}^2} \left(e^{-\phi_{cd}t} + \frac{\phi_{cd}}{n\omega_r} \sin n\omega_r t - \cos n\omega_r t\right) \left[u(t) + u(t-T/2) + \cdots\right] \quad (9)$$

where $u(t)$ = step function at $t = 0$.

This output across R_d, due to a single harmonic frequency, is indicated on a meter having a long time constant. Consequently the long-time average of $v_d(t)$ is to be evaluated. This is

$$v_d(av) = \frac{4A}{n\pi} \frac{1}{\tau_c} \frac{n\omega_r}{n^2\omega_r^2 + \phi_{cd}^2} \text{ Aver. of } e^{-\phi_{cd}t} \left[u(t) + \ldots\right] \quad (10)$$

where the terms $\left[\phi_{cd}/(n\omega_r)\right] \sin n\omega_r t$ and $\cos n\omega_r t$ have been neglected because they give a nearly zero average.

Now, ϕ_{cd} is of the order of 1000 sec.^{-1} for the QP

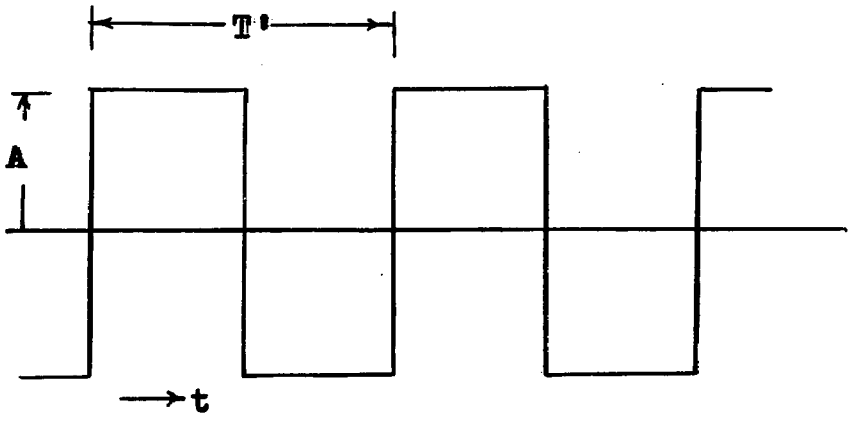

Figure 4. Input Square Wave

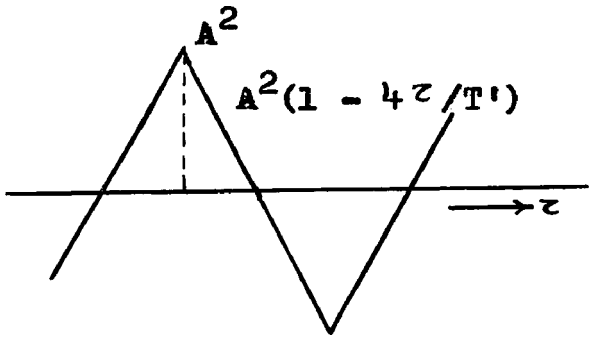

Figure 8. Autocorrelation Function of Square Wave

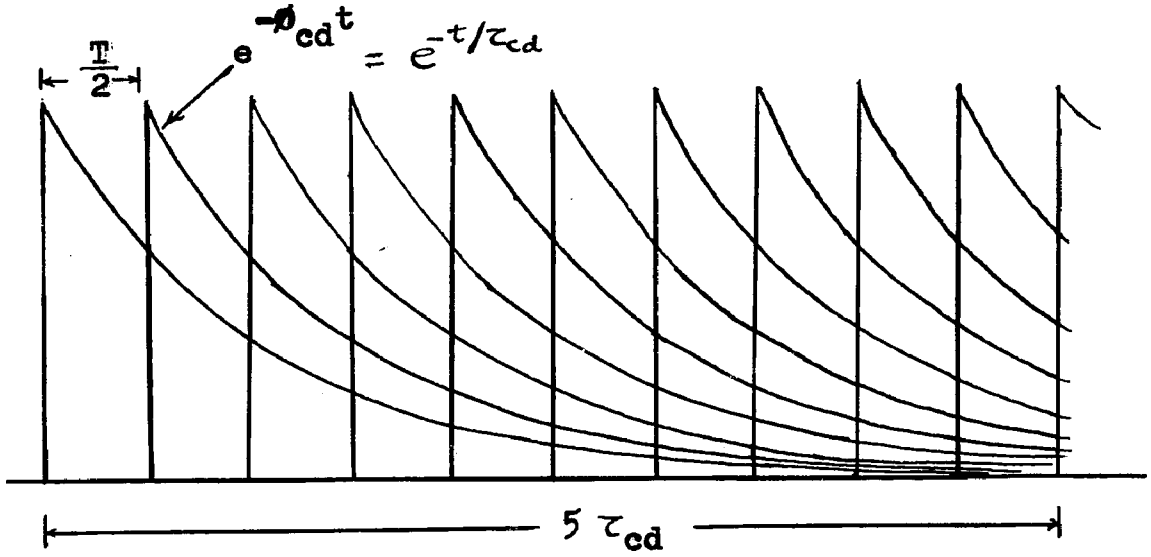

Figure 5

circuit and if the tuned frequency f_o is very high, the terms $u(t) + u(t-T/2)$ ... suggest very fast recurrence of pulses having the waveform $\exp(-\phi_{cd} t)$, as shown in Figure 5. For example, if the tuned frequency is $f_o = 1$ MHz, then $T = 1\ \mu s$, and in one time constant, $\tau_{cd} = \phi_{cd}^{-1}$, there are 1000 pulses of the waveform $\exp(-1000t)$ coming into the meter. The time average value of $\exp(-\phi_{cd} t)\ [u(t) + u(t-T/2) \ldots]$ can be calculated as the average within a time equal to 5 time constants, during which theterm $\exp(-\phi_{cd} t)$ decays to within 1% of zero.

Since pulses given by equation (10) are displaced by T/2, the total number of pulses occuring within the time of $5\ \phi_{cd}^{-1} = 5\ \tau_{cd}$ is $k = 5\ \tau_{cd}/(T/2)$. Then

$$5\ \tau_{cd} \times \text{Average} = \int_0^{5\tau_{cd}} e^{-t/\tau_{cd}}\, dt + \int_{\frac{5}{k}\tau_{cd}}^{5\tau_{cd}} e^{-(t-5\tau_{cd}/k)}\, dt + \ldots\ldots \tag{11}$$

$$\text{or, Average} = \frac{1}{5\ \tau_{cd}} \left\{ k\ \tau_{cd} - \tau_{cd}\ e^{-5/k} \left[1 + e^{-5/k} + \ldots + e^{-5k/k} \right] \right\}$$

$$= \frac{1}{5} \left[k - e^{-5/k}\ \frac{1 - e^{-(k+1)5/k}}{1 - e^{-5/k}} \right] \tag{12}$$

When k is of the order of 1000, the term $(1 - e^{-5/k})$ is negligible compared to unity and the average value simplifies to

$$\text{Average} = 4\ k/25 = 1.6\ \tau_{cd}/T = 1.6\ n\ f_r/\phi_{cd} \ . \tag{13}$$

Finally, equations (10) and (13) yield, with $\tau_{cd}\ \phi_{cd} \approx 1$,

$$v_d(av) = \frac{4A}{n\pi} \quad \frac{1}{\tau_c} \quad \frac{n\omega_r}{n^2\omega_r^2 + \phi_{cd}^2} \quad \frac{1.6\, n\, f_r}{\phi_{cd}}$$

$$= \frac{6.4}{\pi} \; A \; \frac{n\omega_r\, f_r}{n^2\, \omega_r^{\,2} + \phi_{cd}^2} \quad . \tag{14}$$

Furthermore, when the tuned frequency f_o ($= n\omega_r/2\pi$) is in the range of 0.2 to 10 MHz, and $\phi_{cd} \approx 1000$,

$$n^2\omega_r^2 \gg \phi_{cd}^2 \quad . \tag{15}$$

Then the meter indication for one single frequency in the input square wave will be simply

$$v_d(av) = \frac{3.2}{\pi^2} \quad \frac{A}{n} \quad . \tag{16}$$

If the repetition rate, f_r, of the square wave is less than Δf, the bandwidth of the filter, there will be $\frac{1}{2}\Delta f/f_r$ odd harmonic terms which will pass through the filter, with half the number on either side of the tuned frequency f_o. Therefore, for $n \gg 1$ and $f_r < \frac{1}{2}\Delta f$, the output reading of the noise meter at the tuned frequency f_o is

$$v_{qp}(f_o) = \frac{1.6}{\pi^2} \; A \; \frac{\Delta f}{f_r} \; \frac{f_r}{f_o} = A \; \Delta f/\omega_o \tag{17}$$

where $$\omega_o = 2\pi f_o = 2\pi n_o f_r = n_o\omega_r \; . \tag{18}$$

The quasi-peak reading is therefore directly proportional to the pulse amplitude A, and the bandwidth of the meter Δf, but inversely proportional to the tuned frequency f_o. For given pulse amplitude and constant bandwidth at all tuned frequencies, there is

$$v_{qp}\,\omega_o = A\,\Delta f = \text{constant.} \qquad (19)$$

Thus v_{qp} is independent of the frequency of the input square wave but depends on the tuned frequency f_o.

Experimental results obtained with a square wave generator and a Stoddart NM 25T noise meter are shown in Figure 6. It indicates that upto input square wave frequencies of 2500 Hz, the output of the quasi-peak circuit at a tuned frequency f_o= 1 MHz is constant and independent of the input frequency f_r. But beyond this frequency the output of the meter increases with increase in frequency of the input square wave. Variation of v_{qp} with tuned frequency f_o is shown in Figure 7 for input frequencies of 60 Hz and 1000 Hz. These input frequencies correspond to a-c and d-c corona, respectively.

Actual measured value of v_{qp} with tuned frequency can be expressed by a relationship of the type

$$v_{qp} = K/\, f_o^m$$

where the exponent 'm' has a value between 1.14 and 1.2. In case the filter does not have a uniform gain over its pass band but a triangular frequency-gain characteristic, the quasi-peak output reduces to one-half the value given in equation (17).

A physical explanation for the experimentally observed variation of v_{qp} with frequency of the input square wave can be given as follows:

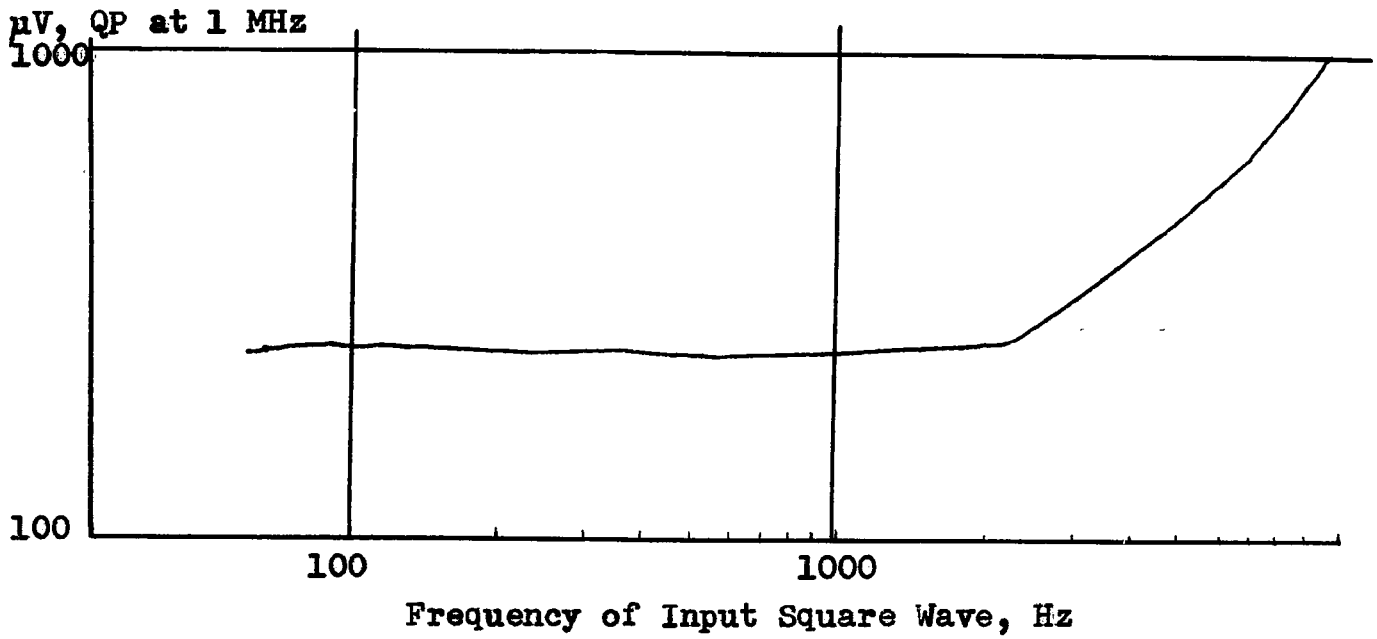

Figure 6. Response of QP circuit. Stoddart NM 25T.

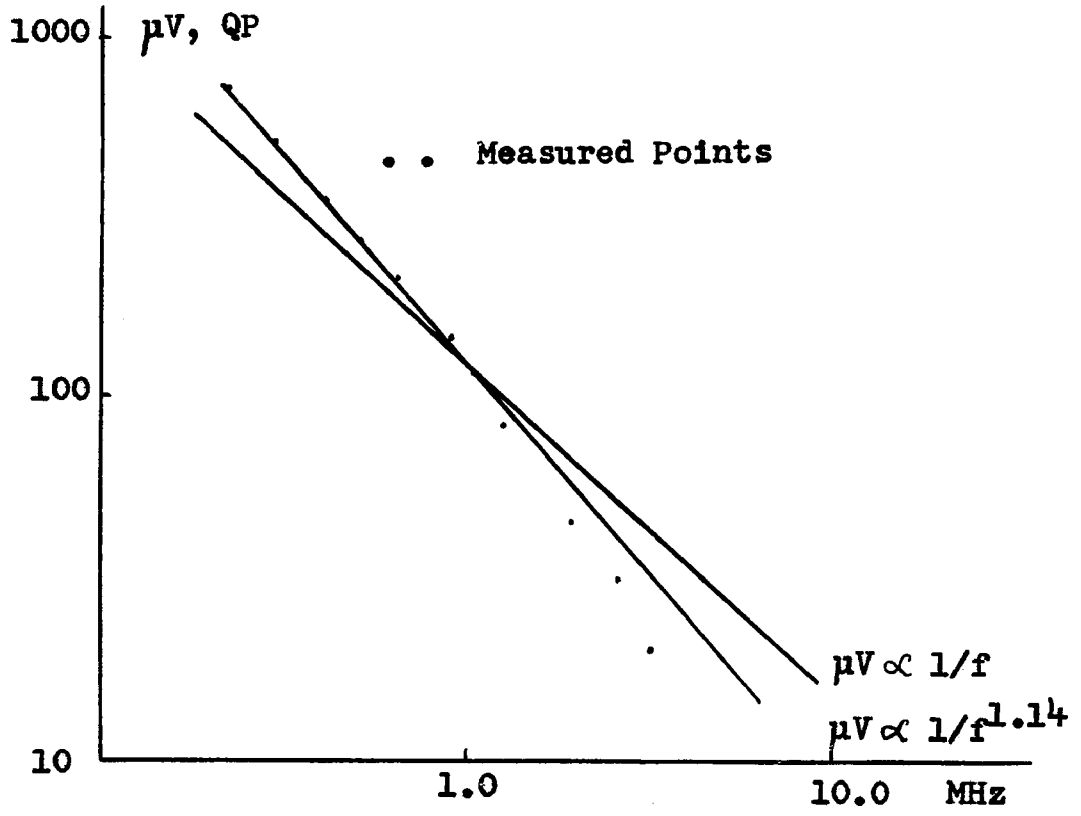

Figure 7. Variation of RIV with Tuned Frequency

The amplitude of the n-th harmonic of the input square wave is inversely proportional to the order of the harmonic as can be seen from the Fourier series for the square wave, equation (5). When the input frequency f_r is less than the bandwidth Δf, the number harmonics passed by the filter increases as the input frequency goes down. Thus the product of amplitude and number of frequencies in the bandwidth remains constant, and hence also the output. When the frequency of the input square wave approaches the bandwidth of the filter, this relation is no longer true and the QP reading does not stay constant. The output of the QP circuit increases with increase in frequency of the input because there is now only one or two harmonic terms corresponding to the tuned frequency or very near it going through the filter, and its amplitude increases as the input frequency increases. This occurs for an input frequency equal to one-half the bandwidth of the filter. For American meters the bandwidth is nearly 5000 Hz and therefore the QP output commences to deviate from a constant level beyond an input frequency of 2500 Hz.

A conclusion obtained from this analysis is that for input frequencies less than one-half the bandwidth of the meter, the QP output remains constant for all tuned frequencies much higher than the input frequency. But for input frequencies higher than one-half the bandwidth of the meter, the QP output increases with input frequency. In usual cases met with in practice under d-c and a-c corona, the pulse

repetition rate is below 1000 per second and therefore there is no difference in performance of a QP circuit within this range under d-c or a-c corona.

In equation (14) it was shown that the average value of indicated voltage of the meter was

$$v_d(av) = \frac{6.4}{\pi} \quad A \quad \frac{n\omega_r f_r}{n^2\omega_r^2 + \phi_{cd}^2} \quad \frac{1}{\tau_c \phi_{cd}} \quad . \qquad (14)$$

For the QP circuit, $\tau_c \phi_{cd} = 1.0$. But for the Field Intensity (FI) circuit, $\tau_c = 0.6$ and $\phi_{cd} = 1/0.6 + 1/0.6$, from equation (4), so that $\tau_c \phi_{cd} = 2.0$. The FI weighting circuit will therefore indicate one-half the QP reading at any given tuned frequency. This is experimentally borne out.

II.3 POWER SPECTRAL DENSITY OF PERIODIC SQUARE WAVE AND COMPARISON WITH QUASI-PEAK READING OF NOISE METER

The autocorrelation function of a square wave with period T' is, (12,13),

$$R(\tau) = \lim_{T\to\infty} \frac{1}{T} \int_{-T/2}^{T/2} f(t)\, f(t-\tau)\, dt \qquad (21)$$

$$= A^2 \,(1 - 4\tau/T') \quad . \qquad (22)$$

It is a triangular wave with the same period T' as the square wave but of amplitude A^2 as shown in Figure 8, page 61. The power spectral density is the Fourier Transform of the autocorrelation function and is

$$\Phi(\omega_o) = 2 \int_0^\infty R(\tau) \cos \omega_o \tau \, d\tau \qquad (23)$$

$$= 8\, A^2/(\omega_o^2\, T') = 8\, A^2\, f_r/\omega_o^2 \qquad (24)$$

We can now compare the QP output of the noise meter with the power spectral density given above, for the input square wave. When the detector has a linear input-output characteristic, the QP output voltage was found in equation (17) to be nearly

$$v_{qp}(\omega_o) = A\ \Delta f/\omega_o \qquad (17)$$

Therefore,

$$\eta = \left(\frac{v_{qp}(\omega_o)}{\Delta f}\right)^2 \Big/ \frac{\Phi(\omega_o)}{f_r} = 1/8 \ . \qquad (25)$$

This shows that the square of the quasi-peak reading per cycle of bandwidth bears a constant ratio to the power spectral density per cycle of the input square wave. Therefore, the noise level of the square wave input can be equally well described by the power spectral density if the input characteristics are known.

II.4 RESPONSE OF QUASI-PEAK CIRCUIT TO PERIODIC CORONA PULSE INPUT

The positive corona pulse has been shown in Chapter I, equation (1) to have the time variation

$$i(t) = A\ (e^{-at} - e^{-bt}) \ .$$

The Fourier series for a pulse train having a period T' (repetition rate f_r) is

$$\mathcal{F}(\omega) = \frac{A}{T'}\frac{b-a}{ab} + \sum_{n=1}^{\infty} \frac{2A}{T'}\left(\frac{a}{a^2+n^2\omega_r^2} - \frac{b}{b^2+n^2\omega_r^2}\right)\cos n\omega_r t$$

$$+ \sum_{n=1}^{\infty} \frac{2A}{T'}\left(\frac{1}{a^2+n^2\omega_r^2} - \frac{1}{b^2+n^2\omega_r^2}\right) n\omega_r \sin n\omega_r t$$

$$\mathcal{F}_h(\omega) = \frac{A}{T'}\frac{b-a}{ab} + \sum_{n=1}^{\infty} \frac{2A}{T'} \frac{b-a}{\left[(a^2+n^2\omega_r^2)(b^2+n^2\omega_r^2)\right]^{\frac{1}{2}}} \cos(n\omega_r t - \phi_n) \quad \ldots (29)$$

where $$\phi_n = \arctan \frac{(b+a)\, n\omega_r}{ab - n^2\omega_r^2} \quad . \qquad (30)$$

The amplitude and phase angles of harmonics are plotted in Figure 9, for $n f_r = 0.1$ to 10 MHz and $f_r = 1/T' = 1000$ pulses per second. The values of the exponents 'a' and 'b' are taken from equation (10) of Chapter I.

We now examine the output of the quasi-peak weighting circuit when the input consists of periodic corona-type pulses. The Laplace Transform of output voltage of the QP circuit has been found to be

$$V_d(s) = \frac{1}{\tau_c} \frac{V_o(s)}{s + \phi_{cd}} \quad . \qquad (1)$$

The input to the filter, $V_i(s)$, consists of the Laplace Transform of the Fourier series given in equation (29), while the output of the filter contains only those frequencies that have been passed within the bandwidth. These harmonics are rectified and form the input $V_o(s)$ of the QP weighting circuit. From equation (29), each of the harmonics passed by the filter contains a cosine term and a sine term as follows:

$$\frac{2A}{T'} \frac{(b-a)(ab - n^2\omega_r^2)}{(a^2+n^2\omega_r^2)(b^2+n^2\omega_r^2)} \cos n\omega_r t$$

$$\frac{2A}{T'} \frac{(b^2-a^2)\, n\omega_r}{(a^2+n^2\omega_r^2)(b^2+n^2\omega_r^2)} \sin n\omega_r t \, .$$

The rectifier is half-wave rectifier and the output can be expressed for the sine wave by

$$\sin n\omega_r t \left[u(t) + u(t-T/2) + u(t-T) + \ldots\right] \quad (31)$$

and its Laplace Transform is

$$\frac{n\omega_r}{s^2+n^2\omega_r^2}\left[1 + e^{-sT/2} + e^{-sT} + \ldots\right] \quad (32)$$

A half-wave cosine consists of one-quarter cycle of cosine followed by sine waves as shown in Figure 10. Its Laplace Transform is

$$\frac{s}{s^2+n^2\omega_r^2} + \frac{n\omega_r}{s^2+n^2\omega_r^2}\, e^{-sT/4}\left[1 + e^{-sT/2} + \ldots\right] \quad (33)$$

$\therefore$ $V_d(s)$ consists of terms such as

$$\frac{1}{\tau_c}\,\frac{n\omega_r}{s^2+n^2\omega_r^2}\,\frac{1}{s+\phi_{cd}}\left[1 + e^{-sT/2} + \ldots\right] \quad (34)$$

and $$\frac{1}{\tau_c}\,\frac{n\omega_r}{s^2+n^2\omega_r^2}\,\frac{1}{s+\phi_{cd}}\, e^{-sT/4}\left[1 + e^{-sT/2} + \ldots\right] \quad (35)$$

and one term

$$\frac{1}{\tau_c}\,\frac{s}{s^2+n^2\omega_r^2}\,\frac{1}{s+\phi_{cd}} \quad . \quad (36)$$

For the sine component in $V_d(s)$, the output of the QP circuit is obtained by taking the inverse transform of equation (1) using equation (34), thus:

$$v_s(t) = \frac{2An\omega_r(b^2-a^2)}{T'(a^2+n^2\omega_r^2)(b^2+n^2\omega_r^2)}\,\frac{n\omega_r}{\tau_c}\,\frac{1}{n^2\omega_r^2+\phi_{cd}^2} \times$$

$$\left[e^{-\phi_{cd}t} + \frac{\phi_{cd}}{n\omega_r}\sin n\omega_r t - \cos n\omega_r t\right]\left[u(t)+u(t-T/2)+\cdots\right] \quad (37)$$

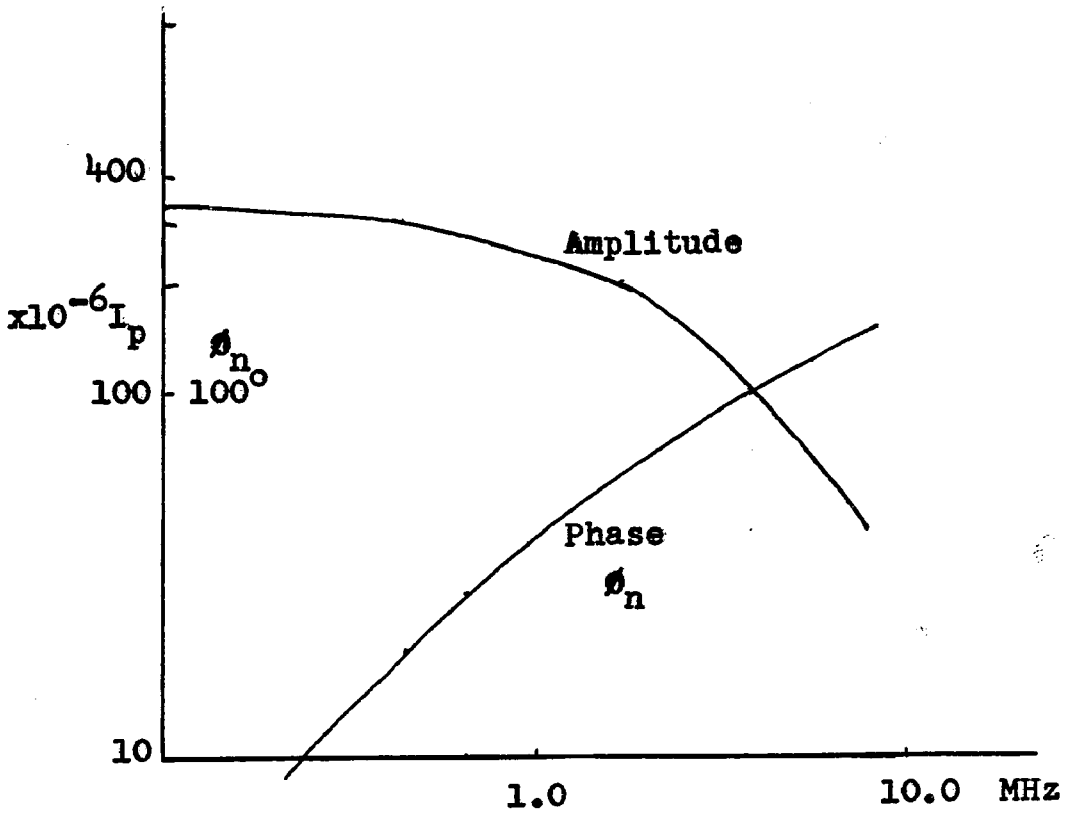

Figure 9. Amplitude and Phase of Harmonics in Positive Corona Pulse. f_r 1000 pps.

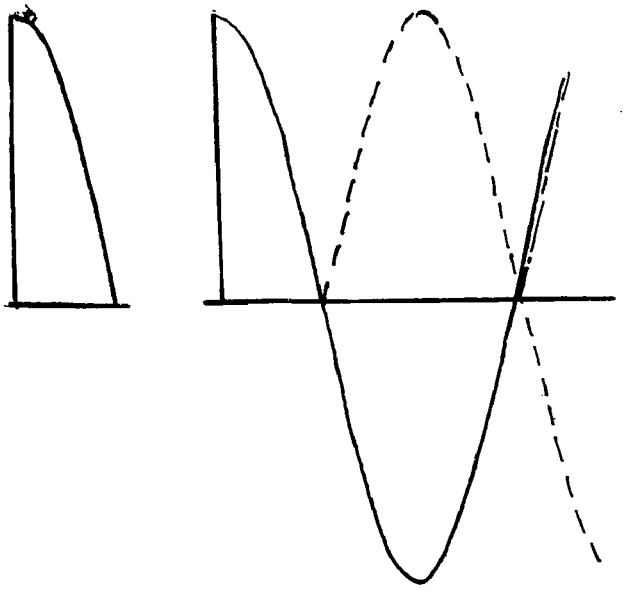

Figure 10

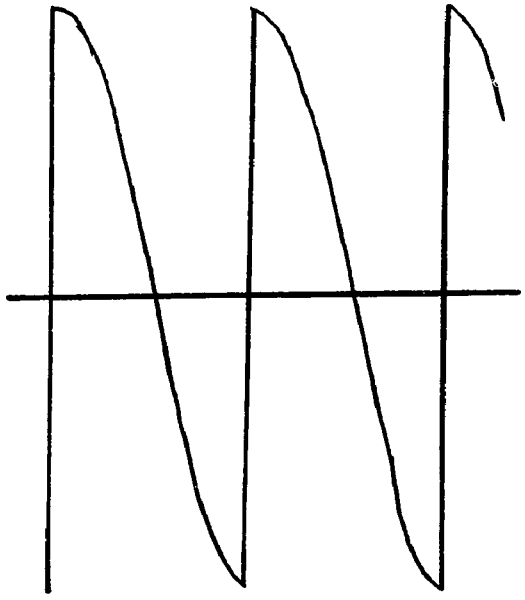

Figure 11

Similarly, the half-wave rectified cosine component of the rectifier output will yield a QP response equal to

$$v_c(t) = \frac{2A}{T'} \frac{(b-a)(ab-n^2\omega_r^2)}{(a^2+n^2\omega_r^2)(b^2+n^2\omega_r^2)} \frac{1}{\tau_c} \left\{ \frac{\phi_{cd}}{\phi_{cd}^2+n^2\omega_r^2} \times \right.$$
$$\left[e^{-\phi_{cd}t} + \frac{n\omega_r}{\phi_{cd}} \sin n\omega_r t + \cos n\omega_r t \right]$$
$$\left. + \frac{n\omega_r}{n^2\omega_r^2+\phi_{cd}^2} \left[e^{-\phi_{cd}t} + \frac{\phi_{cd}}{n\omega_r} \sin n\omega_r t - \cos n\omega_r t \right] \left[u(t-\tfrac{T}{4}) + u(t-\tfrac{3}{4}T) + \cdots \right] \right\} \quad (38)$$

The terms

$$\frac{\phi_{cd}}{n\omega_r} \sin n\omega_r t \left[u(t) + u(t-T/2) + \cdots \right]$$

represent a half-wave rectified sine with amplitude $\phi_{cd}/n\omega_r$. Its average value is $\phi_{cd}/(\pi n\omega_r)$.

The terms

$$\cos n\omega_r t \left[u(t) + u(t-T/2) + \cdots \right]$$

represent a wave as shown in Figure 11 whose average value is zero. Also, at the lowest tuned frequency of 0.2 MHz, the ratio

$$\phi_{cd}/n\omega_r = 1/400\pi \quad .$$

The average value of rectified sine components given by equation (37) is therefore negligible and the only term of concern is $\exp(-\phi_{cd}t)$. Its average value has been found to be $1.6\, n\, f_r/\phi_{cd}$ in equation (13). There is an equal amount contributed to the average value by the rectified cosine terms. The QP reading for one frequency passed through the filter will then be

$$v_d(av) = \frac{2A}{T'} \frac{(b^2-a^2)\, n\omega_r}{(a^2+n^2\omega_r^2)(b^2+n^2\omega_r^2)} \frac{n\omega_r}{\tau_c} \frac{1}{n^2\omega_r^2+\phi_{cd}^2} \frac{1.6nf_r}{\phi_{cd}}$$
$$+ \frac{2A}{T'} \frac{(b-a)(ab-n^2\omega_r^2)}{(a^2+n^2\omega_r^2)(b^2+n^2\omega_r^2)} \frac{1}{\tau_c} \left\{ \frac{n\omega_r}{\phi_{cd}^2+n^2\omega_r^2} \frac{1.6nf_r}{\phi_{cd}} + \frac{1}{n^2\omega_r^2+\phi_{cd}^2} \right\}. \quad (39)$$

The last term is negligible compared to the first two terms and the quasi-peak output is

$$V_{d(av)} = \frac{2A}{T'} \frac{(b-a)(n\omega_r)}{(a^2+n^2\omega_r^2)(b^2+n^2\omega_r^2)} \frac{1}{(\phi_{cd}^2+n^2\omega_r^2)} \times$$

$$\frac{1.6 n f_r}{\tau_c \phi_{cd}} \left[(b+a) n\omega_r + (ab - n^2\omega_r^2) \right] \qquad (40)$$

The final output of the QP circuit will consist of the sum of average voltages of all frequencies passed through the filter within the passband. If the tuned frequency is high and there are only 5 or 6 harmonics passed through the filter, $n\omega_r$ is nearly constant for all these frequencies. For example, if the tuned frequency is $f_o = 1$ MHz and the repetition rate of pulses f_r is 1000 per second, i.e. $n_o = 1000$, then n will range from 997 to 1003. Therefore the term $n\omega_r$ will be nearly equal to $\omega_o = 1000\omega_r$, and the QP reading will be

$$v_{qp} = \frac{1.6}{\pi} \frac{A}{T'} \frac{(b-a)\omega_o^2 \left[ab + (a+b-\omega_o)\omega_o \right]}{(a^2+\omega_o^2)(b^2+\omega_o^2)(\phi_{cd}^2+\omega_o^2)} \frac{1}{\tau_c \phi_{cd}} \frac{\Delta f}{f_r} \qquad (41)$$

But $T' = 1/f_r$ and $\tau_c \phi_{cd} \approx 1$ for the QP circuit. ($\tau_c \phi_{cd} = 2$ for the FI circuit). Also, $\omega_o^2 + \phi_{cd}^2 \approx \omega_o^2$.

Therefore

$$v_{qp} = \frac{1.6}{\pi} A \frac{(b-a)\Delta f}{(a^2+\omega_o^2)(b^2+\omega_o^2)} \left[ab + (a+b-\omega_o)\omega_o \right]. \qquad (42)$$

Once again, for the corona-type pulse input, the output of

the QP circuit is seen to be independent of the pulse repetition rate when the repetition rate is less than one half the bandwidth.

II.5 POWER SPECTRAL DENSITY OF PERIODIC CORONA-TYPE PULSES AND COMPARISON WITH QUASI-PEAK OUTPUT OF NOISE METER

Consider a train of positive pulses having the time variation

$$i(t) = A\,(e^{-at} - e^{-bt})$$

with a repetition rate $f_r = 1/T'$ pulses per second. Its autocorrelation function is, (10),

$$R(\tau) = \lim_{T\to\infty} \frac{1}{T} \int_{-T/2}^{T/2} i(t)\, i(t-\tau)\, dt \quad . \qquad (43)$$

Taking a finite time interval T in which there are N pulses such that $T = N\,T'$, there is

$$\int_{-T/2}^{T/2} i(t)\, i(t-\tau)\, dt = N \int_{-T'/2}^{T'/2} i(t)\, i(t-\tau)\, dt \qquad (44)$$

$$\therefore\ R(\tau) = \lim_{N\to\infty} \frac{N}{NT'} \int_{-T'/2}^{T'/2} i(t)\, i(t-\tau)\, dt$$

$$= \frac{1}{T'} \int_{-T'/2}^{T'/2} i(t)\, i(t-\tau)\, dt$$

$$= \frac{A^2}{T'} \left[\frac{1}{2a} e^{-a\tau} + \frac{1}{2b} e^{-b\tau} - \frac{1}{a+b} (e^{-a\tau} + e^{-b\tau}) \right] \qquad (45)$$

The quantity

$$\frac{T'}{A^2} R(\tau) = \frac{1}{2a} e^{-a\tau} + \frac{1}{2b} e^{-b\tau} - \frac{1}{a+b} (e^{-a\tau} + e^{-b\tau}) \qquad (46)$$

is plotted in Figure 12 for a 50/150 ns positive corona pulse

for which

$$a = 10.5 \times 10^6 \quad \text{and} \quad b = 34.65 \times 10^6 .$$

The power spectral density is the Fourier Transform of the autocorrelation function thus:

$$\Phi(\omega) = 2 \int_0^\infty R(\tau) \cos\omega\tau \, d\tau$$

$$= \frac{A^2}{T'} \frac{(b-a)^2}{(a^2+\omega^2)(b^2+\omega^2)} \qquad (47)$$

The power spectral density can be expressed in terms of the area of the pulse, that is the charge content, and the repetition rate. Now, the area of the pulse is

$$Q = \int_0^{T'} A\,(e^{-at} - e^{-bt})\, dt = A\,\frac{b-a}{ab} . \qquad (49)$$

Therefore,

$$\Phi(\omega) = Q^2 f_r \frac{a^2 b^2}{(a^2+\omega^2)(b^2+\omega^2)} \qquad (50)$$

A comparison between the power spectral density $\Phi(\omega)$ and the response of the QP circuit of the meter can now be made. Figure 13 shows a plot of the following two quantities:

$$\frac{\Phi(\omega_o)}{A^2 f_r} = \frac{(b-a)^2}{(a^2+\omega_o^2)(b^2+\omega_o^2)} \qquad (51)$$

and

$$\left(\frac{\pi v_{qp}}{1.6\, A \Delta f}\right)^2 = \left\{ \frac{(b-a)\left[ab + (a+b-\omega_o)\,\omega_o\right]}{(a^2+\omega_o^2)(b^2+\omega_o^2)} \right\}^2 \qquad (52)$$

On the same figure is also plotted the ratio

$$\left(\frac{\pi v_{qp}}{1.6\, A \Delta f}\right)^2 \Big/ \left(\frac{\Phi(\omega_o)}{A^2 f_r}\right) \qquad (53)$$

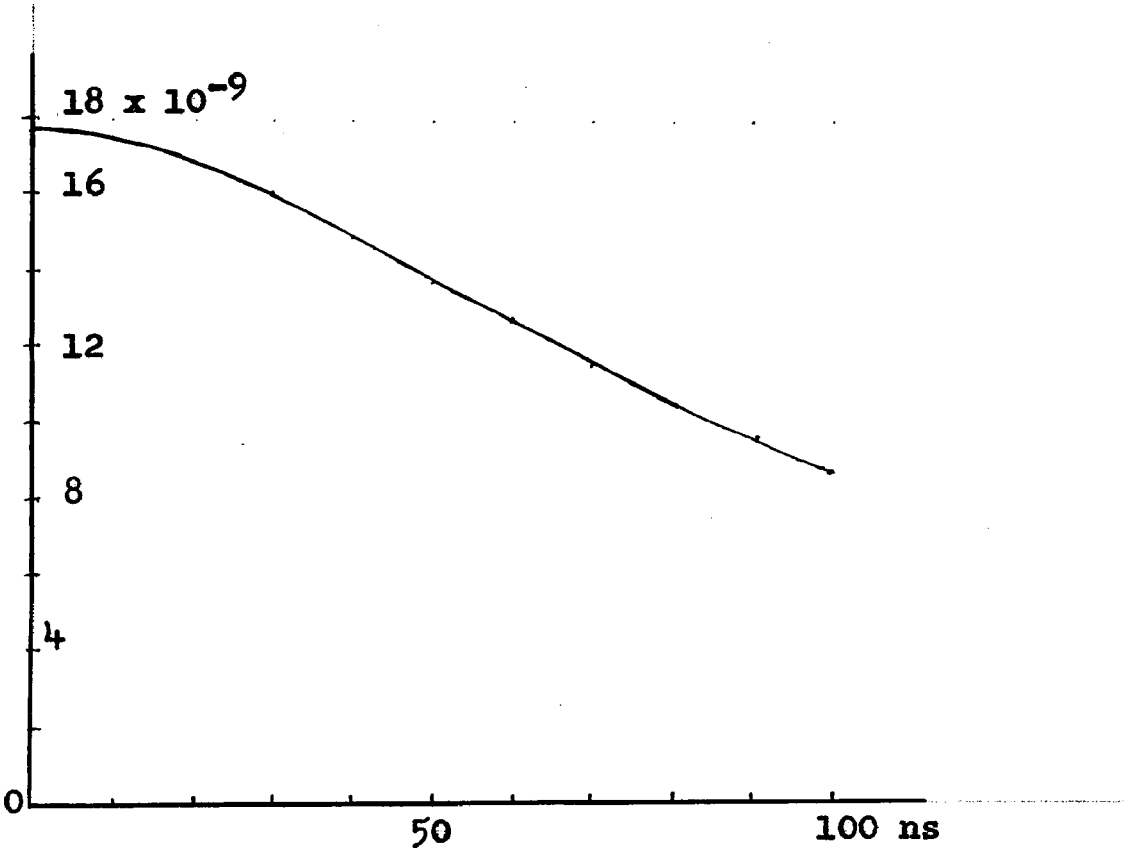

Figure 12. Autocorrelation Function of Positive Pulse

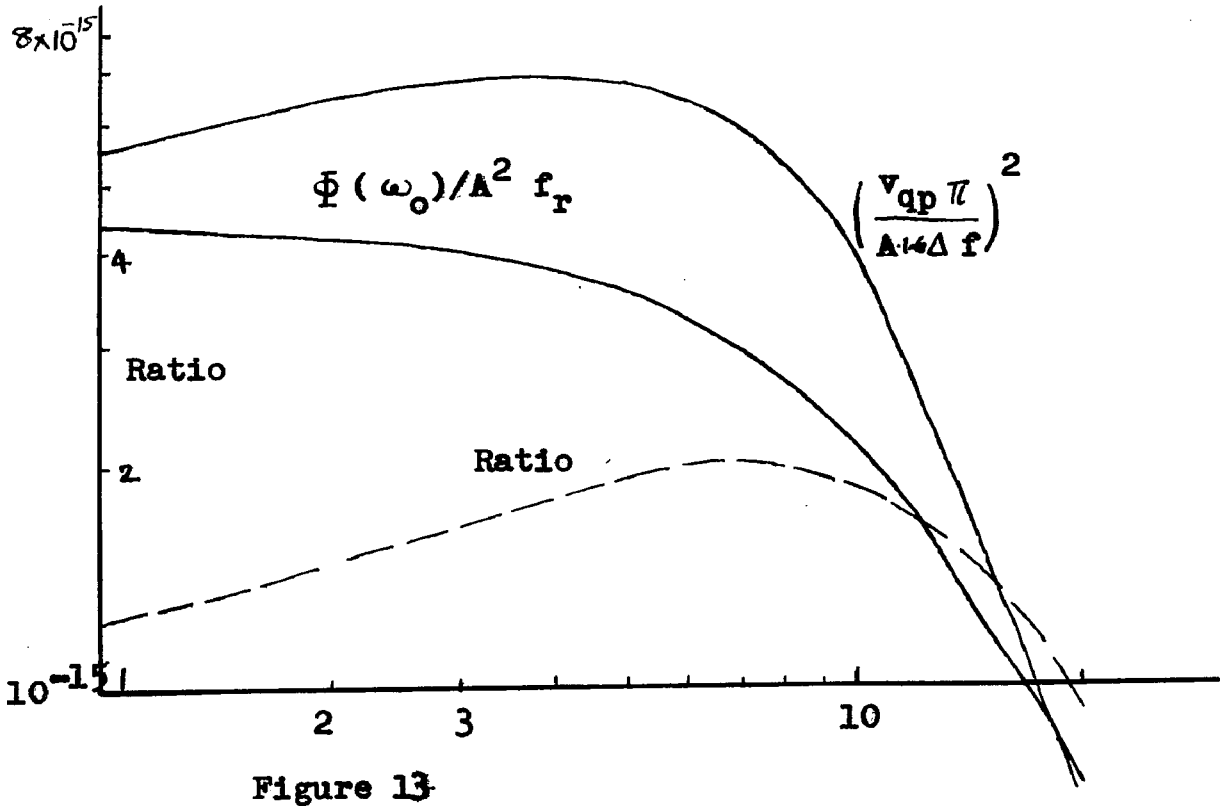

Figure 13

One can observe a very close similarity between the two quantities within a ratio of 2 to 1 in the range of frequencies from 0.2 MHz to 3.2 MHz (ω_o = 1.0 to 20). In the usual range of measurement used in practice, namely between 0.5 MHz to 1.5 MHz, (ω_o = 3 to 9), the ratio lies between 1.7 and 2.0. From this figure it is concluded that the noise level of a transmission line can be equally well expressed by the power spectral density divided by the repetition rate of pulses, $\Phi(f_o)/f_r$, as it can be done by the square of the QP reading per cycle of bandwidth of the instrument, $(v_{qp}/\Delta f)^2$. This places a great emphasis on the need for measuring the characteristics of corona pulses and brings about the importance of the pulse power content on the level of radio interference of a transmission line.

II.6 AUTOCORRELATION FUNCTION AND POWER SPECTRAL DENSITY OF RANDOMLY OCCURING CORONA PULSES

Pulses occuring from a long conductor in corona are not periodic. The time interval between pulses is randomly distributed with a probability density which is either a Gaussian function or an Exponential function, (11). The time interval between pulses from conductors with a polished surface such as newly strung conductors, occur with a Gaussian probability density distribution. From well-weathered conductors, corona discharge takes place at fixed spots and the probability density of time interval between pulses shows an exponential distribution. The autocorrelation function

and power spectral density of corona pulse trains occuring with random distribution of time interval will be examined. The power spectral density at the tuned frequency will then be compared with the output of the quasi-peak weighting circuit of the noise meter in the next section.

The autocorrelation function is

$$R(\tau) = \lim_{T\to\infty} \frac{1}{T} \int_{-T/2}^{T/2} i(t)\, i(t-\tau)\, dt \qquad (54)$$

As mentioned in Chapter I, corona pulses give rise to impulse type of noise and not a random type of noise, that is, the pulses do not overlap one another. Also, the average time interval between pulses is normally much longer than the pulse duration. For example, positive corona pulses are not more than 500 ns (0.5 μs) in duration while the average repetition rate is 1000 pulses per second, that is the average time interval between pulses is 1 ms. Therefore the time interval between pulses is on the average more than 1000 times the pulse duration. Autocorrelation function and spectral density will be derived based on this assumption.

Consider a train of pulses all having identical shape and amplitude. Let the time interval between consecutive pulses be $t_1, t_2, \cdots, t_n$ $(n\to\infty)$ as shown in Figure 14(a). The time interval T to be considered in equation (54) contains $t_1, t_2, \cdots$ as shown. On the same figure is plotted a second train of identical pulses displaced by a time interval τ from the original pulse train. The product

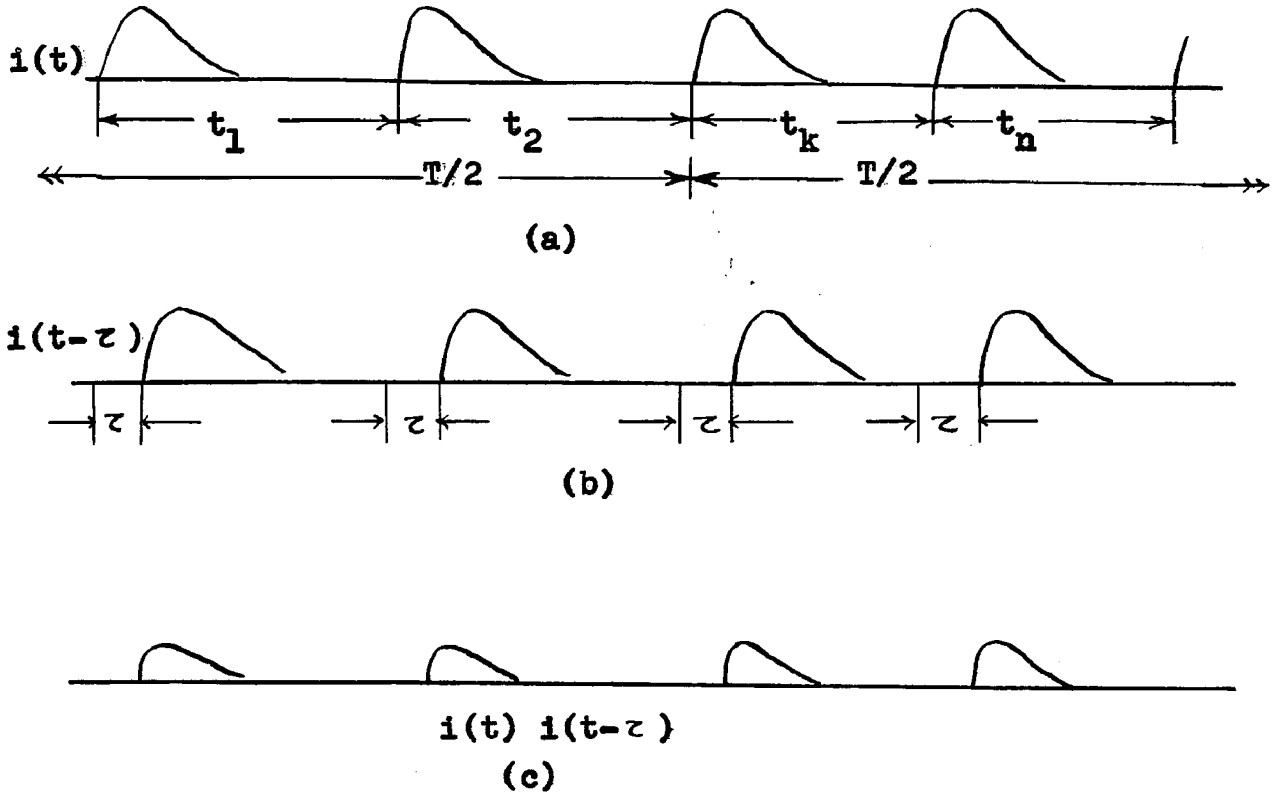

Figure 14. Positive Pulses with Random Intervals

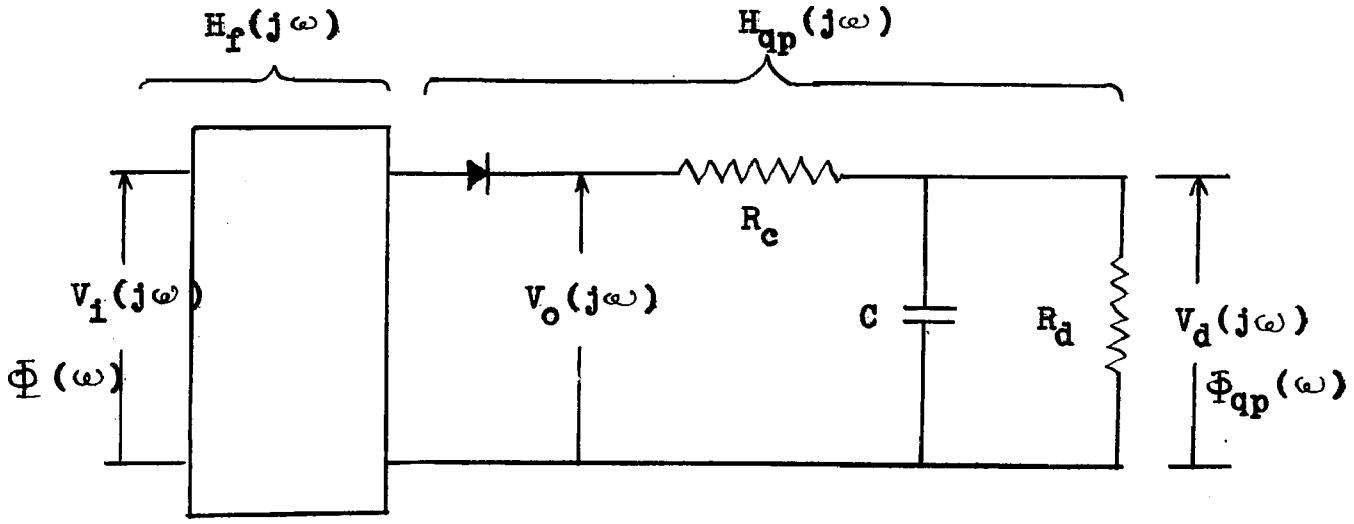

Figure 15. Noise Meter

$i(t)\ i(t-\tau)$ is then obtained and is shown in Figure 14(c).

Now, the integral

$$\int_{-T/2}^{T/2} i(t)\ i(t-\tau)\ dt$$

consists of the sum of a large number of integrals of the type

$$\int_0^{t_1} i(t)\ i(t-\tau)\ dt + \ \ldots \qquad \ldots + \int_0^{t_n} i(t)\ i(t-\tau)\ dt \ . \quad (56)$$

Since the pulses are identical in shape and amplitude, all the integrals in equation (56) have the same value and equal

$$F(\tau) = A^2 \left[\frac{1}{2a}\ e^{-a\tau} + \frac{1}{2b}\ e^{-b\tau} - \frac{1}{a+b}\left(e^{-a\tau} + e^{-b\tau}\right) \right] \ . \quad (57)$$

If $p(k) =$ the probability of occurence of time interval t_k, then

$$T = p(1)\ t_1 + (p(2)\ t_2 + \ldots\ldots + p(k)\ t_k + \ldots + p(n)\ t_n \quad \ldots (58)$$

Also, the number of pulses during time interval T will be

$$N = N(1) + N(2) + \ldots\ldots\ldots\ldots + N(n) \quad (59)$$

where $N(k) =$ number of pulses having a time interval t_k between them.

But $$N(k) = p(k)\ N \ . \quad (60)$$

Therefore, $$N = N\left[p(1) + p(2) + \ldots + p(k) + \ldots\ p(n) \right] \quad (61)$$

or, $$p(1) + p(2) + \ldots\ldots + p(k) + \ \ldots\ + p(n) = 1 \ . \quad (62)$$

Thus,

$$\lim_{T\to\infty} \frac{1}{T} \int_{-T/2}^{T/2} i(t)\ i(t-\tau)\ dt = \lim_{T\to\infty} \frac{N\,F(\tau)}{T} \left[p(1) + \ldots + p(n) \right]$$

$$= \frac{1}{T'} F(\tau) \ , \quad (63)$$

where $T' = T/N$ = average time interval between pulses, obtained from an infinitely large number of sampling of pulses.

The Fourier Transform of autocorrelation function is the power spectral density and is the same as equation (47), thus

$$\Phi(\omega) = \frac{A^2}{T'} \quad \frac{(b-a)^2}{(a^2+\omega^2)(b^2+\omega^2)} , \qquad (47)$$

where $\omega = 2\pi f$.

II.7 RESPONSE OF QUASI-PEAK WEIGHTING CIRCUIT OF NOISE METER AND COMPARISON WITH SPECTRAL DENSITY OF RANDOM PULSES

The response of a quasi-peak weighting circuit to periodic pulses of constant amplitude has been analyzed by Geselowitz, (15), and for periodic pulses with random amplitudes by Haber, (16). An analysis of the response of the QP circuit to constant amplitude corona-type pulses with random repetition rate will be carried out here.

When the spectral density of input to the QP circuit of the noise meter is given by equation (47), the output can be determined by using Figure 15. The transfer function for the bandwidth-limited filter is

$$\left| H_f(j\omega) \right|^2 = 1, \text{ for } f_o - \Delta f/2 \leqslant f \leqslant f_o + \Delta f/2, \qquad (64)$$
$$= 0, \text{ elsewhere,}$$

in which f_o = tuned frequency,

and Δf = bandwidth of filter.

The transfer function of the combination of the rectifier and weighting circuit proper will be

$$\left| H_{qp}(j\omega) \right|^2 = \tfrac{1}{2} \frac{1}{\tau_c^2} \frac{1}{\omega^2 + \phi_{cd}^2} \quad . \qquad (66)$$

Therefore the power spectral density of the output of the QP circuit is

$$\Phi_{qp}(\omega) = \left| H_{qp}(j\omega) \right|^2 \left| H_f(j\omega) \right|^2 \Phi(\omega) \qquad (67)$$

$$= \frac{1}{\tau_c^2} \frac{1}{\omega^2 + \phi_{cd}^2} \frac{1}{2} \frac{A^2}{T'} \frac{(b-a)^2}{(a^2+\omega^2)(b^2+\omega^2)} \quad . \qquad (68)$$

Since the frequencies passed through the filter in its bandwidth is from $f_o - \Delta f/2$ to $f_o + \Delta f/2$, the power content in the output when the meter is tuned to the frequency f_o is

$$\Phi_{qp}(\omega_o) = \frac{1}{2\pi} \int_{\omega_o - \Delta\omega/2}^{\omega_o + \Delta\omega/2} \Phi_{qp}(\omega)\, d\omega \quad , \qquad (69)$$

where $\Delta\omega = 2\pi\Delta f$.

Therefore,

$$\Phi_{qp}(\omega_o) = \frac{1}{4\pi} \frac{A^2(b-a)^2}{\tau_c^2 T'} \int_{\omega_o - \Delta\omega/2}^{\omega_o + \Delta\omega/2} \frac{1}{a^2+\omega^2} \frac{1}{b^2+\omega^2} \frac{1}{\phi_{cd}^2+\omega^2} \, d\omega \qquad \ldots (70)$$

Now,

$$\frac{1}{a^2+\omega^2} \cdot \frac{1}{b^2+\omega^2} \cdot \frac{1}{\phi_{cd}^2+\omega^2} = \frac{1}{(b^2-a^2)(\phi_{cd}^2-a^2)} \cdot \frac{1}{\omega^2+a^2}$$

$$+ \frac{1}{(\phi_{cd}^2-b^2)(a^2-b^2)} \cdot \frac{1}{\omega^2+b^2} + \frac{1}{(a^2-\phi_{cd}^2)(b^2-\phi_{cd}^2)} \frac{1}{\omega^2+\phi_{cd}^2} \qquad (71)$$

Thus,

$$\Phi_{qp}(\omega_o) = \frac{1}{4\pi} \frac{A^2(b-a)^2}{\tau_c^2 T'} \int_{\omega_o - \Delta\omega/2}^{\omega_o + \Delta\omega/2} \left[\frac{1}{(b^2-a^2)(\phi_{cd}^2-a^2)} \cdot \frac{1}{\omega^2+a^2} \right.$$

$$+ \frac{1}{(\phi_{cd}^2-b^2)(a^2-b^2)} \cdot \frac{1}{\omega^2+b^2}$$

$$\left. + \frac{1}{(a^2-\phi_{cd}^2)(b^2-\phi_{cd}^2)} \cdot \frac{1}{\omega^2+\phi_{cd}^2} \right] d\omega$$

$$= \frac{1}{4\pi}\frac{A^2(b-a)^2}{\tau_c^2 T'}\left[\frac{1}{(b^2-a^2)(\phi_{cd}^2-a^2)}\frac{1}{a}\left(\tan^{-1}\frac{\omega_o+\Delta\omega/2}{a}-\tan^{-1}\frac{\omega_o-\Delta\omega/2}{a}\right)\right.$$

$$+\frac{1}{(\phi_{cd}^2-b^2)(a^2-b^2)}\frac{1}{b}\left(\tan^{-1}\frac{\omega_o+\Delta\omega/2}{b}-\tan^{-1}\frac{\omega_o-\Delta\omega/2}{b}\right)$$

$$\left.+\frac{1}{(a^2-\phi_{cd}^2)(b^2-\phi_{cd}^2)}\frac{1}{\phi_{cd}}\left(\tan^{-1}\frac{\omega_o+\Delta\omega/2}{\phi_{cd}}-\tan^{-1}\frac{\omega_o-\Delta\omega/2}{\phi_{cd}}\right)\right] \quad (72)$$

These expressions can be simplified as follows, (17):

Let $\theta_1 = \arctan\frac{\omega_o+\Delta\omega/2}{a}$ and $\theta_2 = \arctan\frac{\omega_o-\Delta\omega/2}{a}$ ..... (73)

Then $\theta = \theta_1 - \theta_2 = \arctan\frac{\omega_o+\Delta\omega/2}{a} - \arctan\frac{\omega_o-\Delta\omega/2}{a}$ (74)

$$\therefore \tan\theta = \tan(\theta_1-\theta_2) = \frac{\tan\theta_1-\tan\theta_2}{\tan\theta_1\tan\theta_2+1}$$

$$= \frac{\Delta\omega/a}{1+\frac{\omega_o^2-(\Delta\omega)^2/4}{a^2}}$$

$$= \frac{a\,\Delta\omega}{\omega_o^2+a^2}, \quad \text{when } \Delta\omega \ll \omega_o, \quad (75)$$

that is, when the bandwidth of the filter is much less than the tuned frequency. Therefore,

$$\arctan\frac{\omega_o+\Delta\omega/2}{a} - \arctan\frac{\omega_o-\Delta\omega/2}{a} = \theta = \arctan\frac{a\,\Delta\omega}{\omega_o^2+a^2}$$

Similarly, $\arctan\frac{\omega_o+\Delta\omega/2}{b} - \arctan\frac{\omega_o-\Delta\omega/2}{b} = \arctan\frac{b\,\Delta\omega}{\omega_o^2+b^2}$

and $\arctan\frac{\omega_o+\Delta\omega/2}{\phi_{cd}} - \arctan\frac{\omega_o-\Delta\omega/2}{\phi_{cd}} = \arctan\frac{\phi_{cd}\,\Delta\omega}{\omega_o^2+\phi_{cd}^2}$ .. (76)

When equation (76) is substituted in equation (72) there is

$$\Phi_{qp}(\omega_o) = \frac{A^2(b-a)^2}{4\pi\tau_c^2 T'}\left[\frac{1}{(b^2-a^2)(\phi_{cd}^2-a^2)}\frac{1}{a}\tan^{-1}\frac{a\Delta\omega}{\omega_o^2+a^2}\right.$$
$$+\frac{1}{(\phi_{cd}^2-b^2)(a^2-b^2)}\frac{1}{b}\tan^{-1}\frac{b\Delta\omega}{\omega_o^2+b^2}$$
$$\left.+\frac{1}{(a^2-\phi_{cd}^2)(b^2-\phi_{cd}^2)}\frac{1}{\phi_{cd}}\tan^{-1}\frac{\phi_{cd}\Delta\omega}{\omega_o^2+\phi_{cd}^2}\right] \quad (77)$$

In practice, $a = 10.5 \times 10^6$, $b = 34.65 \times 10^6$, $\phi_{cd} = 1000$, $\Delta\omega = 2\pi \times 5000$, and $\omega_o = 2\pi \times 10^6$ at a tuned frequency of $f_o = 1$ MHz. Therefore, the following approximations are valid:

$$\frac{a\Delta\omega}{\omega_o^2 + a^2} \ll 1 \; ; \quad \frac{b\Delta\omega}{\omega_o^2 + b^2} \ll 1 \; ; \quad \frac{\phi_{cd}\Delta\omega}{\omega_o^2 + \phi_{cd}^2} \ll 1 \; . \quad (78)$$

Using the power series expansion for arc tan, (18), and taking only the first term, there is

$$\text{arc tan}\frac{a\Delta\omega}{\omega_o^2 + a^2} = \frac{a\Delta\omega}{\omega_o^2 + a^2} \quad (79)$$

Similarly for terms containing 'b' and 'ϕ_{cd}'.

With the above approximations, the power output at the tuned frequency of quasi-peak weighting circuit is finally,

$$\Phi_{qp}(\omega_o) = \frac{\Delta\omega}{2}\frac{A^2(b-a)^2}{\tau_c^2 T'}\left[\frac{1}{(b^2-a^2)(\phi_{cd}^2-a^2)}\frac{1}{\omega_o^2+a^2}\right.$$
$$+\frac{1}{(\phi_{cd}^2-b^2)(a^2-b^2)}\frac{1}{\omega_o^2+b^2}$$
$$\left.+\frac{1}{(a^2-\phi_{cd}^2)(b^2-\phi_{cd}^2)}\frac{1}{\omega_o^2+\phi_{cd}^2}\right] \quad (80)$$
$$= \frac{\Delta\omega\, A^2(b-a)^2}{4\pi\,\tau_c^2\,T'}\frac{1}{(a^2+\omega_o^2)(b^2+\omega_o^2)(\phi_{cd}^2+\omega_o^2)}$$

where use has been made of equation (71).

But the input spectral density at the tuned frequency f_o is obtained from equation (47) with $\omega = \omega_o$, thus

$$\Phi(\omega_o) = \frac{A^2}{T'} \frac{(b-a)^2}{(\omega_o^2 + a^2)(\omega_o^2 + b^2)} . \qquad (81)$$

The ratio between the power spectral density of the output of the QP circuit and the input pulses is

$$\frac{\Phi_{qp}(\omega_o)}{\Phi(\omega_o)} = \frac{\Delta\omega}{4\pi \tau_c^2} \frac{1}{\omega_o^2 + \beta_{cd}^2} \simeq \frac{\Delta f}{2 \tau_c^2 \omega_o^2} \qquad (82)$$

This shows that the output spectral density is related to the input spectral density by the inverse square of the tuned frequency and the known meter constants. Hence it is evident that the quasi-peak voltage of the noise meter is related to the input power spectral density and therefore the noise level of a transmission line may also be described by the power spectral density of the corona pulses.

C H A P T E R - III

DISTRIBUTION OF ELECTRIC FIELD IN THE VICINITY OF A SHORT EXPERIMENTAL LINE WHEN EXCITED BY CORONA PULSES

III.1 INTRODUCTION

Design of a long transmission line requires evaluation of the high-frequency electric field intensity at ground level generated by corona pulses on the conductors at high voltage stresses. A convenient way of assessing this long-line RI field intensity is to first of all determine the RI characteristics of conductors used in short lengths and then extend these results to apply to a long line. Several major utility and research organizations have used this procedure to some extent. Short experimental lines in existence have varied in length from 120 meters to 8500 meters (1/14 mile to 5 miles).

Short experimental lines are normally open-circuited at both ends for the high-frequency voltage or current of the corona pulses by using chokes or resistances to provide the high impedance. A better and more desirable scheme is to connect the line ends to ground through an impedance equal to its characteristic impedance in order to simulate an infinitely long line as far as RIV is concerned. But the cost of this arrangement usually has prevented this scheme from being carried out. Attention in this chapter will therefore be restricted to short open-circuited lines.

When a finite length of conductor, with high impedance to ground at its ends, is excited by a voltage anywhere along

its length, the voltage distribution along the line exhibits standing waves. This is caused by the necessity for the energy of the source of excitation to be trapped in a finite length of conductor. On an infinitely-long conductor, or a short length of conductor terminated at its ends by its characteristic impedance, standing waves are not present. It will be shown in Section III.5, equation (11), that the voltage to ground of such a conductor when excited by an infinitely large number of identical voltage sources, which are uncorrelated in time, is given by the expression

$$V = V_o/\sqrt{\alpha} \quad ,$$

where $V =$ voltage to ground of conductor at frequency f,

$V_o =$ voltage to ground of source at the same frequency,

and $\alpha =$ attenuation of high-frequency voltage on the line in nepers per unit length.

Thus the voltage of an infinitely-long conductor is the same everywhere along its length if the excitation sources are uniformly distributed along the line and they are all identical. This assumption of uniformity of distribution of corona sources is very nearly satisfied in practice; in fair weather the corona sources occur a foot or two from each other whereas in rain they are even more uniformly distributed. On a long line there will always be the possibility of a standing wave being established between towers because the surge impedance of the line undergoes a change at the tower due to the insulator string and the proximity of the grounded structure. In practice, the discontinuity caused by the tower and

insulator to the propagation of high frequency energy is not of sufficient magnitude to be of concern. Therefore this effect is neglected and an infinite line is treated as if its impedance were uniform throughout.

On account of the absence of standing waves on an infinitely long line, the high-frequency energy on the line is not radiated and the field in its vicinity is entirely due to induction.

A finite length of line, on the other hand, being capable of supporting standing waves, gives rise to both an induced field as well as a radiated field. The radiated field from a short experimental line will be neglected within distances equal to 3 or 4 times the line height, especially when the line is supporting several wavelengths of voltage, current or charge. A complete analysis that includes both the radiated and the induced field will not be carried out here. Attention will be restricted to the induced field alone in the vicinity of the short line.

III.2 NATURE OF FIELD NEAR A SHORT LINE: EXPERIMENTAL RESULTS

Experimental results obtained from measurement of electric field at several frequencies in a longitudinal direction under the line are shown in Figure 1. These were obtained when the overhead line was excited by actual corona pulses. Figure 2 shows results of measurements carried out when the conductor was energized at one end by a low-voltage

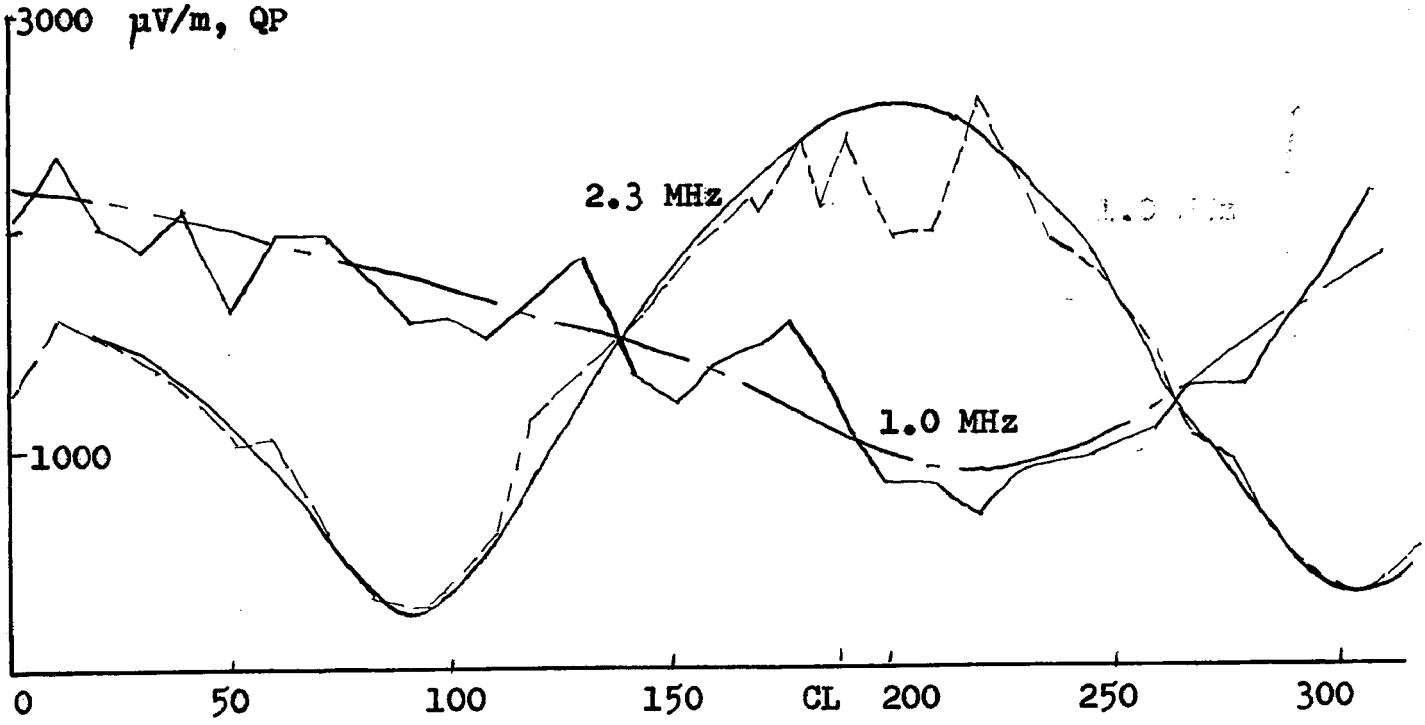

Figure 1. Longitudinal Profile of Electric Field Intensity
Single DRAKE ACSR Conductor, 450 KV Positive

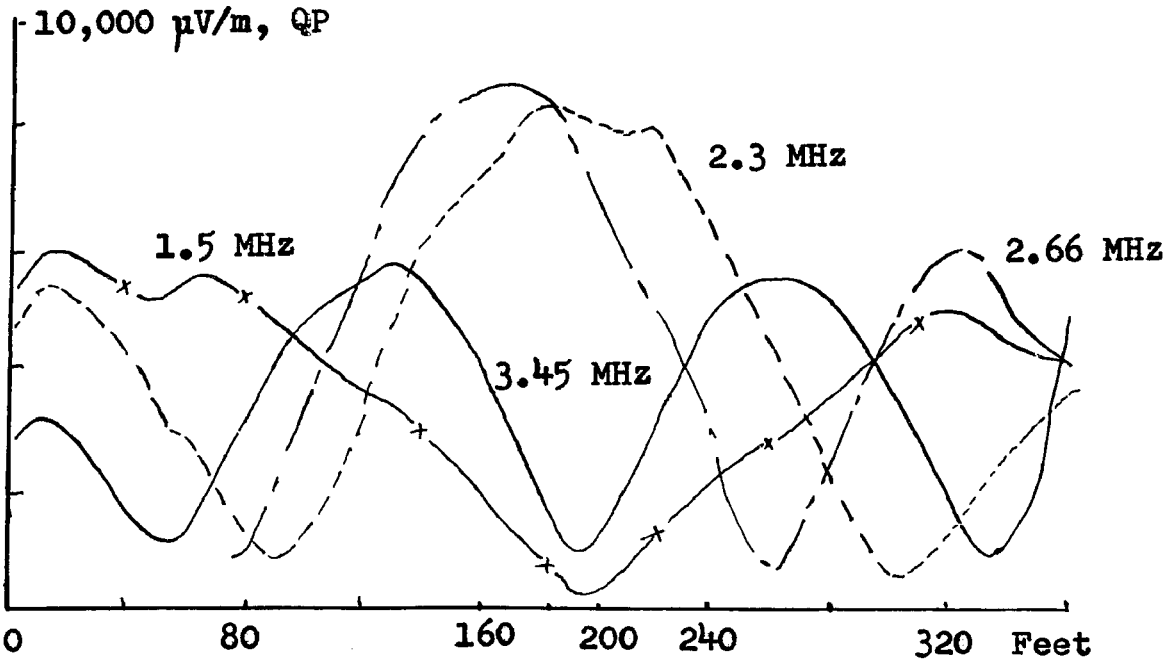

Figure 2. Longitudinal Profile of Electric Field Intensity
Signal Generator Excitation

signal generator yielding sinusoidal voltages at desired frequencies from 0.5 MHz to 15 MHz. The signal generator voltage was held at 1 volt to ground at every frequency and the resulting field intensity was measured by a rod antenna on a Stoddart NM 20A type of noise meter, (1). These curves immediately give an indication of the field factors or the ratio of RIV at conductor to RI measured at ground level under the line.

On this continent the electric field strength measured with a rod antenna has been used exclusively for determining radio interference field intensities and therefore attention will be restricted to this field. In other countries the h-f magnetic field intensities have been measured by means of a loop antenna in addition to or instead of the electric field intensity from a rod antenna. The two measurements are equivalent when proper precautions are taken. When the noise meter is placed on ground surface on a sufficiently large grounded plate and connected to a good ground electrically, the electric field intensity is relatively insensitive to the electrical characteristics of the soil. But the magnetic field intensity measured with a loop antenna is dependent on the magnetic characteristics of the soil and requires the use of suitable correction factors. In all measurements of field intensities these two precautions or restrictions have to be carefully recognized.

In addition to the longitudinal profile of RI along

ground near the line, the 'lateral profile' of r-f electric field intensity is of extreme importance, for design purposes. Lateral decrement of electric field along ground in a direction at right angles to the line gives an indication of the width of right of way required for the infinite line. In the case of a short line, the lateral decrement allows conversion of field intensity measured at a point laterally to the field intensity measured under the line center, from which the expected long line RI level can be predicted. This is necessary because in an actual experimental situation, it is not always practicable to measure RI under the line especially in foul weather. A second practical reason for measuring both the lateral and longitudinal profiles of RI of a short line is that when the ratio of long line RI level to the measured value under the center of the short line is established at the frequency of interest, the noise meter can be moved longitudinally where this ratio is satisfied. The noise meter will then measure the expected long-line RI level which can then be logged continuously.

III.3 TOLERABLE LIMITS OF RI

The lateral decrement of high-frequency field intensity from a long line shows whether or not the line design is properly carried out. A line is well designed if the RI along ground at a specified distance from the line is within limits agreed upon by the power company and the F.C.C. in U.S.A. or the D.O.T. in Canada. It may be of interest to recall

here that Federal authorities in most countries have not specified a definite limit for the RI value, (2). Setting a rigid limit to the tolerable RI level is not a very practical problem and there are several reasons for this.

A power line traverses a variety of countryside, from regions where there is practically no habitation to regions having extremely densely populated cities. A rigid limit would therefore be of no use throughout the length of line. Secondly, federal agencies have taken the attitude of acting as a policing agency rather than a law-making agency in so far as the RI problem is concerned. One of their primary concerns is to obtain 'complaints' from citizens and then recommend to the power companies suitable measures. While RI limits have not been strictly specified, power companies have worked harmoniously with federal agencies as well as citizens to provide as noise-free lines as possible. This has involved a great deal of expenditures on their part in research and development.

A third reason for not specifying the tolerable RI limit is the technical fact that the presence of several conductors on a tower gives rise to an equal number of modes of propagation for the high-frequency energy. The energy in each mode propagates with its own attenuation factor and has its own individual longitudinal and lateral profile for the RI field. The lateral profile is very difficult to estimate at the design stages because of the analytical complexity

and also because of the large number of possible sets of line height and pole separation distances. The interaction between these several modes of propagation also is improperly understood as yet. It will so happen that the field intensity in some cases actually increases beyond a certain lateral distance from the line. Thus, under abnormal conditions of line design, even though the RI level may conform to the set limit at a specified distance from the line, it may actually be higher at a farther distance. Until all these factors are clearly analyzed and the lateral profile is estimated very accurately, it would be of no use to specify rigid RI limits. For the present, power companies have been working with the following approximate limits for RI in fair weather, (3 - 5):

In densely populated areas: below 40 μV/m at 100 feet from the outermost conductor along ground;

In other areas: below 100 μV/m at 100 feet from the outermost conductor along ground, (40 DB above 1 μV/m).

III.4 STANDING WAVES ON A SHORT OPEN-CIRCUITED LINE CAUSED BY CORONA PULSES

Consider a line of length L at a height H above ground and excited by a corona current source at a point x and having a frequency characteristic $I(j\omega)$, as shown in Figure 3. The line is characterized by

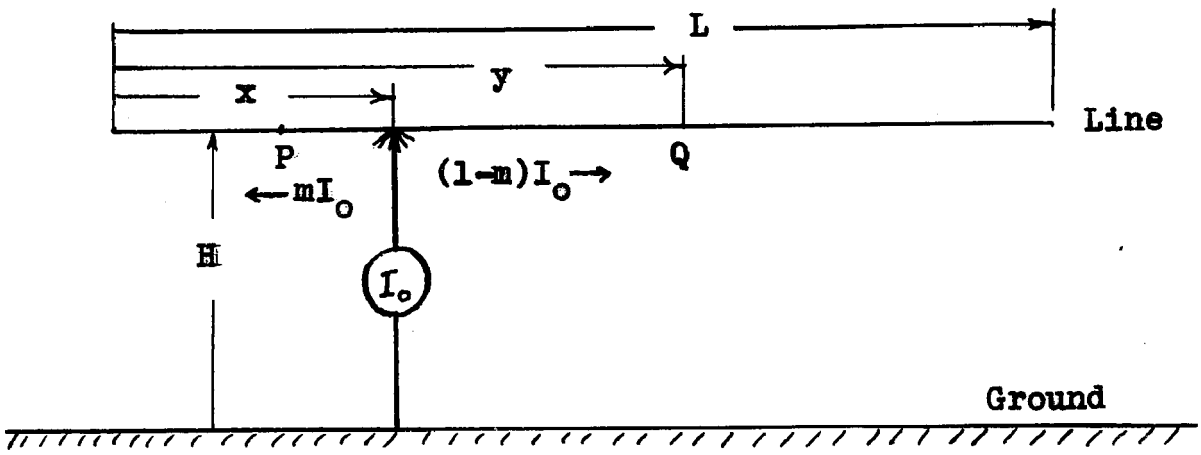

Figure 3. Short line with Corona Current Source

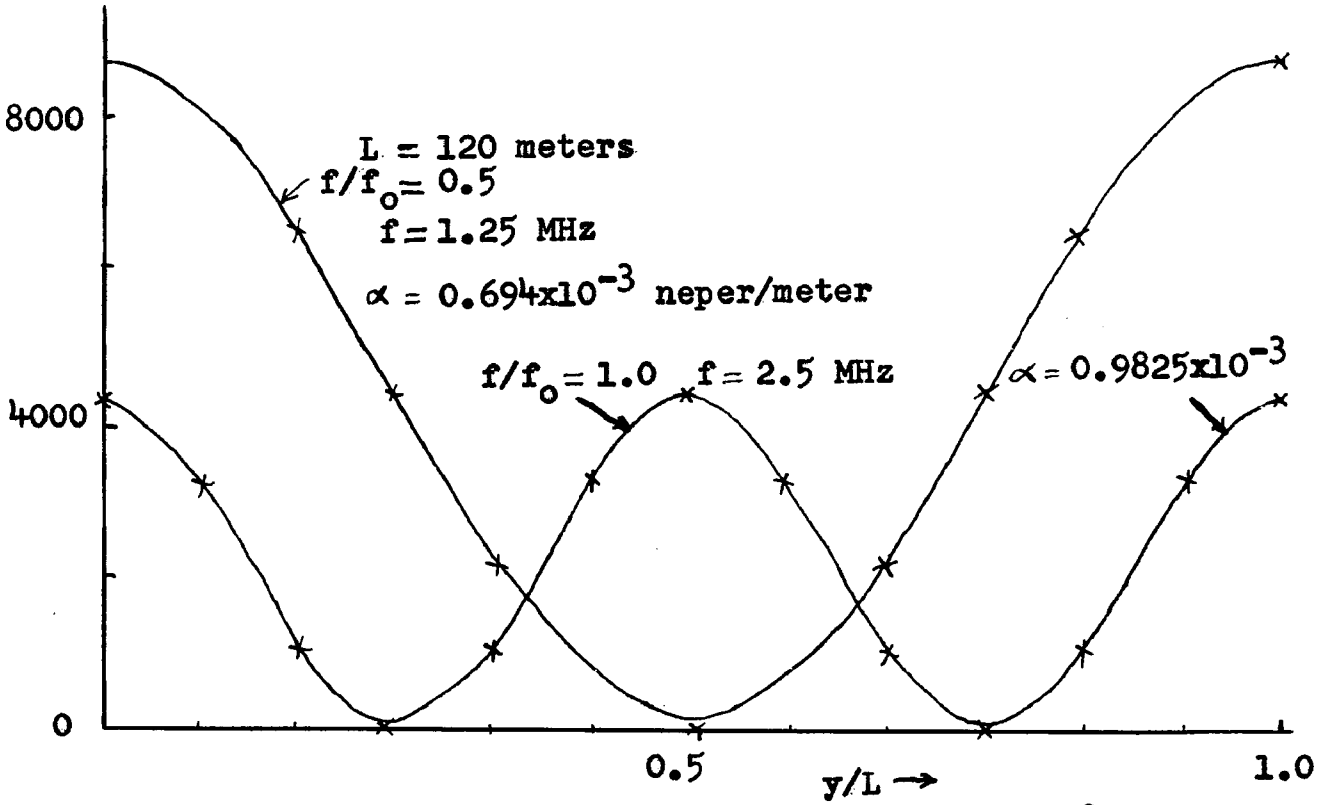

Figure 4. Standing Wave of Voltage Ratio $|E_y/E_o|^2$

a) a characteristic impedance Z_o, and

b) a propagation factor, $p = \alpha + j\beta$,

where α = attenuation factor in nepers per unit length,

β = phase shift factor per unit length

$= 2\pi/\lambda = 2\pi f/f_o L$ at frequency f,

f_o = the first resonance frequency of line = v/L,

and λ, v = wave length and velocity of propagation.

Since the lengths of the line on the two sides of the current source are unequal, the standing waves are unsymmetrical and therefore the current from the corona source divides itself unequally along both sides. Let the current division be $m\ I_o$ and $(1-m)\ I_o$, as shown in Figure 3. The resulting voltage at a point P to the left of the source and a point Q to the right of the source can be obtained by solving the fundamental differential equation of the line with the boundary conditions that the two ends are open and the current at x is equal to $m\ I_o$ and $(1-m)\ I_o$ for the two sides. This gives:

$0 < y < x$: $\qquad x < y < L$

$$E_P = \frac{\cosh py}{\sinh px} Z_o\ m\ I_o \qquad E_Q = \frac{\cosh p(L-y)}{\sinh p(L-x)} Z_o\ (1-m) I_o$$

$$\text{and } I_P = \frac{\sinh py}{\sinh px}\ m\ I_o \qquad I_Q = \frac{\sinh p(L-y)}{\sinh p(L-x)}\ (1-m)\ I_o$$

..... (1)

In order to find the value of 'm', i.e. the current division, the voltage at the current source, $y = x$, must be equal when

looking from both sides. Thus:

$$m \left.\frac{\cosh py}{\sinh px}\right|_{y=x} = (1-m) \left.\frac{\cosh p(L-y)}{\sinh p(L-x)}\right|_{y=x}$$

or,
$$m = \frac{\coth p(L-x)}{\coth px \;\; \coth p(L-x)} \qquad (2)$$

The square of the magnitude of voltage at any point is then obtained from equations (1) and (2) as follows:

$$|E_p(f)|^2 = |I_o Z_o|^2 \left|\frac{\cosh p(L-x) \sinh px}{\sinh pL}\right|^2 \left|\frac{\cosh py}{\sinh px}\right|^2 \qquad (3)$$

$$= \tfrac{1}{2} |I_o Z_o|^2 \frac{[\cosh 2\alpha(L-x) + \cos\beta(L-x)][\cosh 2\alpha y + \cos\beta y]}{\cosh 2\alpha L - \cos 2\beta L} \quad \ldots (4)$$

Similarly,

$|E_Q(f)|^2$ = same as equation (4) with x and y interchanged.

If the current sources are all uncorrelated and uniformly distributed along the line with a linear density of current of $I_o(j\omega)$ per unit length, we may add the square of the magnitude of voltage due to the uniform current sources and obtain the square of the magnitude of RIV at the conductor at any point y along the line. Therefore,

$$|E_y(f)|^2 = \int_y^L |E_p(f)|^2 dx + \int_0^y |E_Q(f)|^2 dx$$

$$= \tfrac{1}{2} |I_o Z_o|^2 (\cosh 2\alpha L - \cos 2\beta L)^{-1}$$

$$\left[\frac{1}{2\alpha} \sinh 2\alpha L + \frac{1}{2\beta} \sin 2\beta L + \frac{1}{2\alpha} \cos 2\beta(L-y) \sinh 2\alpha y \right.$$

$$+ \frac{1}{2\alpha} \sinh 2\alpha(L-y) \cos 2\beta y + \frac{1}{2\beta} \cosh 2\alpha(L-y) \sin 2\beta y$$

$$\left. + (1/2\beta) \cosh 2\alpha y \sin 2\beta(L-y)\right] \quad \ldots (5)$$

This equation may also be obtained from traveling wave analysis, (6 - 8). The electric field intensity along ground level in the vicinity of the short open-circuited line can be calculated from equation (5) when the charge distribution corresponding to the r-f wer is evaluated from it. The amplitude of voltage at a point y along the line is seen to be a function of the attenuation factor α , frequency f, resonant frequency $f_o = v/L$, and line length L.

Equation (5) is plotted in Figure 4 for $f/f_o = 0.5$ and 1.0 for a short line of 120 meters in length. It shows the ratio of square of amplitude of voltage at any point along the line to $|I_o Z_o|^2 = |E_o|^2$. In equation (5), the attenuation factor α deserves special attention because of its dependence on frequency. For a short line 120 meters long, the first resonance frequency f_o is 2.5 MHz based on a value of 3×10^8 meters per second for the velocity of propagation of electromagnetic waves. When $f/f_o = 0.5$, the frequency under consideration is 1.25 MHz. The attenuation factor in Figure 4 must correspond to these frequencies.

Now, from experiments conducted of the attenuation of r-f energy on long alternating current transmission lines the attenuation for the line-to-ground mode of propagation was found to be nearly 1 neper/mile at a frequency of 1 MHz, (9). Also, the attenuation factor is known to vary as the square root of frequency, (10). In this work it will therefore be assumed that the attenuation factor at

any frequency can be described by the following expression:

$$\alpha = 10^{-3}\sqrt{f} \quad \text{nepers/mile}$$
$$= 0.62 \times 10^{-6}\sqrt{f} \quad \text{, nepers/meter.} \qquad (6)$$

This expression yields 1 neper/mile at 1 MHz.

From Figure 4 it is observed that the amplitude of standing wave of voltage along the conductor is very nearly of the same shape as the square of a cosine, that is,

$$|E_y(f)|^2 / |E_o(f)|^2 = A \cos^2 2\pi f\, y/f_o L \ , \qquad (7)$$

where A = the value of this ratio at the line end. Points marked X show the square of a cosinusoidal wave according to equation (7) and shows how closely the latter approximates the actual voltage distribution given by the complicated expression of equation (5). This result is considered to be of great value, especially when an attempt is made to calculate the electric field intensity in the vicinity of the short line.

In equation (5) when $y=0$, the ratio of voltage at the end of the line to the voltage of excitation source per unit length is obtained. This is

$$\left|\frac{E_{y=0}}{E_o}\right|^2 = \left[\frac{1}{2\alpha}\sinh 2\alpha L + \frac{f_o L}{4\pi f}\sin\frac{4\pi f}{f_o}\right] \times \left(\cosh 2\alpha L - \cos 4\pi f/f_o\right)^{-1} \qquad (8)$$

For frequencies which are multiples of one-half the resonant frequency, that is for $f/f_o = \frac{1}{2}k$, $k = 1,2,\ldots,$ it simplifies to

$$\frac{|E_{y=0}|^2}{|E_o|^2} = \frac{1}{2\alpha} \coth \alpha L \quad . \qquad (9)$$

A very important quantity is the voltage at the center of the line obtained from equation (5) when $y = \frac{1}{2} L$. This is

$$\left|\frac{E_{L/2}}{E_o}\right|^2 = \frac{1}{4} \frac{L}{\cosh \alpha L - \cos 2\pi f/f_o} \left[\frac{\sinh \alpha L}{\alpha L} + \frac{\sin 2\pi f/f_o}{2\pi f/f_o} \right] \quad .... \quad (10)$$

This is plotted in Figure 5 for L ranging from 0.1 to 1.0 mile and f/f_o ranging from 0.5 to 10.0. In order that a comparison may be made when α is held constant at all frequencies and when α is assumed to vary as the square root of frequency according to equation (6), curves have been drawn for $\alpha = 1.0$ and for $\alpha = 10^{-3} f^{\frac{1}{2}}$.

Some important observations are made at this stage:

i) when α is constant at 1.0 neper/mile, peaks and nulls are independent of frequency ratio f/f_o. Higher values for peaks and lower values for nulls are indicated as line length L is decreased from 1 mile to 0.1 mile;

ii) when $\alpha = 10^{-3} f^{\frac{1}{2}}$, peaks and nulls depend upon f/f_o ratio. Higher values for peaks are now indicated as L is increased from 0.1 mile to 1 mile. This situation is converse of that occuring when α is held constant because of increasing attenuation encountered at higher frequencies involved in a shorter line;

iii) Nulls appear to be independent of frequency, but not quite. Even though their values are low, they have considerable influence on the evaluation of geometric mean value of the peaks and nulls and thereby estimate the RI values of a long line.

III.5 CONVERSION OF SHORT-LINE RIV TO EXPECTED RIV LEVEL OF LONG LINE

Equation (10) for the ratio of RIV at the line center to the voltage of the source of excitation is one of the most important equations in Radio Interference work, for it allows the conversion of RIV values measured from a short line to the expected value of RIV of a long line with similar configuration.

When the limit of equation (10) is evaluated for $L = \infty$, the RIV value of a long line is obtained, thus:

$$|E(f)|^2_{\text{long line}} / |E_o(f)|^2 = 1/\alpha \quad , \qquad (11)$$

or,

$$|E(f)| = \alpha^{-\frac{1}{2}} |E_o(f)| \quad .$$

Having established the expected long-line level it is now necessary to enquire the method of obtaining the long-line RIV level from measurements made of the standing-wave frequency spectrum, at the center of the short experimental line.

From practical measurement of spectra of frequency of RI under the center of a short experimental line, (11), it has been observed that the peaks of the standing wave occur

at even multiples and nulls or minima occur at odd multiples of one half the resonant frequency. Using these observed properties of RI measured at ground level, it is assumed that a similar property exists for the RIV existing on the conductor.

Evaluation of values of frequency ratio f/f_o at which maxima and minima of equation (10) occur is quite difficult because of the resulting transcendental equation from which f/f_o value has to be solved for. The situation is further complicated when the attenuation factor α is assumed to vary as the square root of frequency f. When α is taken to be a constant and independent of frequency, a numerical calculation shows that successive maxima of the expression in equation (10) occur when f/f_o is an integer. Except for the first minimum value, all other minima of equation (10) occur when the frequency ratio f/f_o equals $\frac{1}{2}(2k+1)$, $k = 1,2,\ldots$, that is at frequencies which are odd multiples of one-half the resonant frequency f_o. The first minimum is displaced from $f/f_o = 0.5$, and occurs at $f/f_o = 0.6$.

In a practical situation, if the measured frequency spectrum of RIV shows a very large number of peaks and nulls, that is maxima and minima, the first null or minimum value may usually be ignored in evaluating the expected RIV level of a long line from the RIV measurement of the short line.

Using the above properties, the maxima of RIV occuring at the line center are obtained by substituting $f/f_o = k$, an integer, in equation (10), thus:

$$\frac{|E(f)|^2_{max}}{|E_o(f)|^2} = \frac{L}{\cosh \alpha L - \cos 2\pi \frac{f}{f_o}} \left[\frac{\sinh \alpha L}{\alpha L} + \frac{\sin 2\pi f/f_o}{2\pi f/f_o} \right] \Bigg|_{\frac{f}{f_o}=k}$$

$$= \frac{L}{\cosh \alpha L - 1} \qquad \frac{\sinh \alpha L}{\alpha L} = \frac{1}{\alpha} \coth \frac{\alpha L}{2} . \qquad (13)$$

This gives the equation to the curve passing through the peaks of the frequency spectrum of RIV.

The minima of the frequency spectrum are given for $f/f_o = \frac{1}{2}(2k - 1)$ in equation (10), thus:

$$\frac{|E(f)|^2_{min}}{|E_o(f)|^2} = \frac{L}{\cosh \alpha L - \cos 2\pi \frac{f}{f_o}} \left[\frac{\sinh \alpha L}{\alpha L} + \frac{\sin 2\pi f/f_o}{2\pi f/f_o} \right] \Bigg|_{\frac{f}{f_o}=\frac{2K-1}{2}}$$

$$= \frac{L}{\cosh \alpha L + 1} \left[\frac{\sinh \alpha L}{\alpha L} \right] = \frac{1}{\alpha} \tanh \frac{\alpha L}{2} . \qquad (14)$$

This is the equation to the curve passing through the minima. The two curves corresponding to equations (13) and (14) are indicated in Figure 6 for a positive corona pulse possessing the frequency spectrum

$$|E_o(f)|^2 = F^2 \left[(a^2 + \omega^2)(b^2 + \omega^2) \right]^{-1} . \qquad (15)$$

When the geometric mean value of the curves passing through the peaks and nulls is evaluated, one has

$$|E_{gm}|^2 = \left[|E_{max}|^2 \cdot |E_{min}|^2 \right]^{\frac{1}{2}} = \alpha^{-1} |E_o(f)|^2 \qquad (16)$$

or,

$$|E_{gm}| = \alpha^{-\frac{1}{2}} |E_o| . \qquad (17)$$

But equation (17) is identical to equation (11) which is the expected RIV level of a long line. Thus the proof of the

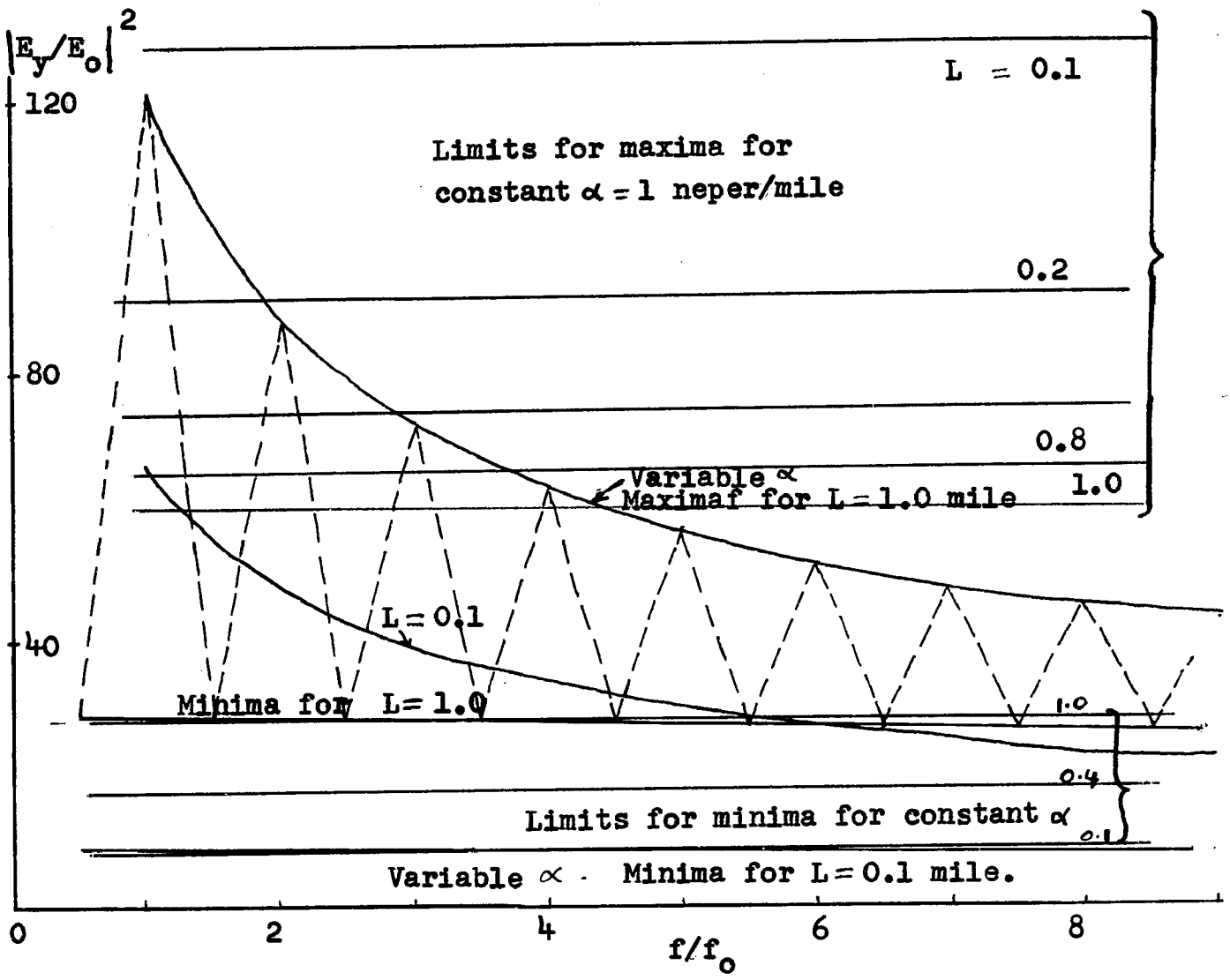

Figure 5. Standing Waves at Line Center for Variable and Constant α .

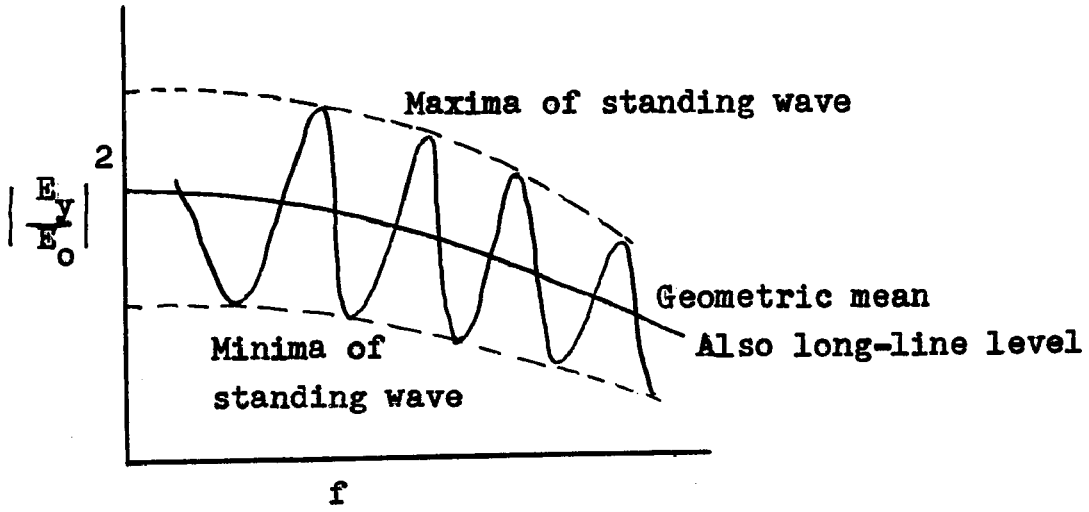

Figure 6. Calculation of Long Line RIV from Short Line Standing Wave Measured under Center

geometric mean method for evaluating the RIV level of a long line from measurements made of RIV at the center of a short line has been established.

One of the important procedures for obtaining the RIV level of an infinitely long line from measurements made of RIV at the center of a short line can now be summarized as follows:

i) Measure the RIV at the center of a short line over a wide range of frequencies.

ii) Draw a curve passing through the maxima of the frequency spectrum thus obtained, and a second curve passing through the minima.

iii) At every frequency, evaluate the geometric mean of the two values obtained from these two curves. This gives a third curve which is the expected RIV level of a long line having the same configuration.

From equations (10) and (11), the ratio of measured value of RIV at the center of a short line to the expected level of a long line is obtained as

$$\frac{|E_{L/2}(f)|^2}{|E|^2} = \frac{\alpha L}{\cosh \alpha L - \cos 2\pi f/f_o}\left[\frac{\sinh \alpha L}{\alpha L} + \frac{\sin 2\pi f/f_o}{2\pi f/f_o}\right] \quad (18)$$

In actual practice, the most important frequency at which RIV is of interest lies near 1.0 MHz. From Figure 5 it may be observed that if this frequency is very close to one half the resonant frequency or its odd multiples, noise readings will be very low at the line center. However, as

mentioned in Section III.2, when the longitudinal profile is available, the noise meter can be moved longitudinally to a location where the meter reading does give the long-line level.

III.6 ELECTRIC FIELD INTENSITY AT GROUND LEVEL IN THE VICINITY OF A SHORT LINE

The distribution of voltage to ground along the conductor of a short line has been derived in Section III.4, equation (8). The corresponding charge distribution is

$$|q_\ell| = |E_\ell| \quad C \quad ,$$

where q_ℓ = charge per unit length,

and C = capacitance of line to ground per unit length.

It is now necessary to evaluate the vertical component of electric field intensity at a pointP along ground in a plane passing through the center of line and at right angles to it. The origin of the coordinate system is taken at one end of the line so that the coordinates of the point P are (L/2, y, H), as shown in Figure 7. The electric potential ϕ_P at P can be determined first, from which the vertical component of electric field intensity can be found out as the negative partial derivative of ϕ_P with respect to z evaluated at $z = H$.

The electric potential at P is the retarded potential caused by the distribution of charge along the entire length of the short line, and is given by the expression, (12),

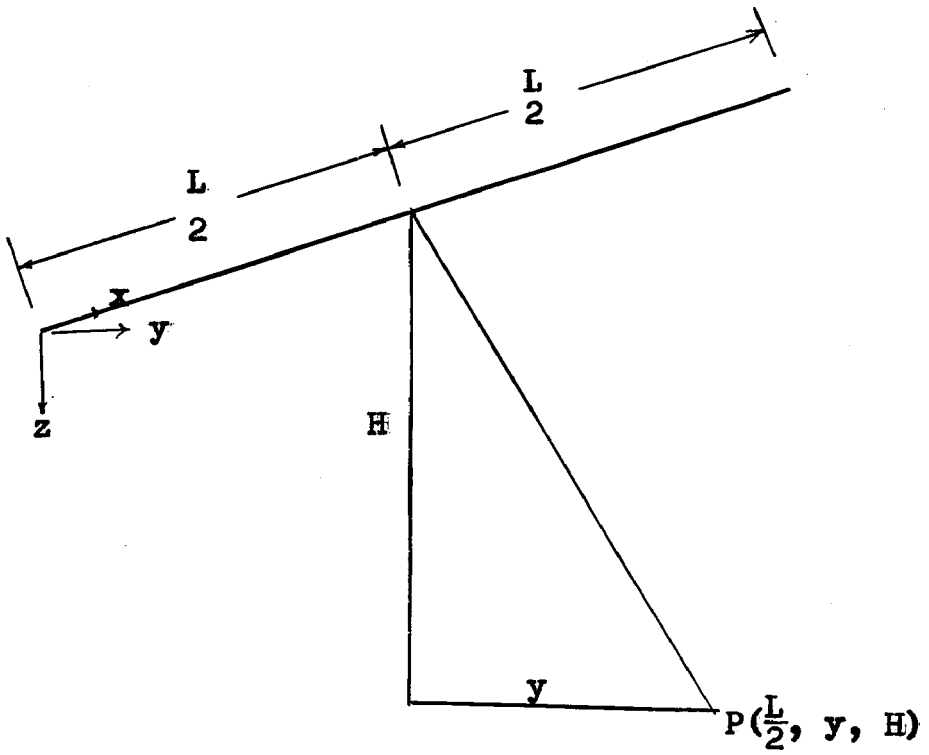

Figure 7

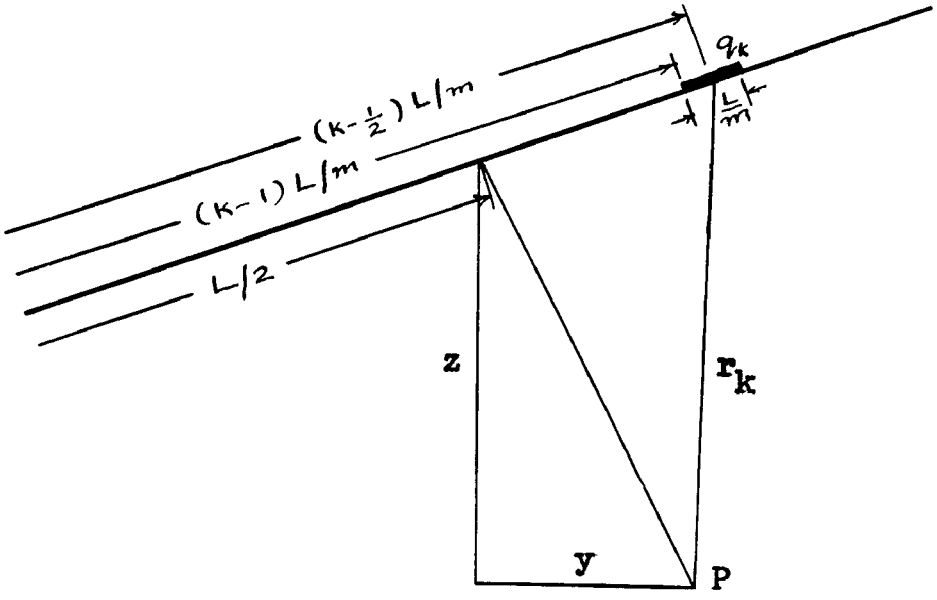

Figure 8

$$\phi_P = \frac{1}{4\pi\epsilon} \int_0^L \frac{q_\ell \; e^{-j\upsilon r}}{r} \, dl \qquad (19)$$

where ϵ = permittivity of free space = 8.854 $\mu\mu$F/m,

$\upsilon = \omega/v = 2\pi/\lambda$,

v = velocity of electromagnetic wave,

and λ = wave length.

Equation (19) applies at a single frequency and the factor exp $(-j\omega t)$ has been omitted from writing.

The integral in equation (19) is extremely difficult to evaluate in closed form on account of the complexity involved in q_ℓ , which is obtained from equation (5) or approximated to a cosinusoidal form as in equation (7). A numerical method is therefore resorted to. The line length is divided into a finite number 'm' equal lengths and the total charge on each part is calculated. The radius vector r_k, $(k = 1,2, \ldots, m)$ from the middle of each part to the point P is then determined and this is used for calculating the retarded potential. The integral then becomes the sum of m terms.

Figure 8 shows the line length divided into m equal parts each of length L/m. The distance from the middle of the k-th part to the point P on ground will be

$$r_k = \left\{ z^2 + y^2 + \left[(k-\tfrac{1}{2}) \, L/m - \tfrac{1}{2} L \right]^2 \right\}^{\frac{1}{2}} . \qquad (20)$$

Therefore, $$\partial r_k / \partial z = z/r_k \; . \qquad (21)$$

The potential at P due to the element of charge q_k of the

k-th part is

$$\phi_k = \frac{1}{4\pi\epsilon} \; q_k \; \frac{1}{r_k} \; \cos \omega (t - r_k/v) \quad . \qquad (22)$$

The vertical component of electric field intensity at P due to the charge q_k and its image below ground is then

$$\begin{aligned} \Delta E_v &= -2 \; \partial \phi_k / \partial z \\ &= \frac{2z}{4\pi\epsilon} \, q_k \left[r_k^{-3} \cos (\omega t - 2\pi r_k/\lambda) \right. \\ &\qquad \left. - r_k^{-2} \sin (\omega t - 2\pi r_k/\lambda) \right] \quad . \qquad (23) \end{aligned}$$

The total contribution to the vertical component of field intensity from the charge along the entire length of line consisting of all the 'm' equal parts will then be

$$E_v = \frac{z}{2\pi\epsilon} \sum_{k=1}^{m} q_k \left[r_k^{-3} \cos (\omega t - 2\pi r_k/\lambda) \right. \\ \left. - r_k^{-2} \sin (\omega t - 2\pi r_k/\lambda) \right] \quad . \qquad (24)$$

The vertical component of field intensity at P on the ground is finally obtained by replacing z by H in equation (24), thus:

$$E_v = \frac{H}{2\pi\epsilon} \sum_{k=1}^{m} \frac{q_k}{r_k^3} \; (1 + r_k^2)^{\frac{1}{2}} \; \cos \left(\omega t - \frac{2\pi r_k}{\lambda} + \psi_k\right), \qquad \ldots (25)$$

where $\tan \psi_k = r_k$.

In practical situations, when the line height is more than 10 meters, the angle ψ_k is 90°. This gives

$$E_v = \frac{H}{2\pi\epsilon} \sum_{k=1}^{m} - q_k \, r_k^{-2} \sin (\omega t - 2\pi r_k/\lambda) \quad . \qquad (26)$$

This amounts to taking only the second term of equation (23). With this approximation, the vertical component of field intensity at P is

$$E_v = -\frac{H}{2\pi\epsilon} \sum_{k=1}^{m} q_k r_k^{-2} \left(\sin\omega t \cos 2\pi r_k/\lambda - \cos\omega t \sin 2\pi r_k/\lambda \right)$$

$$= \frac{H}{2\pi\epsilon}\left[\left(-\sum_{k=1}^{m} q_k r_k^{-2} \cos 2\pi r_k/\lambda \right) \sin\omega t + \left(\sum_{k=1}^{m} q_k r_k^{-2} \sin 2\pi r_k/\lambda \right) \cos\omega t \right]$$

$$= \frac{H}{2\pi\epsilon}\left[\left(\sum_{k=1}^{m} q_k r_k^{-2} \sin 2\pi r_k/\lambda \right)^2 + \left(\sum_{k=1}^{m} q_k r_k^{-2} \cos 2\pi r_k/\lambda \right)^2 \right]^{\frac{1}{2}} \cos(\omega t + \phi) \quad \ldots (27)$$

where

$$\tan\phi = \left(\sum_{k=1}^{m} q_k r_k^{-2} \cos 2\pi r_k/\lambda \right) \Big/ \left(\sum_{k=1}^{m} q_k r_k^{-2} \sin \frac{2\pi r_k}{\lambda} \right) \quad \ldots (28)$$

The amplitude of E_v is

$$|E_v| = \frac{H}{2\pi\epsilon}\left[\left(\sum_{k=1}^{m} q_k r_k^{-2} \cos \frac{2\pi r_k}{\lambda} \right)^2 + \left(\sum_{k=1}^{m} \frac{q_k}{r_k^2} \sin \frac{2\pi r_k}{\lambda} \right)^2 \right]^{1/2} \quad \ldots . (29)$$

Lateral attenuation of this field intensity is determined as the ratio 'μ' of E_v at a given value of y to that at y= 0, that is under the line. This is

$$\mu = \frac{|E_v|_{y=y}}{|E_v|_{y=0}} = \frac{\left[\left(\sum_{k=1}^{m} q_k r_k^{-2} \cos 2\pi r_k/\lambda \right)^2 + \left(\sum_{k=1}^{m} q_k r_k^{-2} \sin 2\pi r_k/\lambda \right)^2 \right]^{1/2}}{\left[\left(\sum_{k=1}^{m} q_k r_{ko}^{-2} \cos 2\pi r_{ko}/\lambda \right)^2 + \left(\sum_{k=1}^{m} q_k r_{ko}^{-2} \sin 2\pi r_{ko}/\lambda \right)^2 \right]^{1/2}} \quad \ldots (30)$$

When the charge distribution on the conductor is assumed to have a cosinusoidal variation, it may be expressed as

$$q = Q \cos 2\pi f \ell / f_o L. \tag{31}$$

Then

$$q_k = \int_{(k-1)L/m}^{kL/m} q \, d\ell$$

$$= \frac{Q f_o L}{\pi f} \cos \frac{2\pi f}{f_o m} (k - \tfrac{1}{2}) \sin \frac{\pi f}{m f_o} . \tag{32}$$

Figures 9 and 10 show calculated values of lateral attenuation 'μ', for line lengths of 120 meters and 800 meters, and line height $H = 12.5$ meters, and for several values of f/f_o. On the same figure are plotted two curves according to the expressions $\mu = 1/r$ and $1/r^2$, where r = the aerial distance of P from the center of the overhead conductor. As the line length is increased (800 meters) and frequency is lowered $(f/f_o = 0.25)$, the variation of electric field intensity from the short line approaches the inverse square law type of attenuation with distance from line.

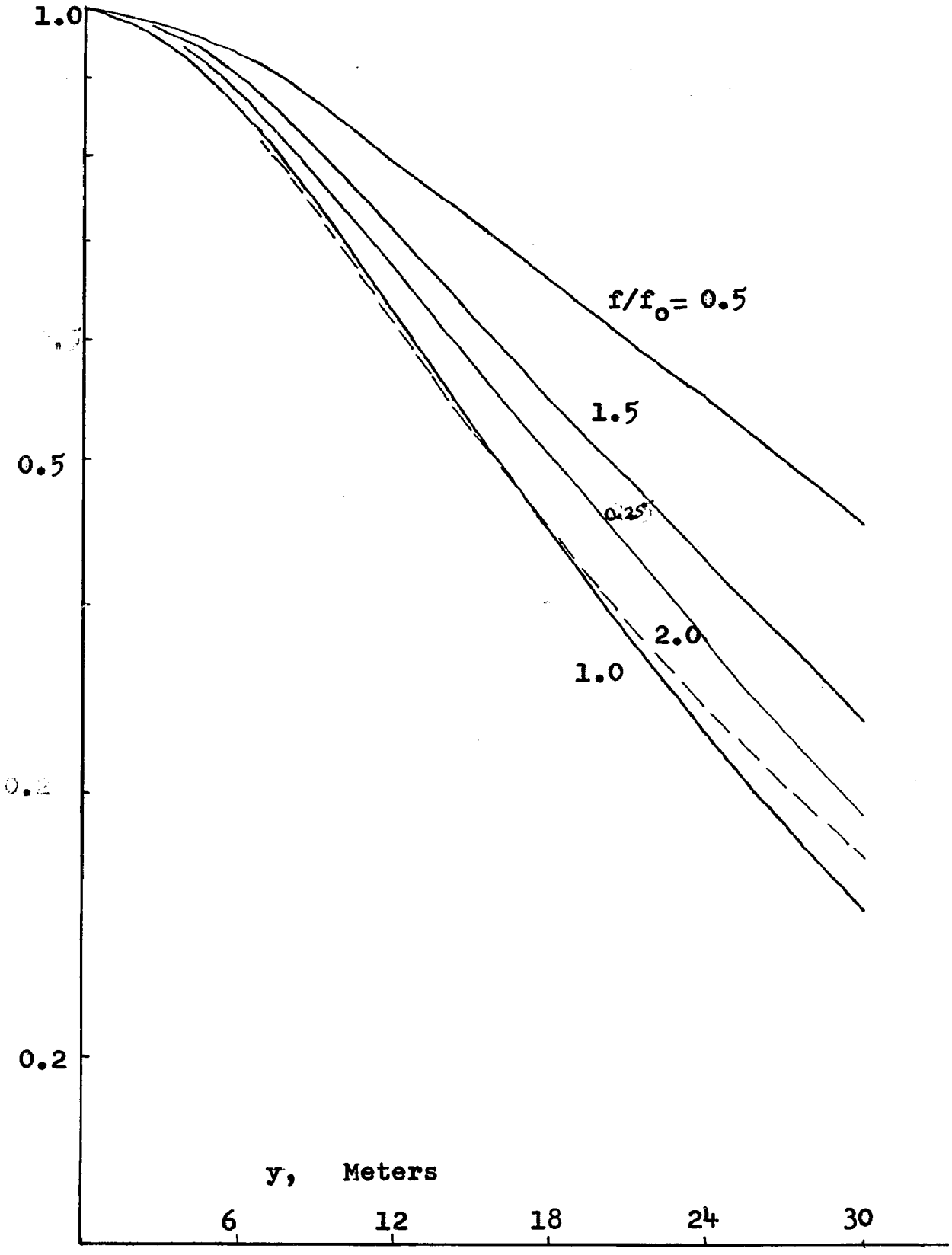

Figure 9. Lateral Attenuatuon of RI. L = 120 meters
H = 12.5 meters

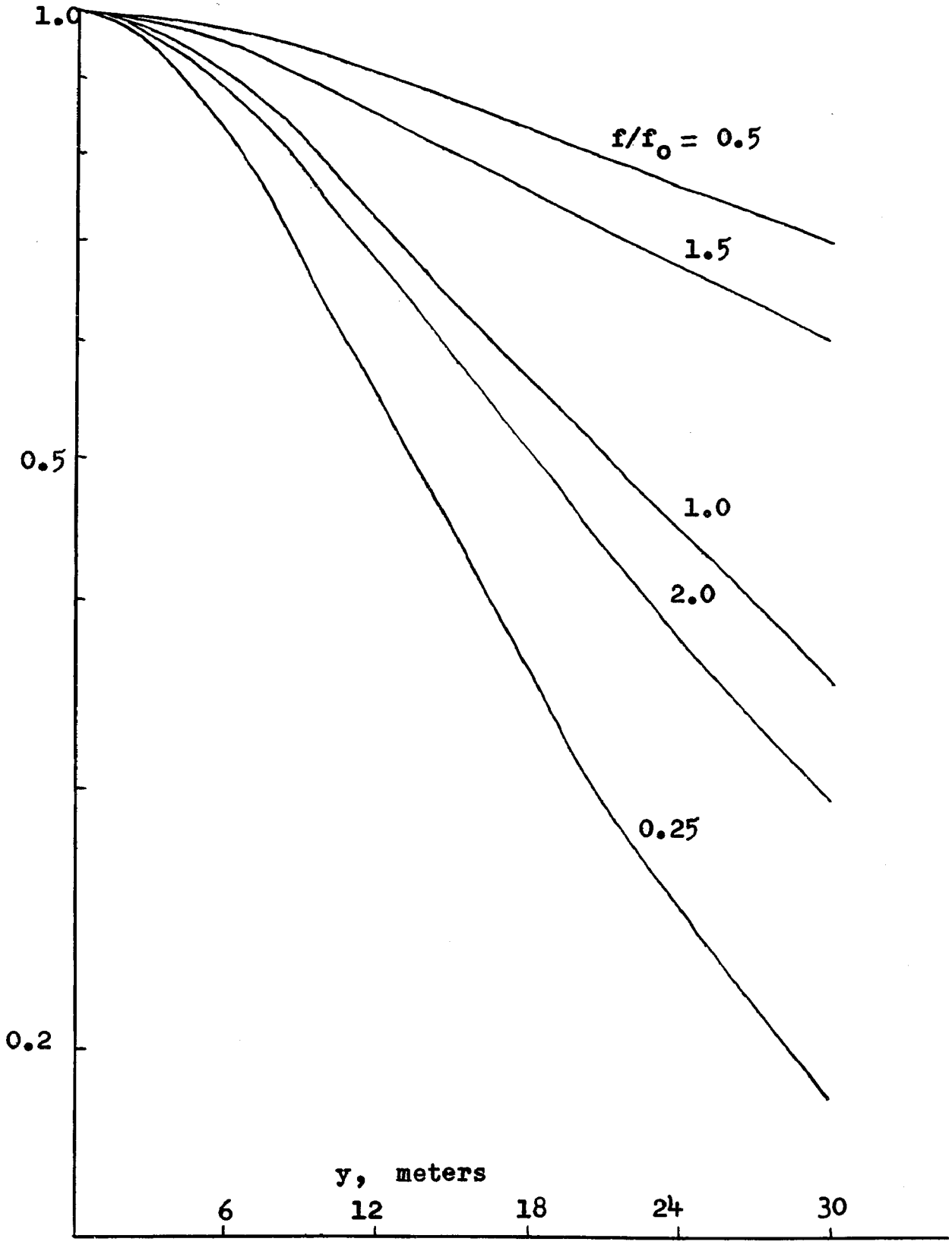

Figure 10. Lateral Attenuation of RI.

L = 800 meters H = 12.5 meters

C H A P T E R IV

PREDICTION OF RADIO INTERFERENCE LEVELS OF LONG D-C TRANSMISSION LINES

IV.1 INTRODUCTION

In selecting the size and configuration of conductors for a given operating voltage from its radio-interference characteristics, several alternative designs have to be worked out before a final choice of design is made. In doing so, it is necessary to have information on the following items:

a) limits for tolerable RI from transmission lines;

b) variation of RIV of conductor with applied voltage;

c) working voltage for conductors of given size and configuration at which the limit of tolerable RI is reached; and

d) comparison of RI levels of the same or different sizes of conductor in different configurations.

Information on the last three topics can be obtained from experiments conducted with short experimental lines, (1 - 8), combined with experience gained from long lines in operation at lower voltages. In the case of d-c transmission only one long line has just been placed in operation in the Western part of U.S.A. after a series of excellent investigations with short lines. Short experimental lines have therefore to be still relied upon to yield information for projected higher voltage d-c transmission lines.

It has become apparent from experience gained all over the world where experimental projects with short lines exist, that it is not feasible to test an extremely large number of conductor sizes in different configurations and thereby obtain design data for use in long lines. In most cases, a conductor size which would be nearly suitable for a chosen voltage level isselected and a size smaller and larger are tested in order to be able to decide on the final size. The choice of conduc- size for use in short lines themselves is based on experience gained with lower voltage lines as well as the designer's background experience. Under these restrictions, it is evident that some method of predicting the RI levels of conductors used for d-c transmission lines should be available so that a large number of alternative designs can be examined.

Obtaining test data on a large number of conductor sizes is very expensive and time consuming because of the predominant role played by weather conditions on radio interference levels. This means that one has to test conductors under all possible weather conditions before being sure that the line when finally designed will operate satisfactorily under all weather conditions without exceeding the set RI limits. It is therefore beneficial to know the variables in the problem and the extent of their effect on RI levels. Many of the important weather variables and their quantitative effect on RI levels of d-c lines are gradually being ascertained with extreme care in the laboratory wherever possible and on actual outdoor conductors. These variables are:

a) cloud conditions;

b) rate and intensity of rainfall;

c) type, rate and intensity of snowfall;

d) wind velocity and direction;

e) humidity;

f) floating particles of organic and inorganic matter in the atmosphere;

g) ice coating; and

h) atmospheric contamination.

Effect of these atmospheric conditions can be included in design procedures by suitable empirical correction factors, except for transient and unforeseen deposits on conductors caused by birds and insects. As data accumulates on the effect of the above factors, either individually or in combinations, design predictions become more certain. In this chapter an analytical method for predicting radio noise levels of conductors will be derived which will include the effect of weather conditions. The results of analysis will then be compared with test results to a limited extent in order to show the validity of the analytical procedure and its results. The procedure set forth is based on relatively few assumptions that are fundamental to the problem and have an experimental basis.

IV.2 RELATIVE INTERFERENCE LEVEL

As mentioned earlier it is a difficult matter, financially and temporally, to obtain RI levels of an extremely

large number of conductors in all possible configurations. Therefore if noise levels of a large number of sizes in many configurations can be compared theoretically, and if experimental results on one or two sizes ofconductors are available, then it follows naturally that the RI levels of any conductor size can be determined. A method of calculating these "relative interference levels" is therefore of basic importance. In this chapter, a method of calculating relative interference level of a conductor in a given configuration will be derived. From experimental data available to the author on a few conductor sizes the validity of the method will be proved. From the analytical procedure the size and configuration suitable for a large number of voltage levels will then be derived. Results of this chapter can be used for the design of transmission lines for d-c from the point of view of their RI limitation.

The following four configurations have been selected for purposes of calculation:

1. Single conductor in monopolar line;
2. Two-bundle conductor in monopolar line;
3. Single conductor in bipolar line; and
4. Two-bundle conductor in bipolar line.

These are the most usual conductor configurations used in practice.

The analytical procedure for calculating relative interference levels is based on the following assumptions which

are derived from experimental results:

1. Radio Influence Voltage (RIV) of a conductor (QP value) follows the following types of variation with excitation voltage:

   i) RIV proportional to voltage;

   ii) Log (RIV), i.e. the DB value, proportional to voltage.

2. Variation of RIV with weather conditions at a given voltage is expressible by a single factor, called the Weather Factor or the w-factor;

3. Corona-inception gradient on a smooth conductor is given by Peek's formula for air density of 1 as follows:

$$G_{os} = 30\ (1 + 0.308\ r^{-\frac{1}{2}})\ \text{kv/cm} \qquad (1)$$

   For stranded conductor with a rough surface, it is

$$G_o = m\ G_{os} = 30\ m\ (1 + 0.308\ r^{-\frac{1}{2}})\ \text{kv/cm.} \qquad (2)$$

   The factor 'm' is called the surface environment factor and is less than unity. Correction for air density is included in m.

4. Every unit surface area of aluminum of a conductor, regardless of its outer diameter, yields the same amount of r-f energy under the same weather and for the same excess voltage gradient above the corona-inception value.

5. The QP reading of a noise meter is proportional to the square root of the r-f energy at a given frequency in the corona discharge.

IV.3 VARIATION OF R-F ENERGY WITH APPLIED VOLTAGE

Variation of RIV at a definite frequency in the corona discharge varies non-linearly with voltage as shown in Figure 1. This variation can be completely expressed by a power series, Thus:

$$RIV = \sum_{i=1}^{\infty} a_i V^i \qquad (3)$$

This expression is quite difficult to handle and is not of much practical use, because the voltage of a conductor in nearly all practical cases does not vary over a wide range, but only within a small range near the corona-inception voltage. Simpler relations between the applied voltage and RIV are sought for which apply within definite ranges of excitation voltage. Two such expressions that are found to apply are

i) linear variation of RIV with applied voltage, V, and

ii) linear variation of decibel value of RIV with applied voltage.

When RIV of a conductor varies linearly with applied voltage, it can be expressed as

$$RIV = A + \frac{1}{w_1' k} V \quad . \qquad (5)$$

Since RIV is zero at the corona-inception voltage V_o, we have

$$RIV = (w_1' k)^{-1} (V-V_o) \qquad (6)$$

where A and w_1' depend on the weather conditions and 'k' is a geometrical constant for a given conductor and line configuration. It converts voltages into surface voltage gradients on the conductor. Its values are discussed in Section IV.8.

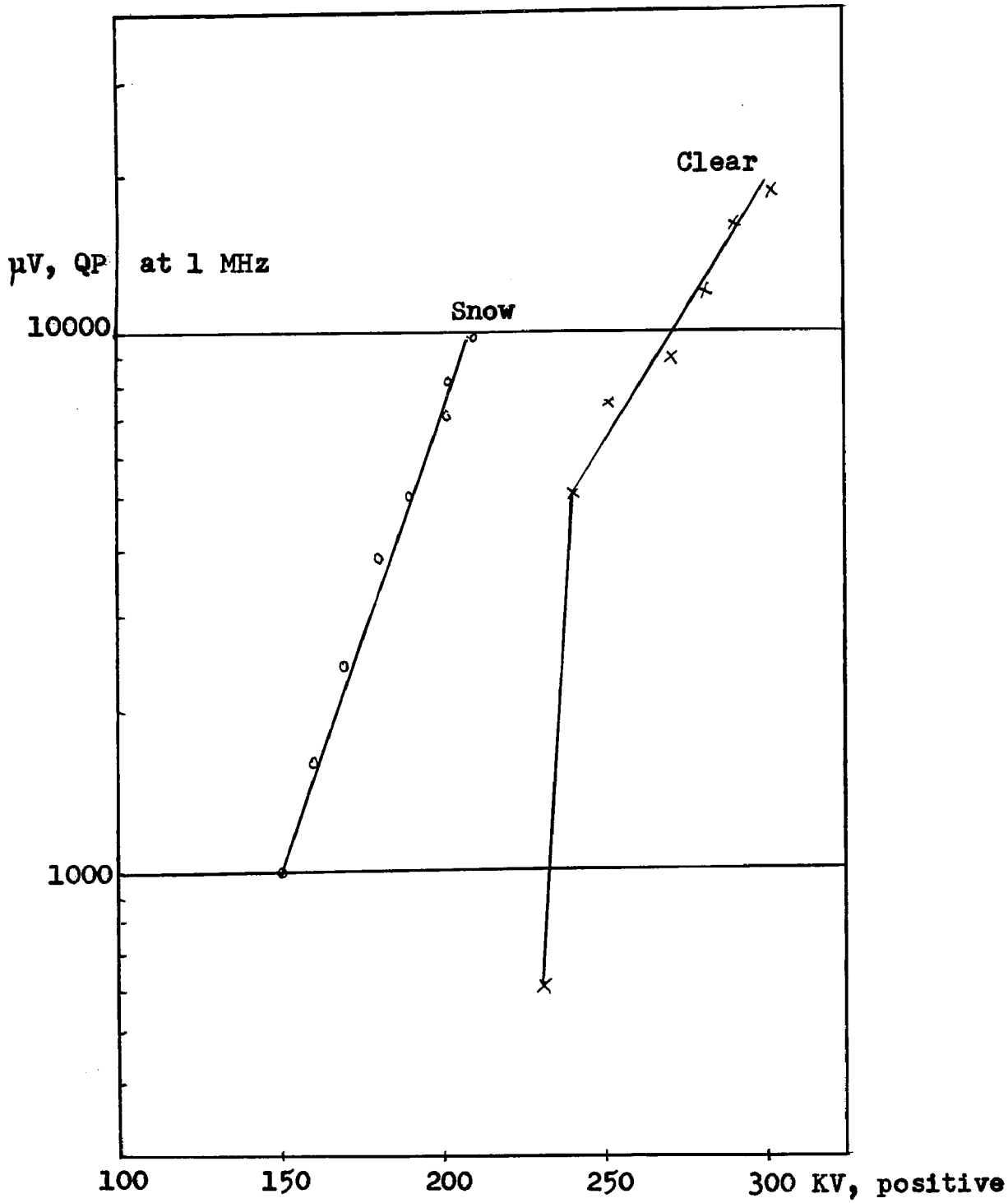

Figure 1. Variation of RIV with Applied Voltage.

Lark Conductor 0.806-inch Diameter

The corona-inception voltage is

$$V_o = G_o\, k = 30\, m\, (1 + 0.308\, r^{-\frac{1}{2}})\, k \,. \qquad (7)$$

The r-f energy per unit area is also assumed to have the same type of variation with voltage as the square of RIV and can be described by the equation

$$\sigma = (w_1\, k^2)^{-1}\ (V - V_o)^2 \,. \qquad (8)$$

This is called the spectral density of r-f energy at a given frequency. The total energy in the corona pulse activity per unit length of conductor will be

$$S_1 = B\, 2\pi\, r\, w_1^{-1}\ k^{-2}\ (V - V_o)^2 \qquad (9)$$

Under the assumption that every unit surface area of conductor gives the same amount of r-f energy for equal values of w_1 and $g = (V-V_o)/k$, the excess gradient above the corona-inception gradient, the value of constant B in equation (9) becomes the same for all conductors. Hence it can be set equal to unity if only comparison of RIV levels are being carried out. Thus

$$S_1 = 2\pi\, r\ w_1^{-1}\, k^{-2}\ (V - V_o)^2 \,. \qquad (10)$$

When the DB value of RIV varies linearly with voltage, it may be expressed by

$$20\ \mathrm{Log}_{10}(\mathrm{RIV}) = (V - V_o)/2\, k\, w_2' \qquad (11)$$

or,

$$\mathrm{RIV} = C\, 10^{(V-V_o)/2\, k\, w_2'} \qquad (12)$$

where

$$w_2 = w_2'/20.$$

Since only the relative values of noise levels are of interest,

the constant C can be set equal to unity and the r-f energy per unit surface area of conductor will be

$$\sigma = 10^{(V-V_o)/k\, w_2} = 10^{g/w_2} \qquad (13)$$

This gives the energy generated by unit length of conductor as

$$S_2 = 2\pi r\ 10^{g/w_2} = 2\pi r\ 10^{(V-V_o)/k\, w_2} \qquad (14)$$

Of these two types of variation, the former applies to laboratory studies as described in Chapter I and the latter applies to larger conductors tested outdoors.

The relative interference levels of conductors can now be derived when the variation of linear energy density is given by equations (10) or (14). They will be carried out for four particular cases of conductor configuration mentioned in Section IV.2, page 116.

IV.4 SINGLE CONDUCTOR IN MONOPOLAR CONFIGURATION

The density of r-f energy per unit area of conductor surface is

$$\text{i)}\quad \sigma = w_1^{-1} g^2 = w_1^{-1} k_{1m}^{-2} (V - V_o)^2 \qquad (15)$$

$$\text{ii)}\quad \sigma = 10^{g/w_2} = 10^{(V-V_o)/k_{1m} w_2} \qquad (16)$$

where w_1 and w_2 are constants and depend on weather,

g = voltage gradient in excess of corona-inception gradient $= G - G_o$,

G_o = corona-inception gradient $= V_o/k_{1m}$,

G = surface voltage gradient on conductor $= V/k_{1m}$,

V = applied voltage,

V_o = corona inception voltage,

and k_{1m} = ratio of voltage to surface voltage gradient

$$= r \text{ Ln } (2H/r) \ . \tag{17}$$

The total energy developed over a unit length of conductor, the linear generation density, is

$$S = 2\pi r \sigma \tag{18}$$

Then the r-f energy over a differential length dl of the conductor is $S\ dl$. This energy divides itself into two equal portions and travels on the conductor on both sides of the source, as shown in Figure 2. In doing so it attenuates by 2α nepers per unit length. The energy received at a point P at distance l from the source will be

$$\tfrac{1}{2} S\ dl\ \ e^{-2\alpha l} \tag{19}$$

and the total energy received at P from the entire line is

$$W = 2 \int_0^\infty \tfrac{1}{2} S\ e^{-2\alpha l}\ \ dl = S/2\alpha = \pi r \sigma / \alpha \tag{20}$$

where thetwo types of variation of σ are given in equations (15) and (16). The quantity W is called the relative interference level of radio influence voltage. It denotes a quantity proportional to the r-f energy present on the conductor at a fixed frequency. Its decibel value is

$$DB = 10 \text{ Log}_{10} W \tag{21}$$

It is afunction of a) conductor radius, r; b) applied voltage, V; c) corona-inception voltage, V_o; d) line height H which enters in the factor k_{1m}; e) the attenuation factor, α ;

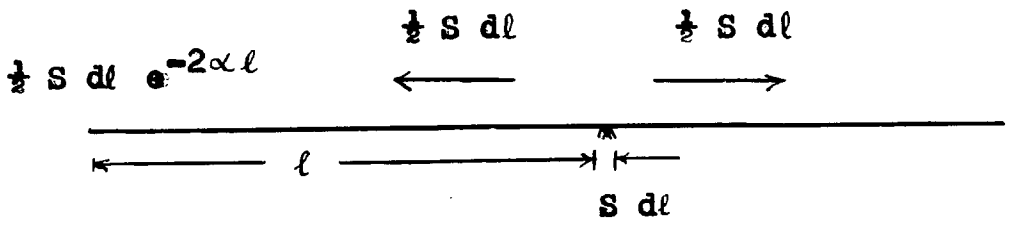

Figure 2

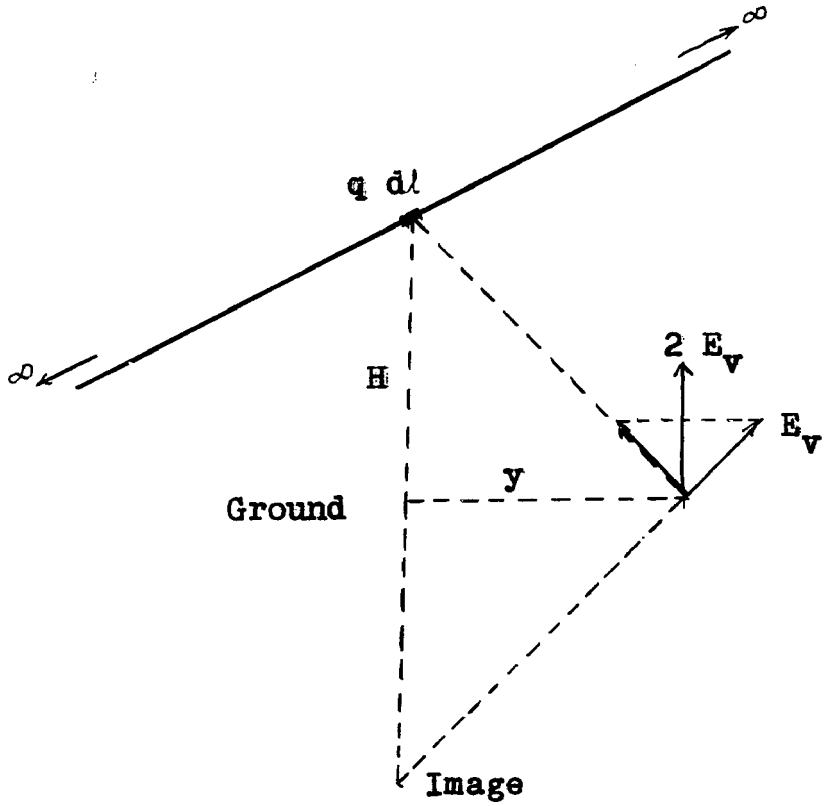

Figure 3

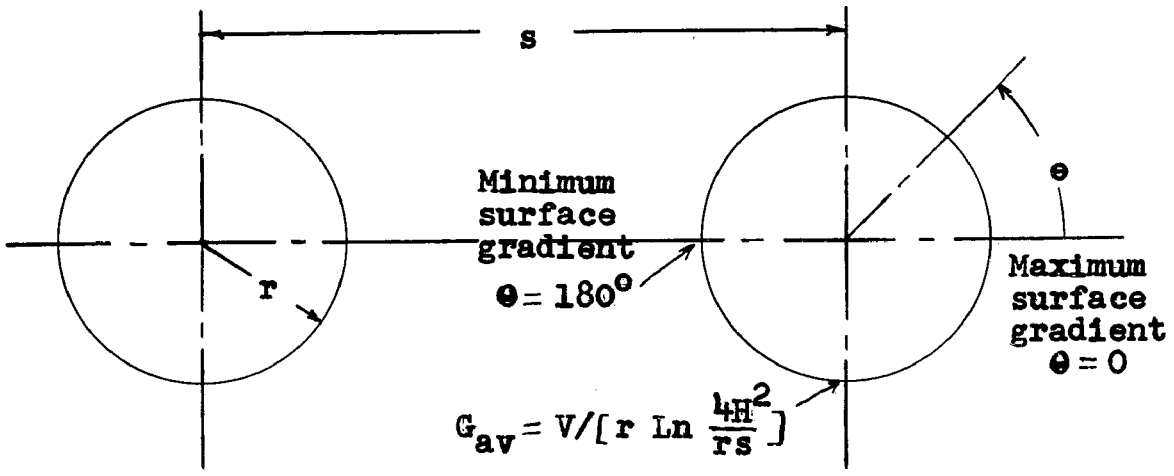

Figure 4. Two-bundle Conductor

and the weather constants, w_1 or w_2. The expression for W of the r-f energy at the conductor, or its DB value, as it stands can be used for making the following types of comparison:

a) RIV levels of a given size of conductor in different weather conditions;

b) RIV levels of two different sizes of conductor under the same weather condition or under different weather conditions;

c) RIV levels of conductors when line height is varied;

and d) RIV levels of single conductor with two-bundle conductor in monopolar configuration.

In order that comparison of RI levels of a monopolar line with a bipolar line may be effected, it is necessary to evaluate the vertical component of electric field intensity at ground level. This can be done when it is realized that the total energy at a point P on the line is proportional to the square of the charge or voltage existing on the conductor. Figure 3 shows a conductor having a charge q per unit length. When the ground surface is assumed to be a good conductor, the electric field intensity at a point on ground can be evaluated from the charge q and its image (-q) at a distance H below the ground surface. One then obtains

$$\mathcal{E} = \frac{\text{vertical comp. of elec. field intensity at point y on ground}}{\text{charge per unit length of conductor}} = (2\pi\epsilon)^{-1} \; 2H\,(H^2 + y^2)^{-1} \qquad (22)$$

Therefore the energy involved in the vertical component of field intensity is

$$W_g = W \mathfrak{Z}^2 \tag{23}$$

and the 'relative' value of ground field intensity, or RI level is

$$E = W_g^{\frac{1}{2}} \quad . \tag{24}$$

Its decibel value is

$$DB_E = 10 \text{ Log}_{10} W_g = 10 \text{ Log}_{10} (W \mathfrak{Z}^2) \tag{25}$$

The final expressions for relative interference level for the two types of variation of W with applied voltage V will be as follows:

i) Linear variation of RIV of conductor with voltage:

$$(RIV)^2 = \pi r (w_1 \alpha)^{-1} k_{1m}^{-2} (V - V_o)^2 \tag{26}$$

$$(RI)^2 = \pi r (w_1 \alpha)^{-1} k_{1m}^{-2} (V - V_o)^2 \left(\frac{2H}{H^2 + y^2}\right)^2 \tag{27}$$

ii) Linear variation of Log (RIV) of conductor with applied voltage:

$$(RIV)^2 = \frac{\pi r}{\alpha} \; 10^{(V-V_o)/w_2} k_{1m} \tag{28}$$

$$(RI)^2 = \frac{\pi r}{\alpha} \; 10^{(V-V_o)/w_2} k_{1m} \left(\frac{2H}{H^2 + y^2}\right)^2 \tag{29}$$

IV.5 TWO-BUNDLE CONDUCTOR IN MONOPOLAR CONFIGURATION

On a two-bundle conductor, the surface voltage gradient varies on the periphery of each conductor, as shown in Figure 4. The maximum voltage gradient on a conductor is

$$G_{max} = \frac{q}{2\pi \epsilon r} \left(1 + \frac{2r}{s+r} \right) , \qquad (30)$$

where q = charge per unit length on each conductor,

and s = distance of separation between conductors.

The factor 2 is included in the second term in parenthesis to account for the fact that when a metallic cylinder is placed in a uniform electric field, the field intensity on the surface of cylinder is twice the intensity of the uniform field. The average surface voltage gradient on any one of the conductors of thebundle is obtained when the effect of charge on second conductor of bundle is neglected and is given by

$$G_{av} = q \, (2\pi \epsilon r)^{-1} = V/k_{2m} \qquad (31)$$

Variation of surface voltage gradient on conductor with the angle θ is expressed approximately by the expression

$$G = G_{av} \left(1 + 2r \cos \theta / (s+r) \right) . \qquad (32)$$

Because the voltage gradient on conductor varies with θ, it will so happen that the entire surface of conductor might not be generating r-f energy at any given voltage, unless the minimum surface voltage gradient G_{min}, exceeds the corona-inception gradient, G_o.

We can now determine the total r-f energy per unit length of the bundle when the spectral energy density has the two types of variation described by equations (8) or (13).

Case (i): Linear variation of RIV with voltage:

When σ is given by equation (8), the energy generated

over a differential angle $d\theta$ is

$$dS = \sigma\, r\, d\theta = w_1^{-1} (G - G_o)^2 r\, d\theta$$

$$= w_1^{-1} \left[G_{av} \left(1 + \frac{2r}{s+r} \cos\theta \right) - G_o \right]^2 r\, d\theta \quad .. \quad (33)$$

Therefore, the total energy generated by one conductor, when only a portion θ on either side of the point of maximum gradient $(\theta = 0)$ is in corona, is

$$S_\theta = \int dS = 2\int_0^\theta \frac{1}{w_1} \left[G_{av} - G_o + G_{av} \frac{2r}{s+r} \cos\theta \right]^2 r\, d\theta$$

$$= \frac{2r}{w_1} \left[(G_{av}-G_o)^2\theta + \frac{2r^2}{(s+r)^2} G_{av}^2\, \theta \right.$$

$$\left. + \frac{4r}{s+r} (G_{av}-G_o) \sin\theta + \frac{r^2}{(s+r)^2} G_{av}^2 \sin 2\theta \right]. \quad (34)$$

In the case when the entire periphery is in corona, the r-f energy generated by one conductor is obtained by using $\theta = \pi$ in equation (34). This is

$$S = \frac{4\pi r}{w_1} (G_{av} - G_o)^2 + \frac{4\pi r^3}{(s+r)^2 w_1} G_{av}^2$$

$$= \frac{4\pi r}{w_1 k_{2m}^2} (V - V_o)^2 + \frac{4\pi r^3}{w_1 (s+r)^2} \frac{V^2}{k_{2m}^2} \quad (35)$$

The total energy generated by the bundle is twice that of equation (35), thus

$$S_2 = \frac{8\pi r}{w_1 k_{2m}^2} \left[(V - V_o)^2 + \frac{r^2}{(s+r)^2} V^2 \right] \quad (36)$$

The value of k_{2m} is

$$k_{2m} = r \, \mathrm{Ln} \, (4H^2 / r\, s) \quad (37)$$

The voltage at which the entire surface of bundle generates r-f energy is determined when

$$V_s \left(1 - \frac{2r}{s+r} \right) = V_o \qquad (38)$$

or,
$$V_s = \frac{s+r}{s-r} V_o$$

$$= 30\, m \left(1 + \frac{0.308}{r^{\frac{1}{2}}}\right) r \, \mathrm{Ln} \left(\frac{4H^2}{rs}\right) \frac{s+r}{s-r} , \qquad (49)$$

upon using equations (2) and (37).

Case (ii): Linear variation of DB of RIV on conductor with voltage

When σ varies with voltage gradient according to equation (13), the energy generated over an angle $d\theta$ will be

$$dS = \sigma \, r \, d\theta = 10^{(G-G_o)/w_2} \, r \, d\theta \, . \qquad (40)$$

The total energy generated by one conductor of the bundle when only a portion θ of the conductor, on either side of $\theta=0$, is in corona will be

$$S_\theta = \int dS = 2r \int_0^\theta 10^{(G-G_o)/w_2} \, d\theta$$

$$= 2r \int_0^\theta 10^{\left[G_{av}(1 + 2r\cos\theta/(s+r)) - G_o\right]/w_2} \, d\theta$$

$$= 2r \int_0^\theta 10^{(G_{av} - G_2)/w_2} \cdot 10^{2r\, G_{av} \cos\theta/(s+r)w_2} \, d\theta$$

..... (41)

This integral can be evaluated by a numerical method using Simpson's 7- or 13- ordinate method. When the entire conductor surface is in corona, the total energy generated by the bundle is

$$S_2 = 4 \int_0^{\pi} r\, 10^{(G-G_o)/w_2}\, d\theta$$

$$= 4\pi r\, 10^{(G_{av}-G_o)/w_2}\, I_o\left(\frac{4.6\, r}{s\, w_2} G\right) \qquad (42)$$

where $I_o(x) =$ Bessel function of second kind and order zero. The integral in (42½ is of the standard form and given by Formula 813.1 in Dwight's Tables of Integrals, (9). Once again, the voltage at which the entire bundle generates r-f energy is determined by equation (39).

The final expressions for relative interference level for the two types of variation of σ with applied voltage, V, will be as follows:

i) Linear variation of RIV with voltage:

$$(RIV)^2 = \frac{4\pi r}{\alpha\, w_1\, k_{2m}^2} \left[(V-V_o)^2 + \frac{r^2}{(s+r)^2} V^2 \right] \qquad (43)$$

$$(RI)^2 = \frac{4\pi r}{\alpha\, w_1\, k_{2m}^2} \left[(V-V_o)^2 + \frac{r^2}{(s+r)^2} V^2 \right] \left(\frac{2H}{H^2+y^2}\right)^2 \qquad (44)$$

ii) Linear variation of DB of RIV with voltage:

$$(RIV)^2 = \frac{2\pi r}{\alpha}\, 10^{(V-V_o)/w_2}\, k_{2m}\, I_o\left(\frac{4.6\, r}{s\, w_2}\, \frac{V}{k_{2m}}\right) \qquad (45)$$

$$(RI)^2 = (RIV)^2 \left(\frac{2H}{H^2+y^2}\right)^2 \qquad (46)$$

All these four expressions are valid for $V > V_s$, the voltage at which the minimum gradient on the inside of the bundle equals the corona-inception gradient, equation (39).

IV.6 SINGLE CONDUCTOR IN BIPOLAR CONFIGURATION

The bipolar configuration differs from the monopolar case basically because of the existence of two modes of propagation for the r-f energy on the line. Figure 5 shows the voltages, currents and surge impedances of a bipolar line, which satisfy the following matrix equation:

$$\begin{bmatrix} v_1 \\ v_2 \end{bmatrix} = \begin{bmatrix} z\ , & z' \\ z', & z \end{bmatrix} \begin{bmatrix} i_1 \\ i_2 \end{bmatrix} \tag{47}$$

The impedance matrix can be diagonilized by finding its eigen values which are

$$\lambda_1 = z + z' \quad \text{and} \quad \lambda_2 = z - z' \tag{48}$$

This gives the eigen vectors

$$\begin{bmatrix} 1 \\ 1 \end{bmatrix} \text{ for } \lambda_1 \text{ and } \begin{bmatrix} 1 \\ -1 \end{bmatrix} \text{ for } \lambda_2 . \tag{49}$$

By this procedure, we obtain the following new equations

$$\tfrac{1}{2}\begin{bmatrix} 1, & 1 \\ 1, & -1 \end{bmatrix} \begin{bmatrix} v_1 \\ v_2 \end{bmatrix} = \tfrac{1}{2}\begin{bmatrix} 1, & 1 \\ 1, & -1 \end{bmatrix} \begin{bmatrix} z\ , & z' \\ z', & z \end{bmatrix} \begin{bmatrix} 1, & 1 \\ 1, & -1 \end{bmatrix} \tfrac{1}{2}\begin{bmatrix} 1, & 1 \\ 1, & -1 \end{bmatrix} \begin{bmatrix} i_1 \\ i_2 \end{bmatrix}$$

or,

$$\begin{bmatrix} v_{(1)} \\ v_{(2)} \end{bmatrix} = \begin{bmatrix} z_{(1)}\ , & 0 \\ 0\ , & z_{(2)} \end{bmatrix} \begin{bmatrix} i_{(1)} \\ i_{(2)} \end{bmatrix} \tag{50}$$

where $v_{(1)} = \frac{1}{2}(v_1 + v_2)$

$v_{(2)} = \frac{1}{2}(v_1 - v_2)$,

$i_{(1)} = \frac{1}{2}(i_1 + i_2)$,

$i_{(2)} = \frac{1}{2}(i_1 - i_2)$,

$z_{(1)} = z + z'$

and $z_{(2)} = z - z'$

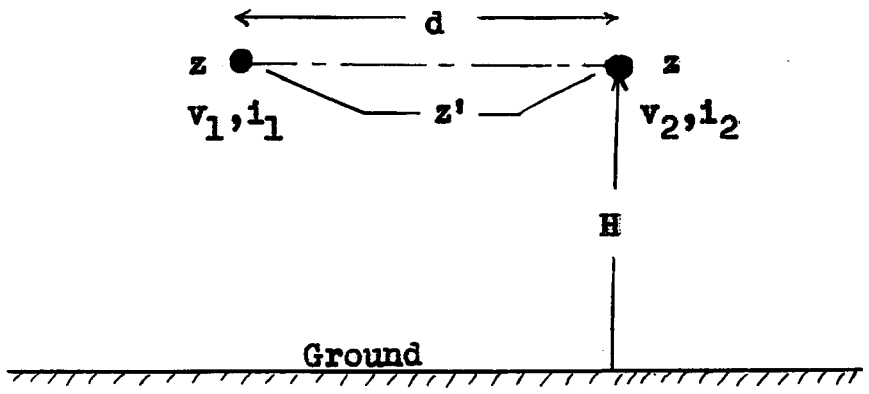

Figure 5

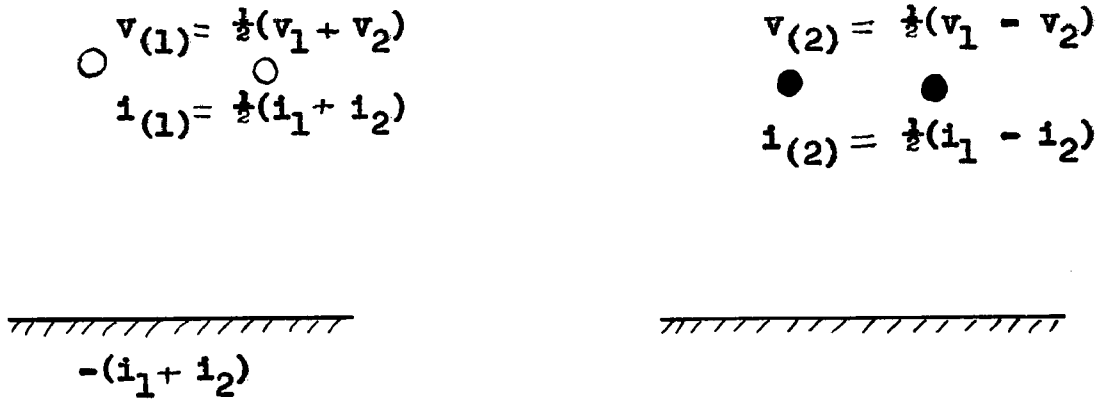

Figure 6

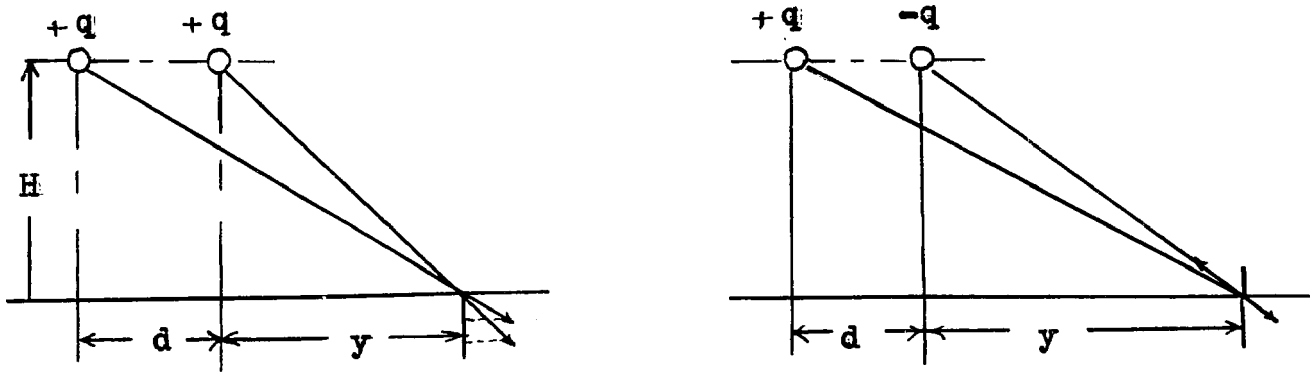

Mode 1: Line-to-ground mode

Mode 2: Line-to-line mode

Figure 7

Equation (50) gives the performance of the r-f voltages, currents and the charges accompanying them in modal form, and together with the eigen vectors of equation (49) can be physically interpreted as follows:

The actual voltages on and currents flowing in the two conductors can be resolved into two components ($v_{(1)}$, $i_{(1)}$) and ($v_{(2)}$, $i_{(2)}$) . The two voltages now have no mutual interaction and propagate independently on conductors with impedances $z_{(1)} = z + z'$ and $z_{(2)} = z - z'$, respectively. In the first mode, a current $i_{(1)} = \frac{1}{2} (i_1 + i_2)$ flows in each conductor in the same direction with return through ground. They are associated with equal charges and of the same polarity on the two conductors. This is the line-to-ground mode.

In the second mode, a current $i_{(2)} = \frac{1}{2} (i_1 - i_2)$ flows in one conductor and the second conductor carries an equal current flowing in the opposite direction. The two conductors form a closed circuit with no current flowing in the ground. This is the line-to-line mode of propagation. The two conductors have equal charges but of opposite polarity. Figure 6 shows the modal voltages, currents and charge distributions

A similar distribution of energies occurs in the two modes. If S_+ and S_- are the r-f energies developed by the positive- and negative- conductor, respectively, the energy associated with the two modes are

$$S_{(1)} = \tfrac{1}{2}\,(S_+ + S_-)$$

and $$S_{(2)} = \tfrac{1}{2}\,(S_+ - S_-) \qquad (51)$$

In normal bipolar lines used in practice, the negative conductor develops very low energy as compared to the positive conductor and can be neglected in comparison. The two modes then possess equal energies

$$S_{(1)} = S_{(2)} = \tfrac{1}{2}\,S_+ \quad . \qquad (52)$$

This property and equation (52) will be used for all subsequent calculations and discussions of relative interference levels.

We now observe the basic difference between an a-c line and a d-c line. In an a-c line, the three phase-conductors generate nearly equal energies. They also give rise to three modes of propagation in a single-circuit line and six modes in a twin-circuit line. The energies associated with different modes are all different. But in a d-c line, the two modes have very nearly equal r-f energies because the negative conductor does not generate r-f energy of any appreciable magnitude.

These two modes of propagation of energy on the d-c transmission line possess different attenuation factors. The line-to-ground mode attenuates faster than the line-to-line mode because ground is involved, the two attenuation factors being nearly in the ratio of 10 to 1. From experiments conducted on long a-c lines, (10), it has been observed that at

1 MHz the line-to-ground mode has an attenuation of 6 DB per mile or 0.7 neper/mile, and the line-to-line mode attenuates 0.7 DB/mile or 0.08 neper/mile. These values for $\alpha_{(1)}$ and $\alpha_{(2)}$ will be used for all calculations.

Now, the energy received at any point P on the conductor can be evaluated from a relation similar to equation (21). The enrgies received at P from the two modes are

$$\left.\begin{aligned} W_{(1)} &= S_{(1)}/2\alpha_{(1)} = S_+/4\alpha_{(1)} \\ \text{and} \quad W_{(2)} &= S_{(2)}/2\alpha_{(2)} = S_+/4\alpha_{(2)} \end{aligned}\right\} \tag{53}$$

The total energy at P is the sum of these two energies, thus:

$$W = \tfrac{1}{4} S_+ \left(\frac{1}{\alpha_{(1)}} + \frac{1}{\alpha_{(2)}} \right) = \frac{\pi r \sigma}{2} \left(\frac{1}{\alpha_{(1)}} + \frac{1}{\alpha_{(2)}} \right). \tag{54}$$

The spectral energy density σ has two types of variation as given by equations (8) and (13).

While equation (54) gives an indication of RIV on the conductor, the vertical component of electric field intensity on ground due to the charges associated with the r-f energy on the conductor yields the RI levels. These can be found out for the two modes.

(a) Line-to-ground mode:

The charge distribution on the two conductors in this mode are equal and of the same polarity, as shown in Figure 7. The vertical component of electric field intensity at a point distant y from the line, due to the charges on the conductors and their images below ground, is

$$\frac{q}{2\pi\epsilon} \; 2H \left[\frac{1}{H^2 + y^2} + \frac{1}{H^2 + (y+d)^2} \right] \quad . \qquad (55)$$

The ratio of this vertical component of field intensity to the charge on the conductor in this mode will be called the "field factor". Thus the field factor in the line-to-ground mode is

$$\mathcal{F}_{(1)} = \frac{2H}{2\pi\epsilon} \left[\frac{1}{H^2 + y^2} + \frac{1}{H^2 + (y+d)^2} \right] \quad . \qquad (56)$$

(b) Line-to-line mode:

The charge distribution on the conductors in this mode consists of equal charges but of opposite polarity, and the field factor is

$$\mathcal{F}_{(2)} = \frac{2H}{2\pi\epsilon} \left[\frac{1}{H^2 + y^2} - \frac{1}{H^2 + (y+d)^2} \right] . \qquad (57)$$

Since only the relative interference values are of interest, the factor $2\pi\epsilon$ in the denominator of equations (56) and (57) may be omitted from all expressions for field factor. These two field factors are plotted in Figure 8 as functions of y/H and for interpolar separation $d = 1.0\ H$ and $0.6\ H$.

The r-f energy at a point P on the conductor in the two modes were found in equation (53) and this is proportional to the squares of charges involved in the two modes. Hence the energy associated with the vertical component of field intensity at ground level in the two modes can be determined as

$$E^2_{(1)} = W_{(1)} \; \mathcal{F}^2_{(1)} = \mathcal{F}^2_{(1)} \; S_+ / 4\alpha_{(1)} \; , \qquad (58)$$

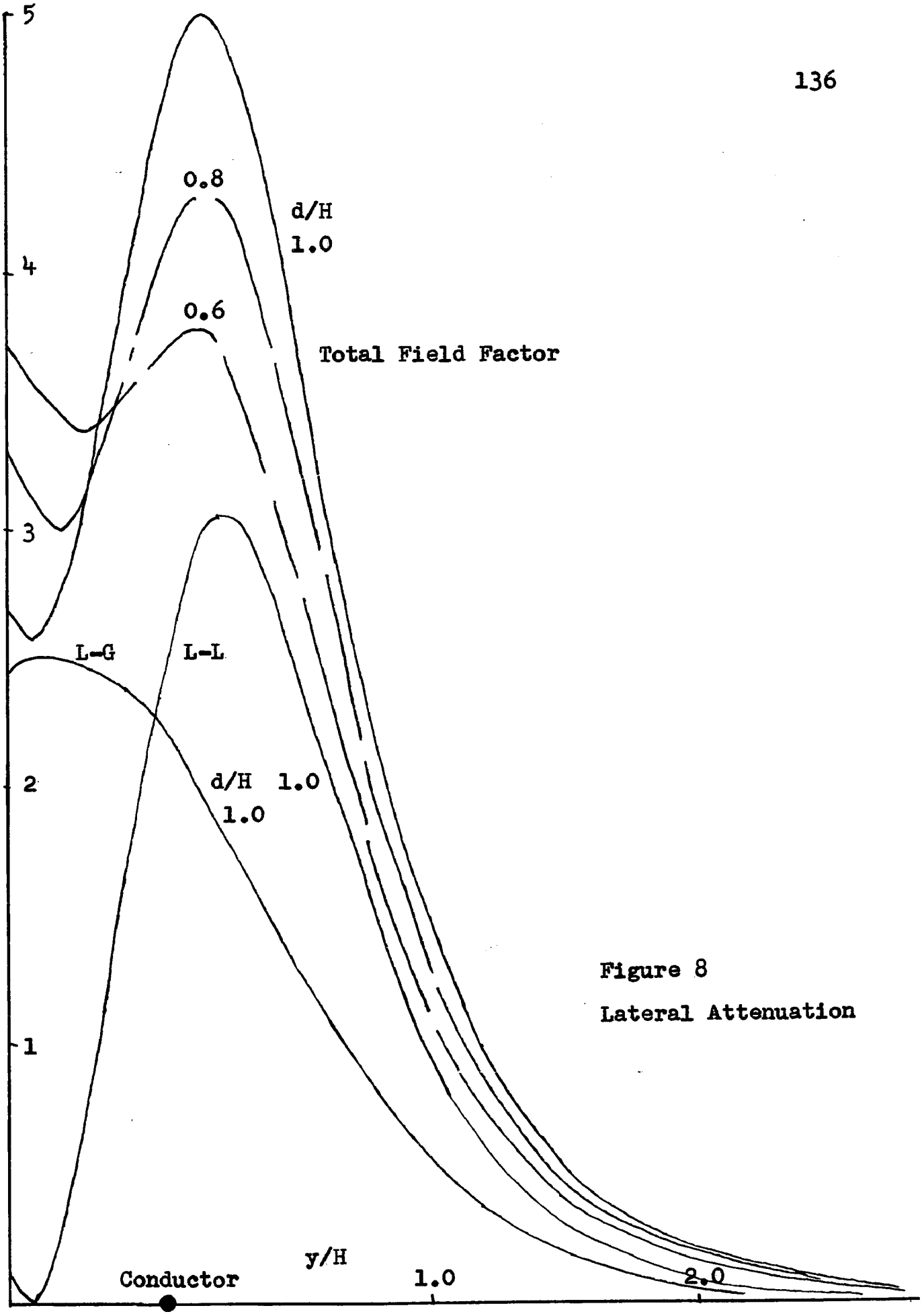

Figure 8

Lateral Attenuation

$$E^2_{(2)} = W_{(2)} \xi^2_{(2)} = \xi^2_{(2)} S_+ / 4\alpha_{(2)} \cdot \qquad (59)$$

Then the total energy content in this field is

$$E^2 = E^2_{(1)} = E^2_{(2)} = \frac{1}{4}\left[\xi^2_{(1)}/\alpha_{(1)} + \xi^2_{(2)}/\alpha_{(2)} \right] S_+$$

$$= \left[\xi^2_{(1)} + \xi^2_{(2)} \frac{\alpha_{(1)}}{\alpha_{(2)}} \right] S_+ / 4\alpha_{(1)} \cdot \qquad (60)$$

The relative RI level of the d-c line with bipolar configuration is finally obtained as E.

From equation (60) the ratio of relative electric field intensity at the point y on ground to that under the line is obtained by evaluating E at $y = y$ and at $y = 0$. This gives the lateral attenuation of electric field strength or the RI level. This ratio is

$$\lambda_{1b} = \left(\xi^2_{(1)} + \xi^2_{(2)} \frac{\alpha_{(1)}}{\alpha_{(2)}} \right)\Big|_{y=y} \Big/ \left(\xi^2_{(1)} + \xi^2_{(2)} \frac{\alpha_{(1)}}{\alpha_{(2)}} \right)\Big|_{y=0}$$

$$= \frac{\left\{ \frac{1}{1+(y/H)^2} + \frac{1}{1+(y/H+d/H)^2} \right\}^2 + \left\{ \frac{1}{1+(y/H)^2} - \frac{1}{1+(y/H+d/H)^2} \right\}^2 \frac{\alpha_{(1)}}{\alpha_{(2)}}}{\left\{ 1 + \frac{1}{1+(d/H)^2} \right\}^2 + \left\{ 1 - \frac{1}{1+(d/H)^2} \right\}^2 \frac{\alpha_{(1)}}{\alpha_{(2)}}} \qquad (61)$$

It is also plotted in Figure 8 for $\alpha_{(1)}/\alpha_{(2)} = 10$, and is called the 'total bipolar field factor'.

One can observe at this stage a fundamental difference between the energies associated with the two modes of propagation of r-f waves on a d-c transmission line and those associated with the modes of propagation of an a-c line. This difference is one of the most noteworthy properties of a d-c line.

Considering a single-circuit a-c line for illustration, all three phase-conductors generate nearly equal amounts of r-f energy. This results in the line-to-ground mode having an extremely large amount of energy compared to the other two line-to-line modes. However, the attenuation of energy in these modes show that the line-to-ground mode attenuates very rapidly as compared to the line-to-line modes. Even with the relatively high attenuation, the line-to-ground mode still possesses a very high value of r-f energy compared to the line-to-line modes. This results in the well-known property of the a-c line that the ground-level electric field intensity is almost entirely caused by the line-to-ground mode of propagation and the line-to-line modes do not affect the RI level. Use of these properties has been made in design of Power Line Carrier, (11).

The situation is quite different in the bipolar d-c line. Since only the positive conductor is generating almost all of the r-f energy (and the negative conductor relatively nothing), the energy involved in the two modes are equal, as shown in equation (52). But now the energy in the line-to-ground mode of propagation attenuates more rapidly than that in the line-to-line mode, nearly in the ratio of 10 to 1. Therefore the line-to-line mode has considerable effect on RI value measured at ground level. The ratio of field intensities contributed by the two modes is obtained as

$$X_b = \frac{\text{line-to-ground mode intensity}}{\text{line-to-line mode intensity}}$$

$$= \frac{\frac{1}{1+(y/H)^2} + \frac{1}{1+(y/H+d/H)^2}}{\left[\frac{1}{1+(y/H)^2} - \frac{1}{1+(y/H+d/H)^2}\right]\left(\frac{\alpha_{(1)}}{\alpha_{(2)}}\right)^{\frac{1}{2}}} \qquad (62)$$

This is plotted in Figure 9 for different values of separation between the positive and negative conductors, i.e. for different values of (d/H), and for $\alpha_{(1)}/\alpha_{(2)} = 10$. It may be observed from this figure that as the bipolar separation increases, the intensity in the line-to-line mode is now greater than in the line-to-ground mode in the shaded area. In practice, d-c lines have a line height between 30 and 50 feet, and the distance at which RI is of interest is $y = 100$ feet, so that the ratio (y/H) lies between 2 and 3. In this range for (y/H), the intensity in the line-to-line mode is at least equal to or greater than the intensity in the line-to-ground mode for bipolar separation d equal to or greater than the line height, ($d/H \geq 1.0$).

One of the most important conclusions obtained from the above reasoning is that in a d-c transmission line, the line-to-line mode of propagation of r-f energy has considerable influence on the RI levels, unlike in an a-c transmission line in which the line-to-line modes of propagation have relatively smaller effect.

Figure 9

Calculated ratio

$$\frac{\text{Line-to-ground mode field intensity}}{\text{Line-to-line mode field intensity}} \quad \text{for} \quad \frac{\alpha_{(1)}}{\alpha_{(2)}} = 10$$

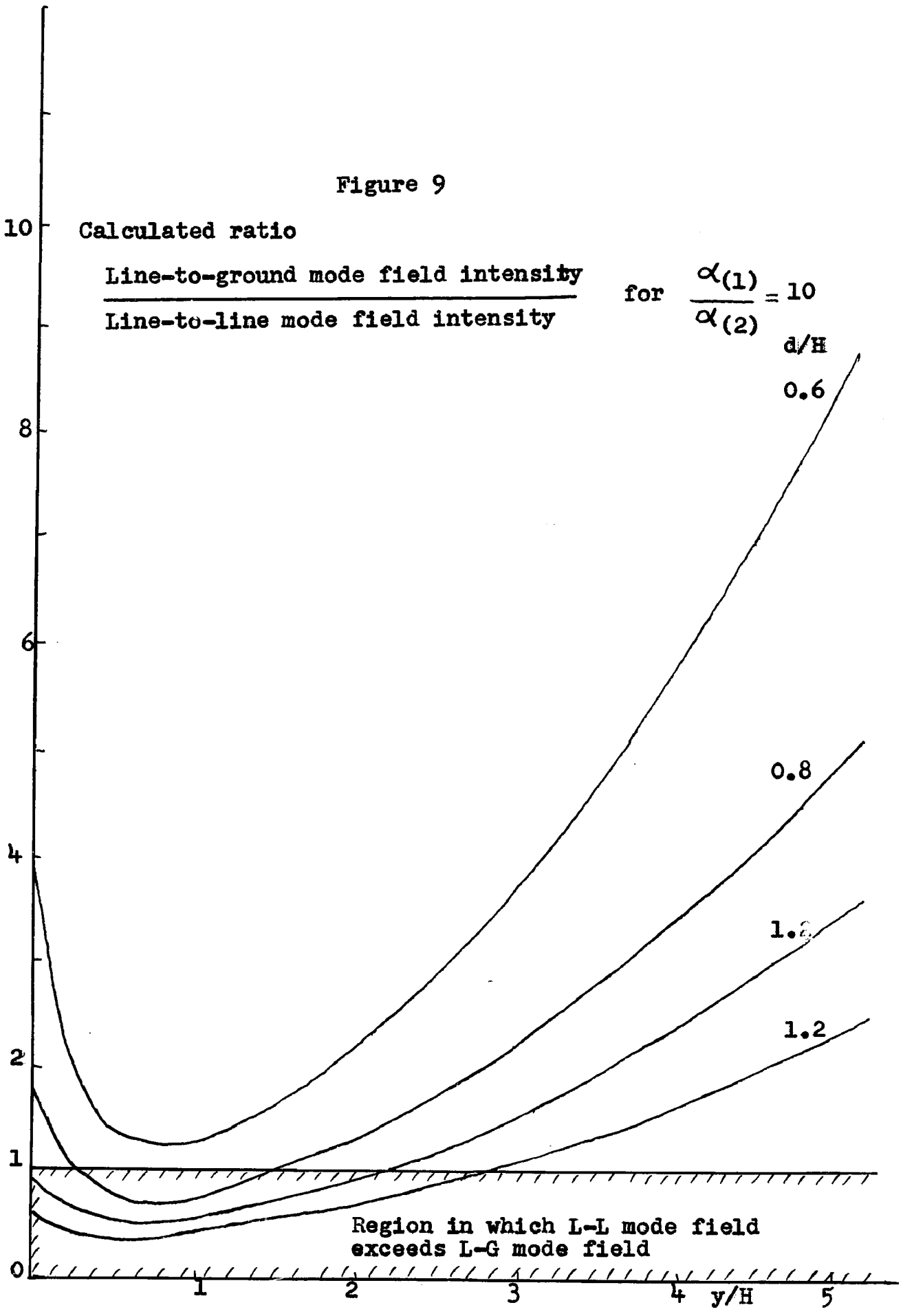

Having discussed the properties of the field factors and obtained the RI level of equation (60), the final forms for RI levels of a single conductor in bipolar configuration can be written when the spectral energy density has the two types of variation given in equations (8) and (13).

Case (i): Linear variation of conductor RIV with voltage:

$$(RIV)^2 = \frac{\pi r}{2\,\alpha_{(1)}\, w_1\, k_{1b}^2}\,(V - V_o)^2\,(1+\frac{\alpha_{(1)}}{\alpha_{(2)}}). \quad (63)$$

$$(RI)^2 = \frac{\pi r}{2\,\alpha_{(1)}\, w_1\, k_{1b}^2}\,(V-V_o)^2\left[\,\xi_{(1)}^2 + \xi_{(2)}^2\,\frac{\alpha_{(1)}}{\alpha_{(2)}}\right]. \quad (64)$$

Case (ii): Linear variation of DB of RIV of conductor with voltage:

$$(RIV)^2 = \frac{\pi r}{2\,\alpha_{(1)}}\;10^{(V-V_o)/w_2\,k_{1b}}\;(1+\alpha_{(1)}/\alpha_{(2)}). \quad (65)$$

$$(RI)^2 = \frac{\pi r}{2\,\alpha_{(1)}}\;10^{(V-V_o)/w_2 k_{1b}}\left[\,\xi_{(1)}^2 + \xi_{(2)}^2\,\frac{\alpha_{(1)}}{\alpha_{(2)}}\right]. \quad (66)$$

In these equations,

$$k_{1b} = r\,\mathrm{Ln}\,(2\,H\,d/r\sqrt{4H^2 + d^2}) \quad . \quad (67)$$

IV.7 TWO-BUNDLE CONDUCTOR IN BIPOLAR CONFIGURATION

The two-bundle conductor in bipolar configuration is the most important type of line and combines the analyses of Sections IV.5 and IV.6. In a manner exactly similar to equations (30) to (35), the total energy generated by the bundle can be calculated for this configuration.

Case i. Linear variation of RIV with voltage:

When the entire bundle is in corona, the r-f energy developed per unit length of conductor is

$$S_+ = \frac{8\pi r}{w_1 k_{2b}^2}\left[(V - V_o)^2 + \frac{r^2}{(s+r)^2} V^2\right] \qquad (68)$$

where the value of k_{2b} is given in the next section, equations (76) and (77).

Case (ii). Linear variation of DB of RIV with voltage:

When the entire bundle is in corona,

$$S_+ = 4\pi r \; 10^{(V-V_o)/w_2 k_{2b}} \; I_o\left(\frac{4.6\, r\, V}{s\, w_2\, k_{2b}}\right) \qquad (69)$$

The voltage at which the entire bundle generates r-f energy is given by an expression similar to (38) and (39), thus:

$$V_s = 30\, m\, (1 + 0.308\, r^{-\frac{1}{2}})\, k_{2b}\, \frac{s+r}{s-r} \; . \qquad (70)$$

Having determined the linear generation density of r-f energy of the bundle, the vertical component of electric field intensity at ground, that is the RI level of the bipolar line, can be found from equation (60).

Case i. Linear variation of RIV with voltage:

$$E^2 = \left[\xi_{(1)}^2 + \xi_{(2)}^2 \frac{\alpha_{(1)}}{\alpha_{(2)}}\right] \frac{8\pi r}{4\alpha_{(1)}} \frac{1}{w_1 k_{2b}^2}\left[(V-V_o)^2 + \frac{r^2}{(s+r)^2} V^2\right], \qquad (71)$$

for $V > V_s$.

Case ii. Linear variation of DB of RIV with voltage:

$$E^2 = \left[\xi_{(1)}^2 + \xi_{(2)}^2 \frac{\alpha_{(1)}}{\alpha_{(2)}}\right] \frac{4\pi r}{4\alpha_{(1)}} 10^{(V-V_o)/w_2 k_{2b}} \times I_o\left(\frac{4.6\, r\, V}{s\, w_2\, k_{2b}}\right), \quad (72)$$

for $V > V_s$.

IV.8 VALUES OF k

The factor 'k' relates the voltage gradient on the surface of conductor to the voltage applied between itself and ground. The expressions for 'k' can be derived from Maxwell's potential coefficients and have the following values:

i) Single conductor in monopolar configuration:

$$k_{1m} = r \text{ Ln } (2H/r) \quad . \quad (73)$$

ii) Two-bundle conductor in monopolar configuration:

$$k_{2m} = r \text{ Ln } (4H^2/sr) \quad . \quad (74)$$

iii) Single conductor in bipolar configuration:

$$k_{1b} = r \text{ Ln } \left(2Hd/\, r\sqrt{4H^2 + d^2}\,\right) \quad . \quad (75)$$

iv) Two-bundle conductor in bipolar configuration:

$$k_{2b} = 2r \frac{\text{Ln } \dfrac{s(d+s)\sqrt{4H^2+d^2}}{r\,d\sqrt{4H^2+(d+s)^2}} \text{ Ln } \dfrac{2H}{s} \dfrac{d}{\sqrt{4H^2+d^2}} + \text{Ln } \dfrac{s(d-s)\sqrt{4H^2+d^2}}{rd\sqrt{4H^2+(d-s)^2}} \text{ Ln } \dfrac{2H}{r} \dfrac{d+s}{\sqrt{4H^2+(d+s)^2}}}{\text{Ln } \dfrac{s^2\,(d^2-s^2)\,(4H^2+d^2)}{r^2\,d^2\sqrt{4H^2+(d+s)^2}\,\sqrt{4H^2+(d-s)^2}}} \quad (76)$$

If the intra-polar conductor separation 's' is such that the approximation $(d-s) \approx (d+s) \approx d$ is made, then equation (76) reduces to the much simpler form

$$k_{2b} = r \, \mathrm{Ln} \frac{4 H^2 d^2}{s \, r \, (4 H^2 + d^2)} \quad . \tag{77}$$

IV.9 COMPARISON OF RADIO NOISE CHARACTERISTICS OF THE FOUR CONFIGURATIONS

In order that a comparison may be effected of the radio noise characteristics of the four configurations, the final equations are brought here for convenience.

1. Single Conductor in Monopolar Configuration:

i. Linear variation of RIV of conductor with voltage:

$$(RIV)^2 = \frac{1}{2\alpha} \frac{2\pi r}{w_1 k_{1m}^2} (V - V_o)^2 \quad . \tag{78}$$

$$(RI)^2 = \frac{1}{2\alpha} \frac{2\pi r}{w_1 k_{1m}^2} (V-V_o)^2 \left(\frac{2H}{H^2+y^2}\right)^2 \quad . \tag{79}$$

ii. Linear variation of DB of RIV of conductor with voltage:

$$(RIV)^2 = \frac{1}{2\alpha} 2\pi r \; 10^{(V-V_o)/w_2 k_{1m}} \quad . \tag{80}$$

$$(RI)^2 = \frac{1}{2\alpha} 2\pi r \; 10^{(V-V_o)/w_2 \, k_{1m}} \left(\frac{2H}{H^2+y^2}\right)^2 \tag{81}$$

$$k_{1m} = r \, \mathrm{Ln} \, (2H/r) \quad . \tag{82}$$

2. Two-Bundle Conductor in Monopolar Configuration:

i. Linear variation of RIV of conductor with voltage:

$$(RIV)^2 = \frac{8\pi r}{2\alpha w_1 k_{2m}^2}\left[(V - V_o)^2 + \frac{r^2}{(s+r)^2} V^2\right] \quad (83)$$

$$(RI)^2 = \frac{8\pi r}{2\alpha w_1 k_{2m}^2}\left[(V-V_o)^2 + \frac{r^2}{(s+r)^2} V^2\right]\left(\frac{2H}{H^2+y^2}\right)^2 . \quad (84)$$

ii. Linear variation of DB of RIV of conductor with voltage:

$$(RIV)^2 = \frac{4\pi r}{2\alpha} 10^{(V-V_o)/w_2 k_{2m}} I_o\left(\frac{4.6\, r\, V}{s\, w_2\, k_{2m}}\right) . \quad (85)$$

$$(RI)^2 = \frac{4\pi r}{2\alpha} 10^{(V-V_o)/w_2 k_{2m}} I_o\left(\frac{4.6\, r\, V}{s\, w_2\, k_{2m}}\right)\left(\frac{2H}{H^2+y^2}\right)^2 . \quad (86)$$

All these four expressions are valid for $V > V_s$ where

V_s = voltage at which minimum gradient on bundle equals the corona-inception gradient

$$= 30\, m\, (1 + 0.308\, r^{-\frac{1}{2}})\, k_{2m}\, \frac{s+r}{s-r} \quad (87)$$

and $$k_{2m} = r\, Ln\,(4H^2/sr) = r\, Ln(2H/r) + r\, Ln(2H/s)$$
$$= k_{1m} + r\, Ln(2H/s) . \quad (88)$$

3. Single Conductor in Bipolar Configuration.

i. Linear variation of RIV of conductor with voltage:

$$(RIV)^2 = \frac{2\pi r}{4 w_1 k_{1b}^2} (V-V_o)^2 \left(1/\alpha_{(1)} + 1/\alpha_{(2)}\right) . \quad (89)$$

$$(RI)^2 = \frac{2\pi r}{4\alpha_{(1)} w_1 k_{1b}^2} (V-V_o)^2 \left[\xi_{(1)}^2 + \xi_{(2)}^2 \frac{\alpha_{(1)}}{\alpha_{(2)}}\right] . \quad (90)$$

ii. Linear variation of DB of RIV of conductor with voltage:

$$(RIV)^2 = \frac{2\pi r}{4} 10^{(V-V_o)/w_2 k_{1b}} \left(1/\alpha_{(1)} + 1/\alpha_{(2)}\right) . \quad (91)$$

$$(RI)^2 = \frac{2\pi r}{4(3)} 10^{(V-V_o)/w_2\, k_{1b}} \left(\xi^2_{(1)} + \xi^2_{(2)} \frac{\alpha(1)}{\alpha_{(2)}} \right). \quad (92)$$

$$k_{1b} = r \, \mathrm{Ln} \frac{2Hd}{r\sqrt{4H^2+d^2}} \quad (93)$$

$$\xi^2_{(1)} = 2H^2 \left[\frac{1}{H^2+y^2} + \frac{1}{H^2+(y+d)^2} \right]^2. \quad (94)$$

$$\xi^2_{(2)} = 2H^2 \left[\frac{1}{H^2+y^2} - \frac{1}{H^2+(y+d)^2} \right]^2. \quad (95)$$

These values of $\xi^2_{(1)}$ and $\xi^2_{(2)}$ are one half of those given in equations (56) and (57) because of the existence of only one half of the energy of the positive conductor in each of the two modes, whereas in the monopolar configuration the entire energy of the positive conductor determines the electric field intensity at ground level.

4. Two-Bundle Conductor in Bipolar Configuration.

i. Linear variation of RIV of conductor with voltage:

$$(RIV)^2 = \frac{2\pi r}{w_1 k^2_{2b}} \left[(V-V_o)^2 + \frac{r^2}{(s+r)^2} V^2 \right] \left(1/\alpha_{(1)} + 1/\alpha_{(2)} \right) \quad .. (96)$$

$$(RI)^2 = \frac{2\pi r}{w_1 k^2_{2b}} \left[(V-V_o)^2 + \frac{r^2}{(s+r)^2} V^2 \right] \left(\xi^2_{(1)} + \xi^2_{(2)} \frac{\alpha(1)}{\alpha_{(2)}} \right). \quad (97)$$

ii. Linear variation of DB of RIV of conductor with voltage:

$$(RIV)^2 = \pi r \, 10^{(V-V_o)/w_2 k_{2b}} \, I_o\left(\frac{4.6r}{s} \frac{V}{w_2 k_{2b}}\right) \left(\frac{1}{\alpha_{(1)}} + \frac{1}{\alpha_{(2)}} \right). \quad (98)$$

$$(RI)^2 = \frac{\pi r}{\alpha_{(1)}} 10^{(V-V_o)/w_2 k_{2b}} I_o\left(\frac{4.6r}{s} \frac{V}{w_2 k_{2b}}\right) \left(\xi^2_{(1)} + \xi^2_{(2)} \frac{\alpha(1)}{\alpha_{(2)}} \right) \quad ... (99)$$

These four expressions apply when $V > V_s$, the voltage at which the entire periphery of the bundle is generating r-f energy.

The above equations for $(RIV)^2$ and $(RI)^2$ have been numerically calculated when the variation of RIV of conductor is assumed to be such that its DB value varies linearly with voltage applied to the conductor. This will afford a comparison with a-c line designs for which a similar variation has been assumed. This has been done for the following conductor sizes:

a) Lark conductor: 0.806-inch in diameter;
b) Drake conductor: 1.108-inch in diameter, with cross-sectional area equal to twice that of a Lark;
c) Falcon conductor: 1.6-inch in diameter, with cross-sectional area equal to twice that of a Drake;
d) Special conductor: 1.8-inch diameter; and
e) Special conductor: 2-inch in diameter.

The average line height has been selected as 30 feet above ground. In the case of a bundle conductor, the spacing is 18 inches; and for a bipolar line, the pole separation is 25 feet.

For the above dimensions, Figure 10 shows values of k_{1m}, k_{2m}, k_{1b}, and k_{2b} calculated according to equations (73), (74), (75), and (77). Figures 11 through 14 show the variation of $(RIV)^2$ at conductor as a function of applied voltage for the five conductors. In these figures, the

weather factor, w_2, has been chosen as 4 when voltages are measured in kilovolts, and the surface environment factor, m, has been set equal to 0.6. These values for w_2 and m are average values found in practice in fair weather and for well-weathered conductors. In the case of the bundle, the $(RIV)^2$ values shown in Figures 12 and 14 are for $V > V_s$ when the entire periphery of the bundle is in corona. The factor $I_o(4.6\ r\ V/s\ w_2\ k)$ varies very slowly with the applied voltage on the two-bundle conductor and therefore the plot of $(RIV)^2$ against voltage on semi-log paper is nearly a straight line. A straight line has therefore been drawn connecting the value of $(RIV)^2$ at $V = V_o$, the corona-inception voltage, and at any other chosen voltage. A convenient value chosen is 100 KV above the corona-inception value.

Figure 15 shows values of $(RI)^2$, the relative ground-level field intensity, at a distance of 100 feet along ground, $(y = 100)$, for these four line configurations.

Several practical conclusions on the use of such figures are drawn. They are:

1. Consider one size of conductor in monopolar and bipolar configurations. The cost of conductor in bipolar case is twice that in monopolar case. Referring to Drake conductor in Figures 11 and 13, a level of 100 for $(RIV)^2$ is reached at 215 KV in bipolar arrangement and at 292 KV in monopolar arrangement. The ratio of these two voltages is $215/292 = 0.735$. For an $(RIV)^2$ level of 1000, the

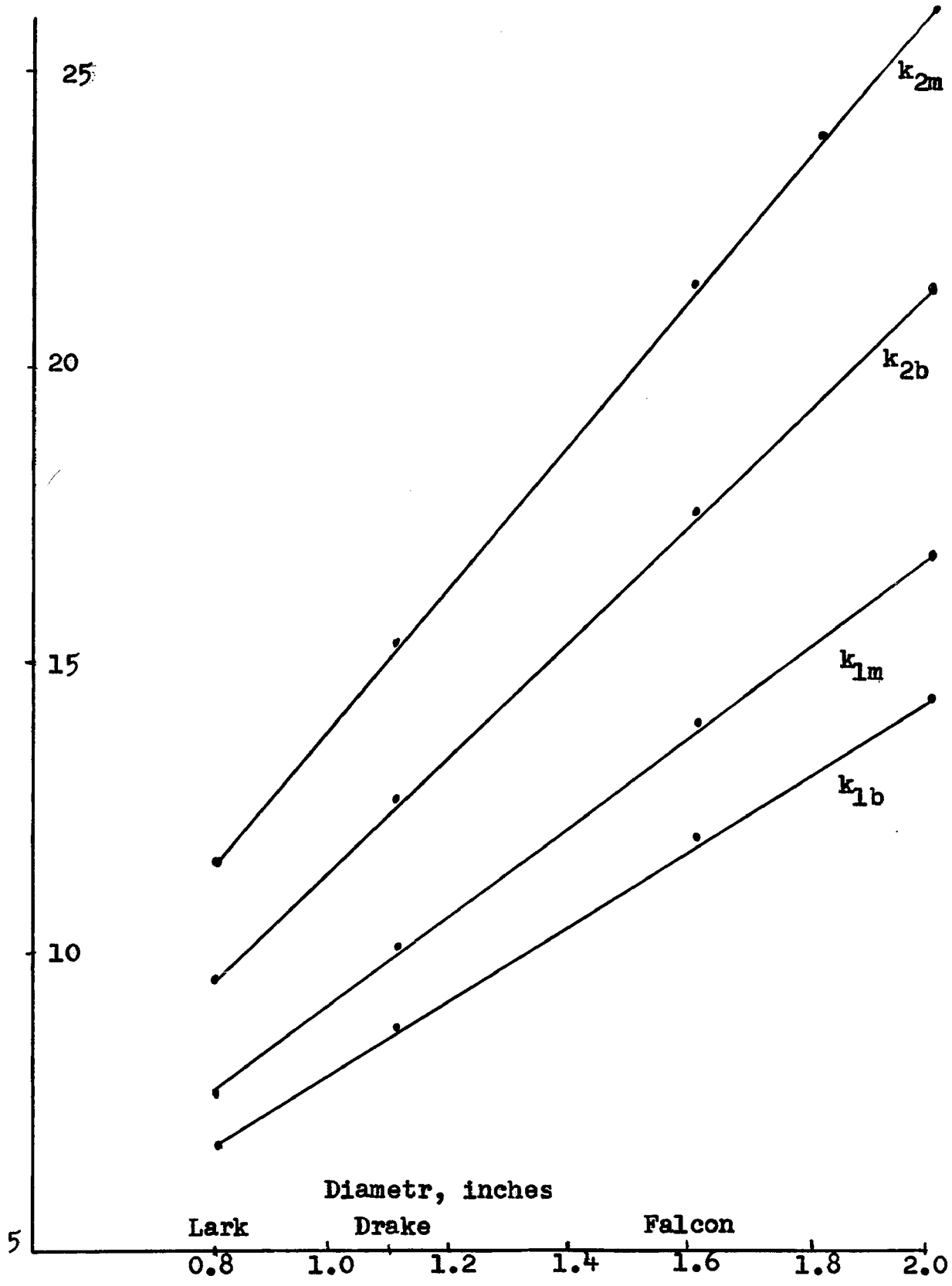
25
20
15
10
5
k_{2m}
k_{2b}
k_{1m}
k_{1b}
Diametr, inches
Lark
Drake
Falcon
0.8
1.0
1.2
1.4
1.6
1.8
2.0

Figure 10

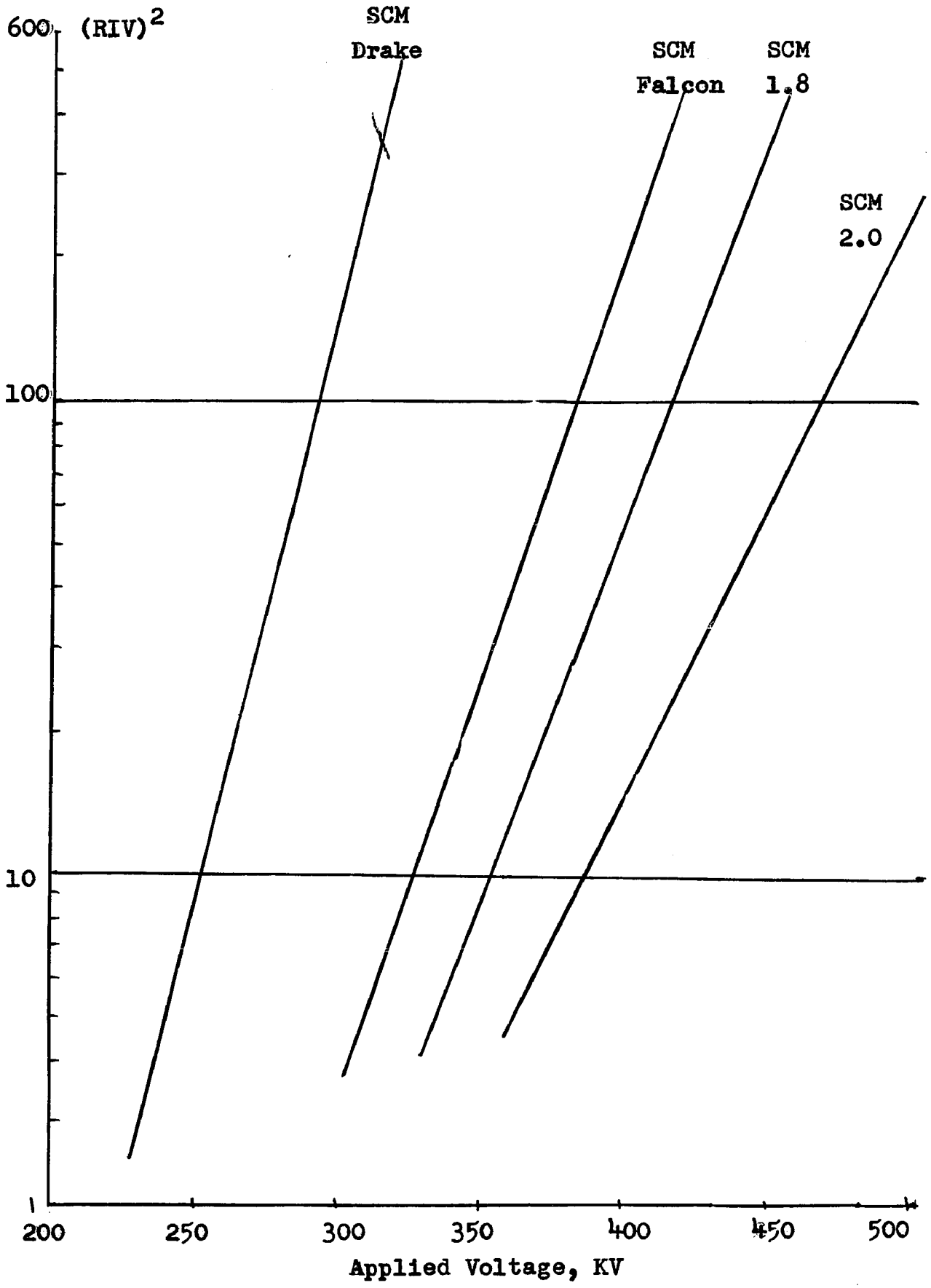

Figure 11. Relative RIV Levels of Single Conductor Monopolar

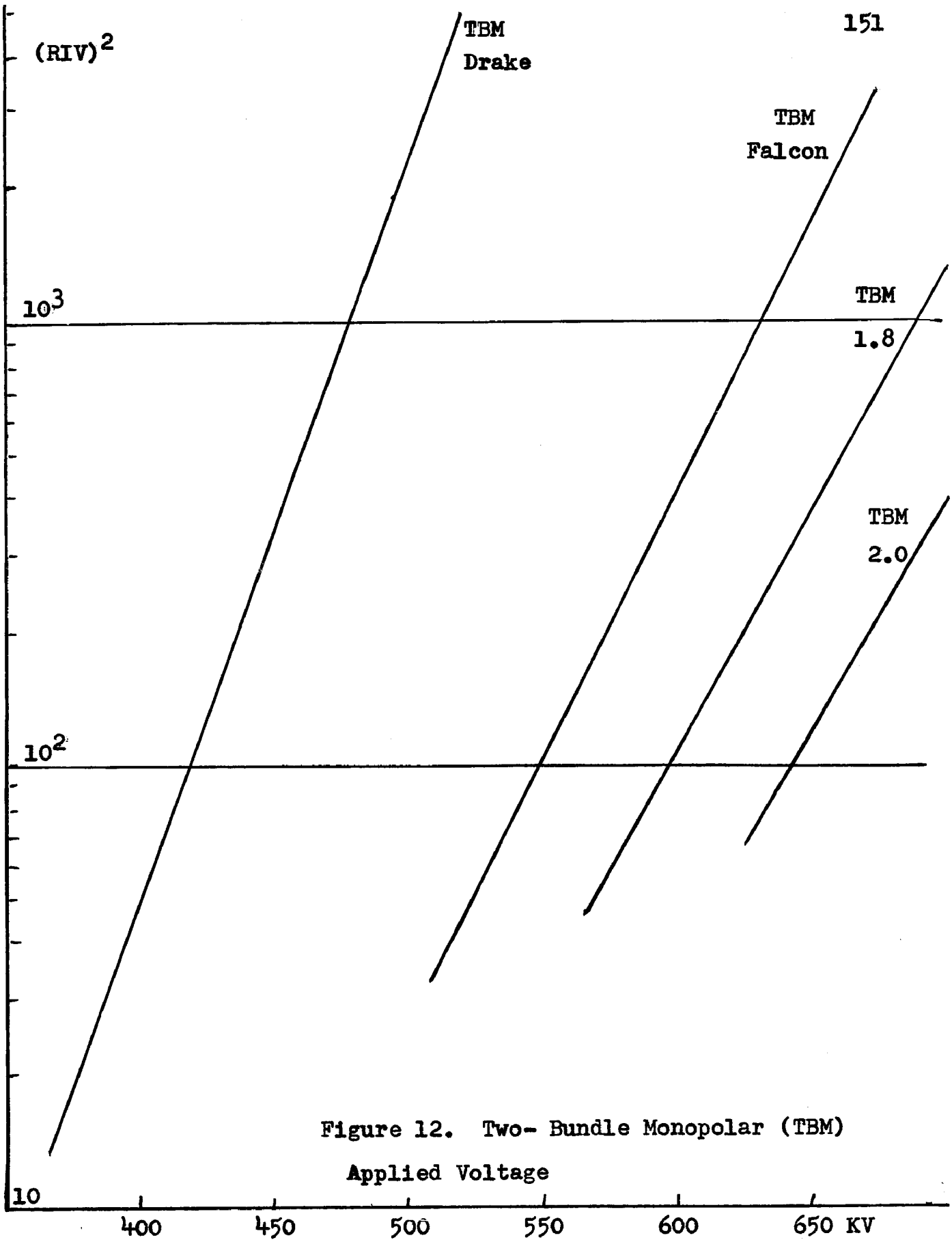

Figure 12. Two- Bundle Monopolar (TBM)

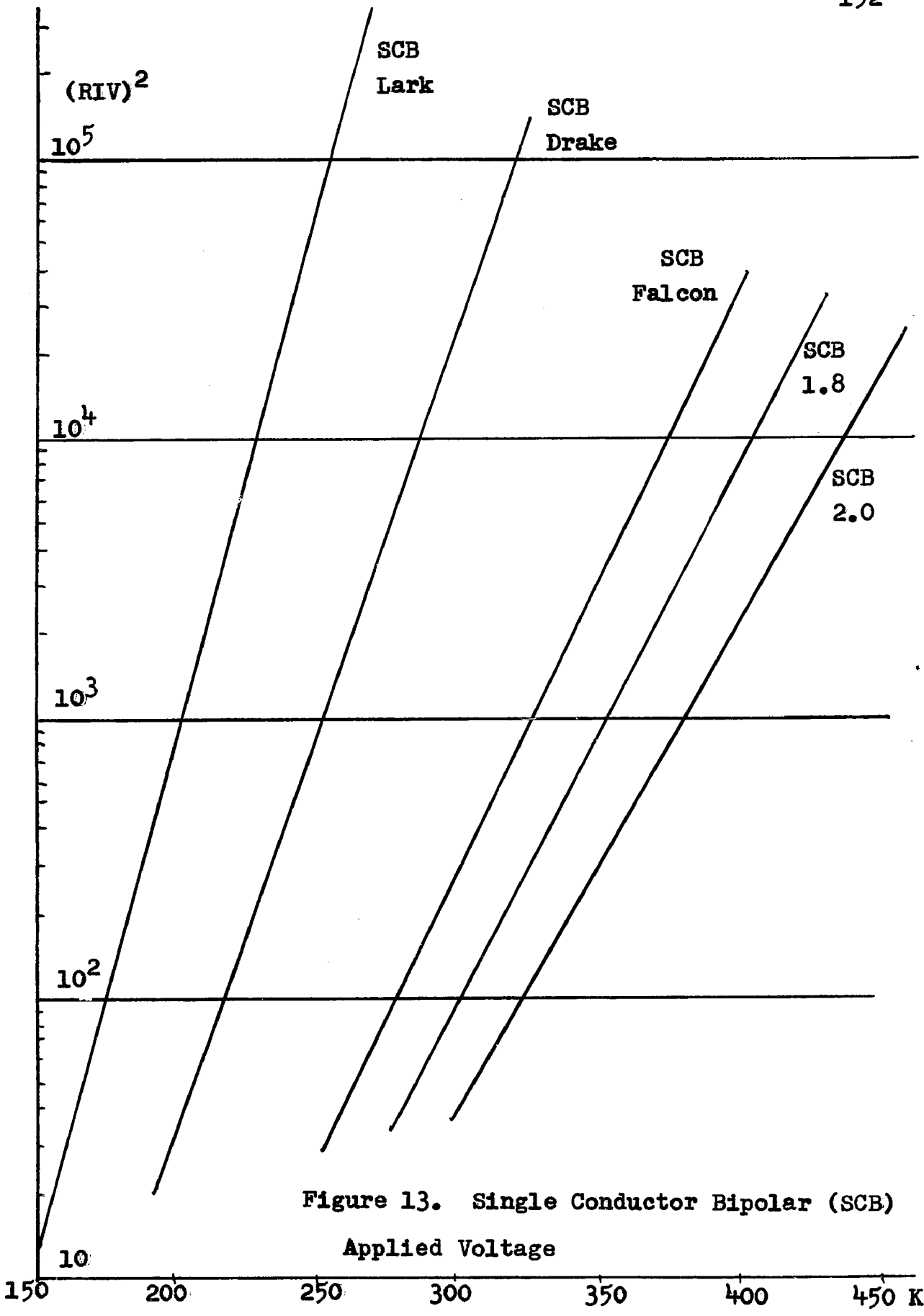

Figure 13. Single Conductor Bipolar (SCB)

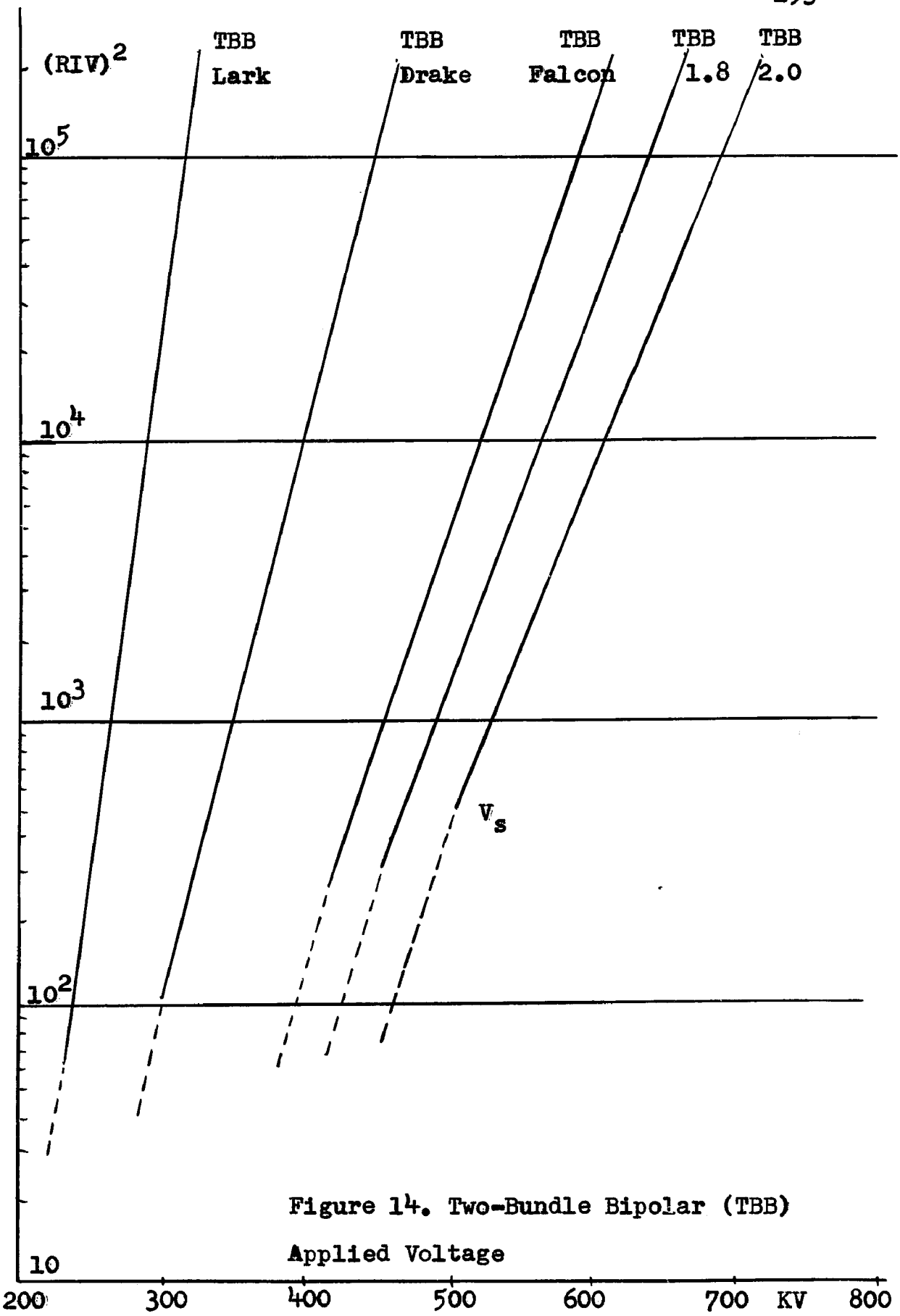

Figure 14. Two-Bundle Bipolar (TBB)

Applied Voltage

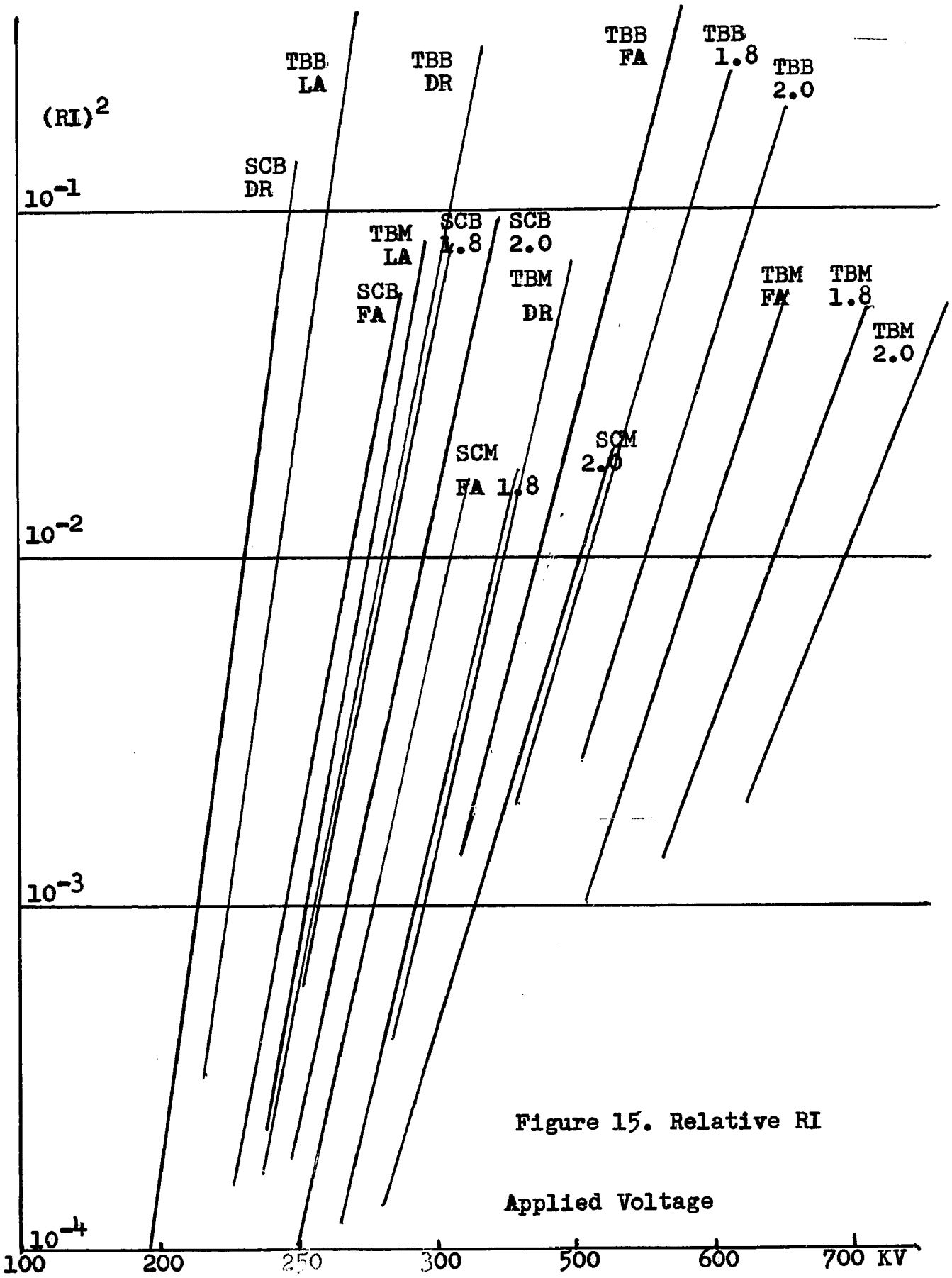

Figure 15. Relative RI

voltage ratio is 250/332 = 0.75. Similarly for the Falcon conductor, the voltage ratios are 0.72 and 0.74 at $(RIV)^2$ levels of 100 and 1000, respectively. These numbers show that for equal RIV level in bipolar and monopolar configurations, the working voltage of a given conductor in bipolar configuration is 70 to 75% of the voltage of the monopolar arrangement. Based on equal RIV levels, the power handling capacity of a conductor in bipolar configuration is only 150% while the conductor cost is 200% that for a monopolar configuration. The reduction in voltage in the bipolar case is caused by the increased surface voltage gradient on the conductor due to the presence of a negatively charged conductor.

2. In a bipolar configuration, Figures 13 and 14, consider a single conductor and a two-bundle conductor having equal cross-sectional areas, that is the same conductor cost. Comparing a two-bundle Lark with a single Drake, an $(RIV)^2$ level of 1000 is reached at 265 KV and 251 KV, respectively. For $(RIV)^2$ level of 10,000 the voltages are 290 KV and 285 KV. Thus there appears to be no benefit gained by using a two-bundle Lark as compared to a single Drake conductor. Again, comparing a two-bundle Drake with a single Falcon which have the same cross-sectional areas and costs, levels of 1000 are reached at equal voltages of 350 KV, while a level of 10,000 for $(RIV)^2$ is reached at 400 KV and 375 KV, a difference of 6%. The two-bundle Drake conductor can

therefore be operated at about 5% higher voltage than a single Falcon conductor. Thus even for the larger size of conductors there is not much benefit obtained by bundling, from the radio noise point of view.

3. Consider two alternate designs for the same operating voltage which yield equal RI levels, Figure 15. A single Falcon conductor in monopolar configuration and a single conductor 2.0-inch in diameter in bipolar configuration yield the same $(RI)^2$ level of 10^{-2} at nearly 400 KV. The cost of conductors is in the ratio of 1 to 5 and the power-handling capacity is also 5.

4. As mentioned in the introduction to this chapter in Section IV.1, when experimental results of operating voltage on one conductor size is ascertained for a set tolerable RI limit, then these figures can be used to ascertain the size and configuration of conductor that shall be suitable for any other operating voltage. This aspect of the problem is discussed in the next section where experimental results are given and compared with theory.

IV.10 COMPARISON OF THEORY WITH EXPERIMENTAL RESULTS

Experimental results obtained of the RI levels of six different configurations of conductors using Lark and Drake conductors are given in Reference 12. Some of these results will be used to verify the analytical method presented in the previous sections and also establish suitable conductor

configurations and sizes for several operating voltages for a limit of 100 μV/m for the RI level at 100 feet from the line at ground level, occuring over an average of 80% of the time. Two different configurations are selected for this purpose, a) a single Lark conductor, 0.806-inch in diameter, in bipolar configuration with a pole separation of 30 feet and average height H = 30 feet above ground; and b) a two-bundle Lark conductor in monopolar configuration with average height of 30 feet above ground. The two lines are shown in Figure 16.

The first step is to obtain the variation of RIV on a conductor sample with excitation voltage in order to find the weather factor w_2. From equation (12), for any conductor, variation of RIV with voltage is expressed as

$$RIV = 10^{(V-V_o)/2\ k\ w_2} .$$

If R_1 and R_2 are the RIV values at two voltages V_1 and V_2, then

$$R_1 = 10^{(V_1-V_o)/2\ k\ w_2}$$

and

$$R_2 = 10^{(V_2-V_o)/2\ k\ w_2} .$$

From these two equation,

$$w_2 = (V_2 - V_1)/\ k\ Log_{10}(R_2/R_1) \qquad (100)$$

From Figure 17, which shows average variation of RIV with voltage obtained from several runs, the following values for w_2 are obtained:

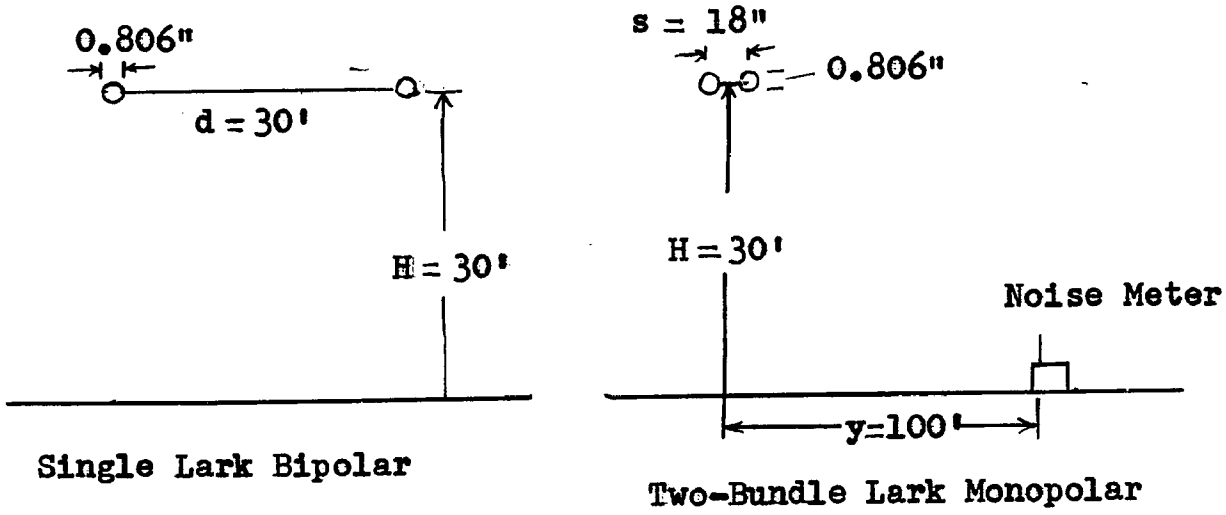

Figure 16

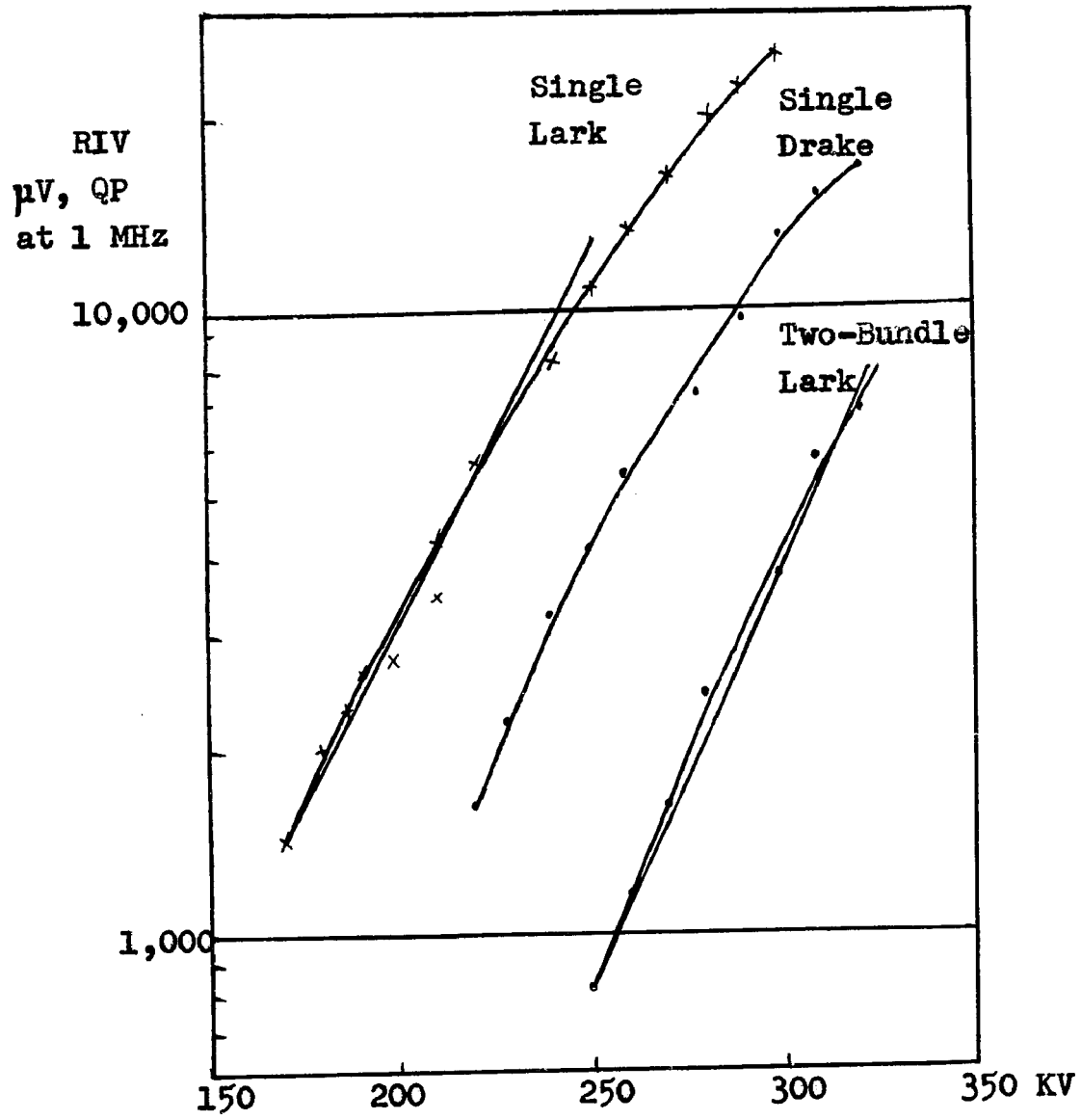

Figure 17. Variation of RIV

i) For single Lark conductor, at $V_2 = 230$ KV, $R_2 = 8{,}000$ μV and at $V_1 = 200$ KV, $R_1 = 3200$ μV.

These RIV values are QP values at 1 MHz.

$$\therefore \quad w_2 = \frac{230 - 200}{2 \times 6.7 \times \text{Log}_{10}\left[\frac{8000}{3200}\right]} = 5.6 \ .$$

From Figure 10, the value of k_{1b} for Lark is 6.7.

ii) For the two-bundle Lark, at voltages of 300 KV and 250 KV, the RIV values are 3,600 and 800 μV, respectively.

$$\therefore \quad w_2 = \frac{300 - 250}{2 \times 11.5 \times \text{Log}_{10}\left(\frac{3600}{800}\right)} = 3.33 \ .$$

From Figure 10, the value of $k_{2m} = 11.5$ for Lark.

The corona-inception voltages are 170 and 250 KV for these two conductors. But these tests are conducted in monopolar arrangement and therefore a correction must be applied when the corona-inception for bipolar arrangement is sought for. Going down from k_{1m} curve to k_{1b} curve for the Lark conductor in Figure 10, the corona-inception voltage in bipolar arrangement reduces from 170 KV to 152 KV.

The field factors are calculated from equations (94) and (95) for the bipolar line and from equation (23) for the monopolar line. These are:

i) for bipolar configuration with $H = 30$, $d = 30$, and $y = 100$:

$$\xi^2_{(1)} = 4 H^2 \left[\frac{1}{H^2 + y^2} + \frac{1}{H^2 + (y+d)^2}\right]^2 = 7.9 \times 10^{-6}.$$

$$\xi^2_{(2)} = 4H^2\left[\frac{1}{H^2+y^2} - \frac{1}{H^2+(y+d)^2}\right]^2 = 4.68 \times 10^{-6} .$$

$$\therefore \quad \xi^2_{(1)} + \xi^2_{(2)} \frac{\alpha_{(1)}}{\alpha_{(2)}} = 126 \times 10^{-6} .$$

ii) for monopolar configuration:

$$\left(\frac{2H}{H^2+y^2}\right)^2 = 30.3 \times 10^{-6} .$$

The RI values at 100 feet from conductor along ground calculated from equations (86) and (92) are:

i) for bipolar single Lark conductor:

$$(RI)^2 = \frac{2\pi r}{4\alpha_{(1)}} \; 10^{(V-V_0)/w_2} \, k_{1b} \left(\xi^2_{(1)} + \xi^2_{(2)} \frac{\alpha_{(1)}}{\alpha_{(2)}}\right)$$

$$= 1.14 \times 10^{-4} \; 10^{(V-152)/42.5} .$$

At $V_o = 152$ KV, $(RI)^2 = 1.14 \times 10^{-4}$.

At $V = 252$ KV, $(RI)^2 = 2.62 \times 10^{-2}$.

ii) for two-bundle Lark conductor in monopolar configuration:

$$(RI)^2 = 2 \; \frac{2\pi r}{\alpha_{(1)}} \left(\frac{2H}{H^2+y^2}\right)^2 \; 10^{(V-V_o)/w_2} \, k_{2m} \, I_o\left(\frac{4.6 \, r \, V}{s \, w_2 \, k_{2m}}\right)$$

$$= 220 \times 10^{-6} \; 10^{(V-250)/38.3} \; I_o(0.268 \times 10^{-2} \, V) .$$

At $V_o = 250$ KV, $(RI)^2 = 2.45 \times 10^{-4}$.

At $V = 350$ KV, $(RI)^2 = 1.10 \times 10^{-1}$.

The above values are plotted in Figure 18 and are straight lines on semi-log paper.

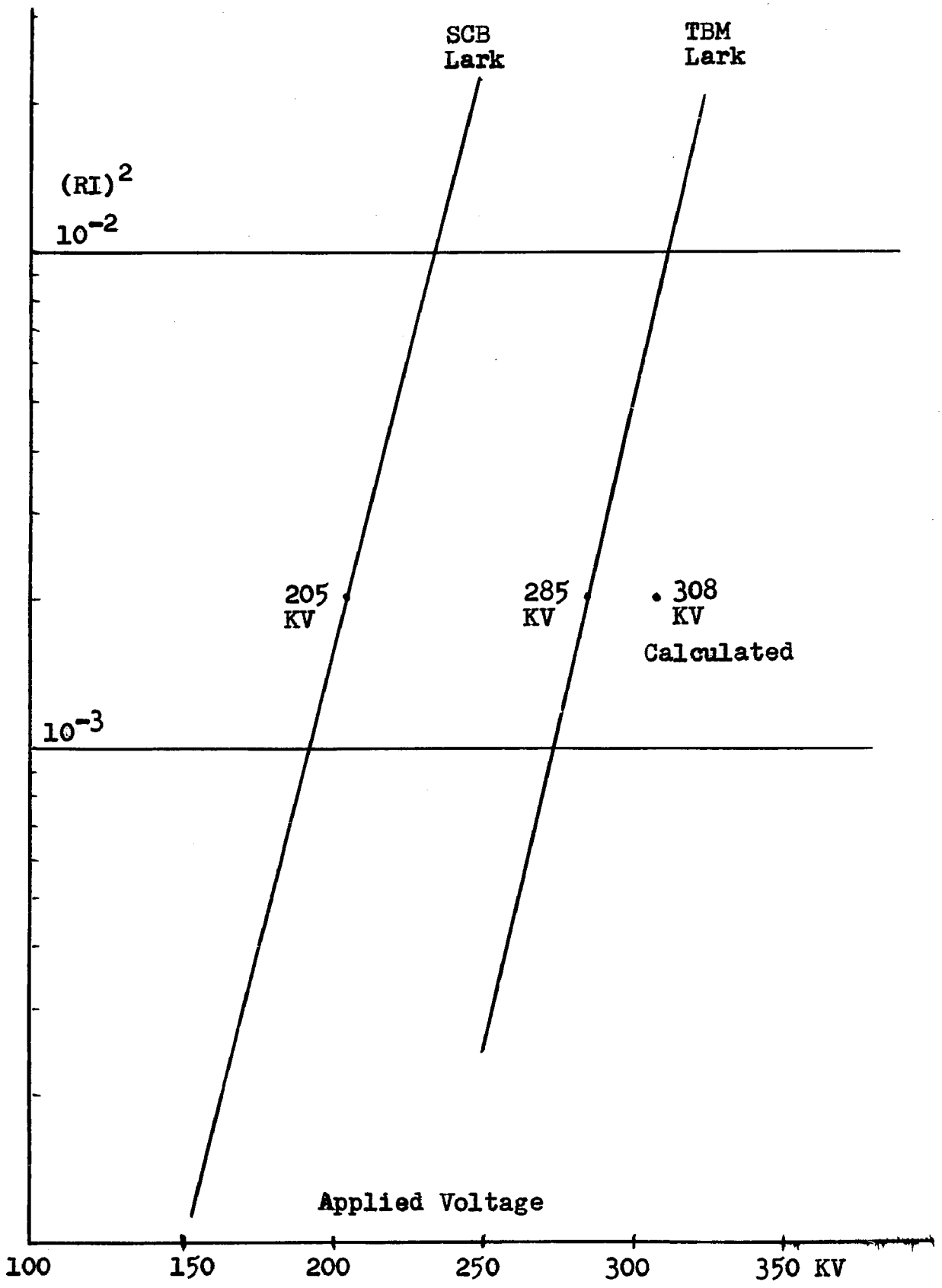

Figure 18. Comparison of Experimental and Calculated RI levels

From experimental results, it has been observed, (12), that an RI level of 100 μV/m at 100-foot distance along grounnd is obtained on the two configurations as follows:

i) single Lark in bipolar arrangement: 205 KV;

ii) two-bundle Lark in monopolar arrangement: 308 KV.

Now, from Figure 18 which shows calculated values, the relative $(RI)^2$ level at 205 KV on the single Lark conductor in bipolar arrangement is 2.0×10^{-3}, and this level is reached on the two-bundle Lark conductor in monopolar arrangement at 285 KV instead of the experimentally found value of 308 KV. Therefore the theoretical calculation gives voltage value within 8.5% of experimental results. Considering the random nature of the entire phenomenon, it is observed that this is a good prediction of voltage values. Furthermore, noise levels obtained from experiments are based on average long-term results and therefore provide a check on expected long-term RI performance of lines. The range of discrepency between calculated and experimental results are not differing by more than the variation of radio noise itself from day to day or from season to season. Design predictions can therefore be carried out to within this accuracy by the mathematical model derived in this chapter.

The usefulness of curves such as in Figure 15 can be stated as follows:

If the voltage level of a conductor subjected to test in a given configuration for a chosen RI level is known,

then the voltage level of any other conductor in a different or the same configuration and in the same or different weather can be found out. As an example, for $w_2 = 4$, if the allowable limit of RI on a two-bundle Lark conductor in monopolar configuration is reached at 300 KV, positive, then the voltages at the same weather for reaching the same RI level are read off from Figure 15 from a constant $(RI)^2$ value of 7×10^{-4} as follows:

Monopolar configuration: Single Falcon ..... 350 KV;
Single Special 1.8" ... 378 KV;
Single Special 2.0" ... 415 KV;
Two-bundle Drake ..... 380 KV.

Bipolar configuration: Single Drake ..... 220 KV;
Single Falcon ..... 283 KV;
Single Special 1.8" ... 308 KV;
Single Special 2.0" ... 328 KV;
Two-bundle Lark ..... 245 KV;
Two-bundle Drake ..... 308 KV.

In order to design a d-c transmission line for a given operating voltage, figures such as 11 through 15 must be calculated with many sets of values of line height, conductor diameter, bipolar separation, weather factor, and surface environment factor. These will provide relative interference values which can be used for selecting the proper line configuration for given operating voltage.

BIBLIOGRAPHY

INTRODUCTION (pp. 4 - 8)

1. B. Rakosh-Das, and R.M. Morris, "Investigation of corona on overhead conductors at high voltage d-c. - A progress report on radio interference," Research Report No.ERB-602, Division of Radio & Electrical Engineering, National Research Council, Ottawa, Ontario, March 1962.
2. R.M. Morris, and B. Rakosh-Das, "An investigation of corona loss and radio interference from transmission line conductors at high direct voltages," Trans. I.E.E.E., vol. PAS-83, pp. 5-16, January 1964.
3. H. Witt, "Insulation levels and corona phenomena on h.v. d.c. transmission lines," Thesis, Chalmers University, Goteborg, Sweden, 1961.
4. B. Rakosh-Das, "Radio interference from high-voltage d-c transmission lines," Bulletin of the Radio & Electrical Engineering Division, National Reseach Council, Ottawa, vol.14, No.2, pp. 19-29, 1964.
5. B.M. Bailey, "Progress report on B.P.A. high-voltage d-c test line radio noise and corona loss," Trans. I.E.E.E., vol. PAS-86, No.10, pp.1141-45, October 1967.
6. E.H. Gehrig, C.F. Clark, A.C. Peterson, and T.C. Rednour, "B.P.A.'s 1100-KV test project; II- radio interference and corona loss," ibid., pp.278-90, March 1967.
7. M.M. Khalifa, and R.M. Morris, "A laboratory study of the effects of wind on d-c corona", ibid., pp.290-8, Mar. 1967.

8. M. Akazaki, "Corona phenomena from water drops on smooth conductors under high direct voltages," ibid., vol. PAS-84, pp.1-8, January 1965.

9. G.E. Adams, "The calculation of radio interference level of transmission lines caused by corona discharges," Trans. A.I.E.E., vol 75, pt.III, pp.411-19, June 1956.

10. C.J. Miller, Jr., "Mathematical prediction of radio and corona characteristics of smooth bundled conductors," ibid., pp.1029-37, October 1956.

11. G.E. Adams, "An analysis of the radio interference characteristics of bundled conductors," ibid. vol.76, pp.1569-1584, February 1957.

12. A.K. Abboushi, and L.O. Barthold, "Digital calculation of radio noise levels," ibid., vol.80, pp.841-6, Dece. 1961.

13. J. Laforest, L.O. Barthold, R.L. Thompson, and C.B. Lindh, "500-kv line design, III- conductors," ibid., pp.587-92, August 1963.

14. L.O. Barthold, W.S. Price, and R.H. Schlomann, "Some important assumptions in calculation of radio noise levels of e.h.v. lines," C.I.G.R.E. Proc., paper 303, 1962.

15. C.J. Miller, Jr., "The calculation of radio and corona characteristics of transmission line conductors," Trans. A.I.E.E., vol.76, pt.III, pp.461-75, August 1957.

16. J. Reichman, and J.R. Leslie, " Radio interference studies for e.h.v. lines in Ontario," ibid., vol.79, pp.153-60, June 1960.

C H A P T E R - I (pp. 9 - 54)

1. L.B. Loeb, " Basic processes in gaseous electronics," Book, University of California Press, Berkeley, 1959.

2. M.R. Amin, "Fast-time analysis of intermittent point-to-plane corona in air, II- positive pre-onset streamer corona," Journal of Applied Physics, vol.22,p.358,1951.

3. M. Akazaki, "Corona phenomena from water drops on smooth conductors under high direct voltages," Trans. I.E.E.E., vol. PAS-84, pp.1-8, January 1965.

4. L.S. Perel'man and M.I. Chernobrodov, "Study of impulses of positive corona and the radio influence of a conductor in actual conditions," Electrical Technology, U.S.S.R., April 1967, pp.218-29.

5. S. Gupta, "Investigation of corona from concentric spherical arrangement of electrodes," Thesis, Univ. of Toronto, 1964.

6. H. Heindl, " Radio interference caused by d-c corona in a co-axial cylindrical field," Archiv der Elektrischen Ubertragung, Wiesbaden, 9(2), pp.93-98, 1955.

7. L.B. Loeb, "Electrical coronas," Book, University of California Press, Berkeley, 1965.

8. C.A.E. Uhlig, "The ultra corona, a new discharge phenomenon occuring on thin wires," Proc. of the high-voltage symposium, National Research Council, Ottawa, 1956.

9. B.J. Jakubczyk, and L. Boulet, "Alternating corona in foul weather, part I - above freezing point,"

Trans. I.E.E.E., vol. PAS-83, pp.508-12, May 1964.

10. J.B. Jordan, "Foul weather corona," Research Report, Electrical Engineering Department, Université Laval, Quebec, Canada, 1965.
11. L.V. Bewley, "Traveling waves in transmission systems," Book, John Wiley & Sons, New York, 1951. (Dover Publications, New York, 1963).
12. R.C. Fletcher, "Impulse breakdown in the 10^{-9}- second range of air at atmospheric pressure," Physical Review, vol.76, no.10, pp.1501-11, November 1949.
13. W. Heintz, "Investigation of the high-frequency spectrum of periodic discharges," Zeit. fur Angew. Math. und Phys., Verlag Burkhauser, Basel, Switz., 11(2), pp.51-6, 1959.
14. H.E. Raether, "Electron avalanches and breakdown of gases," Book, Butterworths, London, 1964.
15. D. Würstlin, "Corona discharges in coaxial cylindrical field," Thesis, Technical Univ. of Karlsruhe, North Baden, Germany, 1959.
16. E. Baumann, "Corona pulses: r-f spectra and their relation to non-ionizing collision and cross sections," in Gas discharges and the electricity supply industry," Book, ed. J.C. Forrest, Butterworths, London, 1962, pp. 238-49.
17. J.D. Cobine, "Gaseous conductors," Book, Dover Publications, New York, 1958, p.254.
18. F.W. Peek, Jr., "Dielectric phenomena in high-voltage engineering," Book, McGraw-Hill, New York, 1929, p.66.

19. D.W. ver Planck, "Calculation of initial breakdown voltages in air," Trans. A.I.E.E., vol.60, pp.99-104, Mar. 1941.

20. W. Shockley, "Currents to conductors induced by a moving point charge," Journal of Applied Physics, vol.9, pp.635-6, October 1938.

21. J.A. Morrison, and D. Edelson, "Solution of the space charge problem for a pulsed Townsend dischage," ibid., vol.33, no.5, pp.1714-20, May 1962.

22. A.S. Denholm, "The pulses and radio influence voltage of power-frequency corona," Trans. A.I.E.E., pt.III, vol.79, pp.698-707, October 1960.

23. B. Rakosh-Das, " Pulses and radio influence voltage of direct voltage corona," Trans. I.E.E.E., vol. PAS-83, pp.483-91, May 1964.

CHAPTER - II (pp. 55 - 85)

1. C.V. Aggers, D.B. Foster, and C.S. Young, "Instruments and methods of measuring radio noise," Trans. A.I.E.E., vol.59, pp.178-92, March 1940.

2. "Methods of measuring radio noise, a report of the joint committee on radio reception of E.E.I., N.E.M.A., and R.M.A.," E.E.I. Publication, No. G9, 1940.

3. S.F. Pearce, " The measurement of radio interference," Proc. International conference on Gas Discharges , Central Electricity Research Laboratories, ed. J.S.Forrest, Butterworths, London, 1962.

4. N.D. Diamentidis, "Correlational and spectral techniques in modern communication and control systems," Electrical Engineering, pp.860-5, November 1961.

5. G.E. Adams, "The calculation of radio interference level of transmission lines caused by corona," Trans. A.I.E.E., vol.75, pt. III, pp.411-19, June 1956.

6. G.E. Adams, "An analysis of radio interference characteristics of bundled conductors," ibid., vol.76, pp.1569-84, February 1957.

7. A.K.Abboushi, and L.O. Barthold, "Digital calculation of radio noise levels, " ibid., vol.80, pp.841-6, Dec. 1961.

8. L.O. Barthold, W.S. Price, and R.H. Schlomann, "Some important assumptions in calculation of radio noise levels of e.h.v. lines," C.I.G.R.E. Proc., paper 303, 1962.

9. F.J. Trebby, "Development of a square law radio noise meter," Trans. A.I.E.E., vol.78, pt.III, pp.522-28, August 1959.

10. F.J. Trebby, "Development of a square-law radio noise meter - II," ibid., pp.1186-91, December 1959.

11. A. Reed, "Corona pulse characteristics and their relationship to radio noise," Research Report No. ERB-711, Radio & Electrical Engineering Division, National Research Council, Ottawa, October 1964.

12. C.V. Lago and D.L. Waidelich, "Transients in Electrical Circuits," Book, Ronald Press Co., New York, 1958, ch.9.

23. W.B. Davenport and W.L. Root, "An introduction to the

theory of random signals and noise," Book, McGraw-Hill, New York, 1958, Chapters 6,7, and 12.

14. M. Schwartz, "Information transmission, modulation, and noise," Book, McGraw-Hill, New York, 1959, Ch. 7.

15. D.B. Geselowitz, "Response of ideal radio noise meter to continuous sine wave, recurrent impulses, and random noise," Trans. I.R.E., Radio Frequency Inetrference, vol. RFI-3, pp.2-11, May 1961.

16. F. Haber, "Response of quasi-peak detector to periodic impulses with random amplitudes," Trans, I.E.E.E., on Electromagnetic Compatibility, vol. EMC-9, no.1, pp.1-6, March 1967.

17. L.V. Bewley, "Two-dimensional fields in electrical engineering," Book, Dover Publications, New York, 1963.

18. H. B. Dwight, "Tables of integrals and other mathematical data," MacMillan Co., New York, 1960, Formula 120.1 and 505.1.

CHAPTER - III (pp. 86 - 112)

1. B. Rakosh-Das, and R.M. Morris, "Investigation of corona on overhead conductors at high voltage d.c., a progress report on radio interference," Research Report No.ERB-602, National Research Council, Ottawa, March 1962.

2. K.Ia. Kafieva, "A study of radio interference from corona on transmission lines," Elektrichestvo, Electical Technology, U.S.S.R., vol.12, pp.598-612, 1960.

3. F.L. Taylor, C.J. Crockford, and R.V. Nicolson, "Investigation of radio noise from existing lines and equipment to aid in the design of future e.h.v. lines," Trans., A.I.E.E., vol.76, pt.III, pp.436-45, August 1957.

4. J. Reichman and J.R. Leslie, "Radio interference studies on e.h.v. lines," ibid., pp.261-70, June 1961.

5. R. Bartenstein, and E. Schafer, "Continuous measurements of the high-frequency interference level of high-voltage transmission lines and their statistical evealuations," C.I.G.R.E. Proc., paper No. 409, 1962.

6. M.C. Perz, "Characterisics of corona noise," Ontario Hydro Research News, pp.1-12, Oct.-Dec. 1960.

7. M.C. Perz, "Method of evalaating corona noise generation from measurements on short test lines," Trans. A.I.E.E., vol.82, pt.III, pp.833-44, December 1963.

8. C.W. Helstrom, "The spectrum corona noise near a power transmission line," ibid., vol.80, pp.831-37, Dec. 1961.

9. G.E. Adams, T.W.Liao, M.G. Poland, and F.J. Trabby, "Radio noise propagation and attenuation tests on B.P.A.'s McNarry-Ross 345-kv line," ibid., vol.78, pp.380-88, June 1959.

10. G.E. Adams, and L.O. Barhhold, "The calculation of attenuation constants for radio noise analysis of overhead lines," ibid., vol.79, pp.975-81, December 1960.

11. R.M. Morris, and B. Rakosh-Das, "An investigation of corona loss and radio interference from transmission line con-

ductors at high direct voltages," Trans. I.E.E.E., vol. PAS-83, pp.5-16, January 1964.

12. S. Ramo, J.R.Whinnery, and T. van Duzer, "Fields and waves in communication electonics," Book, John Wiley & Sons, New York, 1965.

C H A P T E R - IV (pp. 113 - 163)

1. R.M. Morris, and B. Rakosh-Das, "An investigation of corona loss and radio interference from transmission line conductors at high direct voltages," Trans. I.E.E.E., vol. PAS-83, pp.5-16, January 1964.

2. J. Reichman and J.R. Leslie, "Radio interference studies for e.h.v. lines in Ontario," Trans. A.I.E.E., vol.79, pt.III, pp.153-60, June 1960.

3. E.H. Gehrig, C.F. Clark, A.C. Peterson, and T.C. Rednour, "B.P.A.'s 1100-kv test project, II- radio interference and corona loss," Trans. I.E.E.E., vol. PAS-86, pp.278-290, March 1967.

4. H. Witt, "Insulation levels and corona phenomena on h.v. d.c. transmsssion lines," Thesis, Chalmer's University, Göteborg, Sweden, 1961.

5. R. Bartenstein, and E. Schafer, "Continuous measurements of the high-frequency interference level of high voltage transmission lines and their statistical evaluations," C.I.G.R.E. paper No.409, 1962.

6. F.L. Taylor, C.J. Crockford, and R.V.Nicolson, "Investigation of radio noise from existing lines and equipment

to aid in the design of future e.h.v. lines," Trans. A.I.E.E., vol.76, pt.III, pp.436-45, August 1957.

7. M.C. Perz,"Methods of evaluating corona noise generation from measurements on short test lines," Trans. A.I.E.E., vol.82, pt.III, pp.833-44, December 1963. Also see discussion by O. Nigol and J. Reichman.

8. J. Laforest, L.O. Barthold, R.L. Thompson, and C.B. Eindh, "500-kv line design, III- conductors," Trans. A.I.E.E., vol.82, pt. III, p.587, August 1963.

9. H.B. Dwight, "Tables of integrals and other mathmatical data," Book, Macmillan Co., New York, 1958, No.813.1.

10. G.E. Adams, T.W. Liao, M.G. Poland, and F.J. Trebby, "Radio niose propagtion and attenuation tests on B.P.A.'s MacNarry-Ross 345-kv line," Trans. A.I.E.E., vol.78, pt. III, pp.380-88, June 1959.

11. M.C. Perz, "Characteristics of corona noise," Ontario Hydro Research News, vol.12, No.4, pp.1-12, October-December 1960.

12. B. Rakosh-Das, "Radio interference from high-voltage direct-current transmission lines," Bulletin of the Radio & Electrical Engineering Division, National Research Council, Ottawa, vol.14, No.2, pp.19-29, Apr.-Jun. 1964.

V I T A

Beegamudre RAKOSH-DAS was born in March 1926 at Bangalore, Mysore State, India, to Sriman B. Krishna-Rau (deceased) and Srimathi B. Bhagirathi-Bai. He holds the degree of Bachelor of Science in combined Electrical and Mechanical Engineering from Banaras University (1949) and the graduate diploma Associate of the Indian Institute of Science, Bangalore, in Electrical Engineering (1952).

During1948-49 he was employed by the Mysore Government in the Mahatma Gandhi Hydro-electric power station at Jog Falls. From November 1951 to September 1953, he worked in Japan, first as a graduate trainee in the power plant machinery factories of Messrs Hitachi Ltd., and later for one year as a graduate reasearch student at the Kyoto University under the direction of Professor Shigenori HAYASHI.

From January 1954 to August 1957, he was Assistant Professor at Mysore, Lecturer for M.Sc. classes in Electrical Machine Design at the Roorkee University, and Reader in Electrical Machinery at the Banaras University.

In September 1957, he came to Lehigh University as a graduate student and Instructor in Electrical Engineering. From June 1961 to August 1964, he worked as an Assistant Research Officer at the Electrical Engineering Section of the National Research Council of Canada at Ottawa and was assigned to the HIGH-VOLTAGE D.C. transmission research project.

In September 1964, he joined the Royal Military College of Canada and until July 1967, has held successively the posts of Lecturer, Assistant Professor and Associate Professor in Electrical Engineering. Since September 1967, he is working at the Lehigh University.

Mr. Rakosh-Das is a Senior Member of the Institute of Electrical & Electronics Engineers (New York), a Member of the American Physical Society (NEw York), a Member of the Institution of Electrical Engineers (London), Chartered Electrical Engineer in the United Kingdom, and a Registered Professional Engineer in the Province of Ontario. He is a founding member of the Corona Research Group, which is an informal group of all engineers interested in problems concerning corona and its effects.

He is married to Dr. Chintakindi LAKSHMI-BAI and they have one son, VENKATESWAR.